DEVELOPMENT OF FUNCTIONALLY GRADED ALUMINUM MATRIX COMPOSITE MATERIALS FOR DEFENSE INDUSTRY APPLICATIONS

A THESIS SUBMITTED TO
THE GRADUATE SCHOOL OF NATURAL AND APPLIED SCIENCES
OF
MIDDLE EAST TECHNICAL UNIVERSITY

BY

TAHA YILMAZ

IN PARTIAL FULFILLMENT OF THE REQUIREMENTS
FOR
THE DEGREE OF MASTER OF SCIENCE
IN
METALLURGICAL AND MATERIALS ENGINEERING

SEPTEMBER 2019

Approval of the thesis:

DEVELOPMENT OF FUNCTIONALLY GRADED ALUMINUM MATRIX COMPOSITE MATERIALS FOR DEFENSE INDUSTRY APPLICATIONS

submitted by **TAHA YILMAZ** in partial fulfillment of the requirements for the degree of **Master of Science in Metallurgical and Materials Engineering Department, Middle East Technical University** by,

Prof. Dr. Halil Kalıpçılar
Dean, Graduate School of **Natural and Applied Sciences** _____

Prof. Dr. C. Hakan Gür
Head of Department, **Met. and Mat. Eng.** _____

Prof. Dr. Ali Kalkanlı
Supervisor, **Met. and Mat. Eng., METU** _____

Examining Committee Members:

Prof. Dr. Bilgehan Ögel
Met. and Mat. Eng., METU _____

Prof. Dr. Ali Kalkanlı
Met. and Mat. Eng., METU _____

Prof. Dr. Rıza Gürbüz
Met. and Mat. Eng., METU _____

Assist. Prof. Dr. Simge Çınar
Met. and Mat. Eng., METU _____

Assist. Prof. Dr. Ayşe Kalemtaş
Met. and Mat. Eng., BTU _____

Date: 10.09.2019

I hereby declare that all information in this document has been obtained and presented in accordance with academic rules and ethical conduct. I also declare that, as required by these rules and conduct, I have fully cited and referenced all material and results that are not original to this work.

Name, Surname: Taha Yılmaz

Signature:

ABSTRACT

DEVELOPMENT OF FUNCTIONALLY GRADED ALUMINUM MATRIX COMPOSITE MATERIALS FOR DEFENSE INDUSTRY APPLICATIONS

Yılmaz, Taha
Master of Science, Metallurgical and Materials Engineering
Supervisor: Prof. Dr. Ali Kalkanlı

September 2019, 122 pages

Functionally graded materials (FGMs) are advanced class of composite materials that have a gradual change in composition and structure over the entire material and many different properties can be obtained by altering the structure. Therefore, they have many different application areas. This study aims to develop functionally graded aluminum matrix composite materials for defense applications. Firstly, porous ceramic pellets and preforms, made of alumina (Al_2O_3) and olivine ($(Mg,Fe)SiO_4$), were produced with conventional pressing and sintering processes for frontal layer of FGM. Effect of different sintering temperatures, different particle size fractions (for olivine) and different amount of metal powder addition (for alumina) on relative densities of pellets were measured. Secondly, porous ceramic preforms were infiltrated with high strength aluminum alloy AA7075 (Al-Zn-Cu-Mg) by using metal infiltration method. Thirdly, metal matrix composites (MMCs) were produced by melt stirring and squeeze casting methods for backing layer of FGMs using AA7075 (Al-Zn-Cu-Mg) as matrix material and olivine 5-7.5-10 wt. % as reinforcement material. Some of MMCs were T6 heat treated to observe the effect of heat treatment on mechanical properties. All samples were characterized mechanically, physically and microstructurally. Density measurements of pellets showed that from 38 % to 87 % relative densities were achieved with different sintering temperatures, particle

fractions and metal alloy addition. T6 heat treatments increased both hardness and flexure strength properties of MMCs. Maximum hardness was measured from 10 wt.% olivine reinforced MMC as 183 HB and maximum flexure strength was measured as 636 MPa from 5 wt.% olivine reinforced MMC. In melt infiltrated preforms maximum hardness was measured as 458 HB from melt infiltrated alumina preforms sintered at 1400 °C and maximum flexure strength was measured as 487 MPa from melt infiltrated olivine preforms sintered at 1250 °C.

Olivine as a reinforcement material in MMC and as a preform in melt infiltration process was used successfully with this thesis study for the first time in the literature. By changing process and material parameters preforms with different densities were produced for FGM layers.

Keywords: Functionally Graded Materials, Ballistic Armors, AA7075 Aluminum Alloy, Olivine

ÖZ

SAVUNMA SANAYİİ UYGULAMALARI İÇİN FONKSİYONEL DERECELİ ALÜMİNYUM MATRİKSLİ KOMPOZİT MALZEME GELİŞTİRME

Yılmaz, Taha
Yüksek Lisans, Metalurji ve Malzeme Mühendisliği
Tez Danışmanı: Prof. Dr. Ali Kalkanlı

Eylül 2019, 122 sayfa

Fonksiyonel dereceli malzemeler (FDM) tüm malzeme boyunca kademeli yapı ve kompozisyon değişimine sahip olan ileri kompozit malzemelerdir ve yapının değiştirilmesi ile birçok farklı özellikler yakalanabilir. Bundan dolayı, birçok uygulama alanına sahiptirler. Bu çalışma savunma sanayi uygulamaları için fonksiyonel dereceli alüminyum matriksli kompozit malzmelerin geliştirilmesini amaçlamaktadır. İlk olarak, alümina (Al_2O_3) ve olivinden ($(Mg,Fe)SiO_4$) gözenekli seramik pellet ve preformlar geleneksel presleme ve sinterleme prosesleri ile FDM'nin ön tabakası için üretilmiştir. Farklı sinterleme sıcaklıklarının, farklı tane boyut oranlarının (olivin için) ve farklı metal toz ilave oranının (alumina için) peletlerin görece yoğunluklarına etkisi ölçülmüştür. Ikinci olarak, gözenekli preformlar yüksek dayançlı AA7075 (Al-Zn-Cu-Mg) ile metal infiltrasyon yöntemi kullanılarak infilte edilmiştir. Üçüncü olarak, eriyik karıştırma ve sıkıştırma döküm yöntemleri ile FDM'nin arka plakası için AA7075 (Al-Zn-Cu-Mg) matriks malzemesi olarak, ve olivin 5-7,5-10 ağ. % takviye malzemesi olarak kullanılarak metal matriksli kompozit malzemeler (MMK) üretilmiştir. Bazı MMK'lara mekanik özelliklere etkisini görmek için T6 ısıl işlemi yapılmıştır. Tüm numuneler mekanik, fiziksel ve mikroyapısal olarak karakterize edilmiştir. Peletlerin yoğunluk ölçümlerinde farklı sinterleme sıcaklıkları, farklı tane boyut oranları ve farklı metal ilaveleri ile görece %38 ile %87

yoğunluklar elde edilmiştir. MMK'lara uygulanan T6 ısıl işlemi hem eğme dayanımına hem de sertlik özelliklerini iyileştirmiştir. Maksimum sertlik değeri ısıl işlem görmüş ağ. %10 olivin içeren MMK'dan elde edilmiştir (183 HB). Maksimum eğme dayanımı ağ. %5 olivin içeren ısıl işlem görmüş MMK'dan elde edilmiştir (636 MPa). Metal infilte edilmiş preformlardan maksimum sertlik 1400 °C'de sinterlenmiş alümina preformdan 458 HB olarak ölçülmüş ve maksimum eğme dayanımı 1250 °C'de sinterlenmiş olivine preformdan 487 MPa olarak ölçülmüştür.

Bu çalışma ile olivin ilk kez başarılı bir şekilde MMK ve preform infiltrasyon çalışmalarında kullanılmış olup, farklı yoğunluklarda gözenekli seramik preformlar değişken proses ve malzeme parametreleri ile FDM için başarılı bir şekilde üretilmiştir.

Anahtar Kelimeler: Fonksiyonel Dereceli Malzemeler, Balistik Zırh, AA 7075 Alüminyum Alaşımı, Olivin

To my family,

ACKNOWLEDGEMENTS

This thesis would not have been submitted without the help and contribution of several individuals who provided their valuable supports.

Firstly, I would like to express my utmost gratitude to my supervisor dear Prof. Dr. Ali Kalkanlı for his guidance, support and tolerance.

I would like to thank to the technical staff of the Department of Metallurgical and Materials Engineering, METU and especially Ali Osman Atik, Cemal Yanardağ, Önder Şahin and Arif Atalay Özdemir for their contributions to this study.

I would like to thank to my manager Assoc. Prof. Dr. Özgür Birer and my colleagues Mustafa Akbostancı, Hansu Birol, Orçun Ergün, Merve Ergin Örek, Gizem Tütün, Burcu Aksoy, Hande Hanedan and Hüseyin Yurdakul from ASELSAN Inc. for their valuable recommendations, guidance and helps.

I also would like to thank to my support, life energy and my fiancée Zuhal Aktaş for her presence, tolerance, love and understanding. Life is much more beautiful and tolerable with her.

Finally, I cannot thank enough to my dear parents, Belgin Yılmaz and Levent Yılmaz and sisters, Beyza Elif Yılmaz, Zeynep Sude Yılmaz, Zehra Nur Betül Yılmaz whose encouragement, support and presence provide all the success that I have.

TABLE OF CONTENTS

LIST OF TABLES

TABLES

LIST OF FIGURES

FIGURES

CHAPTER 1

INTRODUCTION

In today, defense industry is one of the most important industry branch for countries. Countries makes many investments for their defense expenses. In defense industry, there are many different systems are being studied like weapons (rifles, missiles, rockets, guns, grenades, et cetera), avionics, cameras, electronics, materials, structural elements for aircrafts, ships and ground vehicles et cetera. Among all these systems, ballistic armor protection systems and materials are important features and they have been a topic for many researches, since they are designed to protect people, vehicles, systems, buildings.

Preliminary personal protective armors were made of various animal skins and heavy metal shields and to protect cities, city walls and ditches had been built. However, with developing battle technologies and weapon systems, these materials have been insufficient to protect the things mentioned above high enough. And, heavy metal shields and clothes were too heavy to carry. They were adding more than 20 kilograms on armies. Later, rolled homogenous steels were developed. They have been used and still being used by systems due to its weldability, high hardness and relatively good ductility properties. But it still puts on much weight on systems. In 1970s high strength ballistic fibers were started to use. Ceramic faced fiber backed armor plates are still in use. But ceramic materials do not have multi-hit capacity. A novel material called functionally graded material has been studied. This material has variable properties in one or more than one direction thanks to its compositional or structural difference in its structure. In ballistic armor applications starting with a high ceramic content frontal layer and ending with high metal layer by changing the composition of layers could be a good solution. And this can be provided by functionally graded materials.

In this thesis study, functionally graded metal matrix composite materials were produced. Layers were produced and characterized separately. For matrix material AA 7075 (Al-Zn-Cu-Mg) aluminum alloy was chosen for its superior mechanical properties which make it suitable for an armor system. For reinforcement material, olivine (a natural occurring mineral composed of iron and magnesium silicates), and alumina (Al_2O_3) were used. Firstly, ceramic preforms were produced to get a high ceramic percent frontal layer using conventional pressing and sintering processes and preforms were infiltrated using squeeze casting method. For intermediate and backing layers, reinforcements were added into liquid metal and they were stirred to be wet by liquid metal. And they were squeeze casted. 5-7.5 and 10 weight percent reinforcements used. At the same time, various compositions ceramic pellets were produced and sintered at different temperatures to examine optimum processing parameters for these materials. After the production step all specimens were mechanically, physically and microstructurally examined using mechanical testers (3-point bending machine, hardness measurement instrument), Archimedes' density measurement, and Scanning electron microscopy and optical microscope. It is proposed from this study that, functionally graded metal matrix composite materials can be a new solution to new ballistic protection systems.

CHAPTER 2

LITERATURE REVIEW

2.1. Ballistic Armors

Ballistic armors are equipment that are developed and used to protect ordnance, people and buildings from various size and shape shell fragments and bullets. Humankind has always been studied to protect themselves from threats that are coming from outside and consequently, ballistic science has been developed throughout the history. The ballistics is a science that examines the barrel characteristics and ambient conditions of a bullet from the barrel until it hits the target, as well as the behavior of energy discharge and deformation after impact. Ballistic science is divided into three with respect to its work item. These are interior ballistics, exterior ballistic and terminal ballistic. In interior and exterior ballistics, movement of a projectile in barrel and during flight is studied and in terminal ballistic, deformations on target material and projectile is studied after collision occurs [1].

Ballistic armors are separated into three groups for their area of utilization [1,2]:

1. Personnel Armors (bullet-proof vests and helmets, eye-glasses)
2. Light Armors (armors used in helicopters and aero planes)
3. Heavy Armors (armors used in vehicles and tanks)

Personnel protection armors are composed of soft and hard layers. Soft layers are generally made from fibers (for example ultra-high molecular weight polyethylene (UHMWPE)) and hard layers are made from ceramic materials. For weapon and small arms only fibers can be enough. However, for rifle attacks, ceramic materials are needed as additional material [2].

Both light and heavy armors are used in vehicle protection. Nevertheless, the distinction in between two is the platforms that they are used. Sea, ground and air are three class of the platforms. Ground vehicles, ships, and airplanes. In every platform, meeting different mission requirements is an issue. While in a severe war environment, heavy and hard armors are needed especially in ground vehicles, in air vehicles and boats, light armor materials and system should be used to keep weight at minimum and increase the payload volume [2].

Figure 2.1. shows an example for armor design process. When there is a new threat, conceptual design of armor system is done. Here, the geometry and design requirements are determined. After that, a materials research team selects the appropriate materials that can meet design requirements and ballistic test or modelling simulations are done. If the model or ballistic shoot pass the test, it can be said that new armor can be used in the field [4].

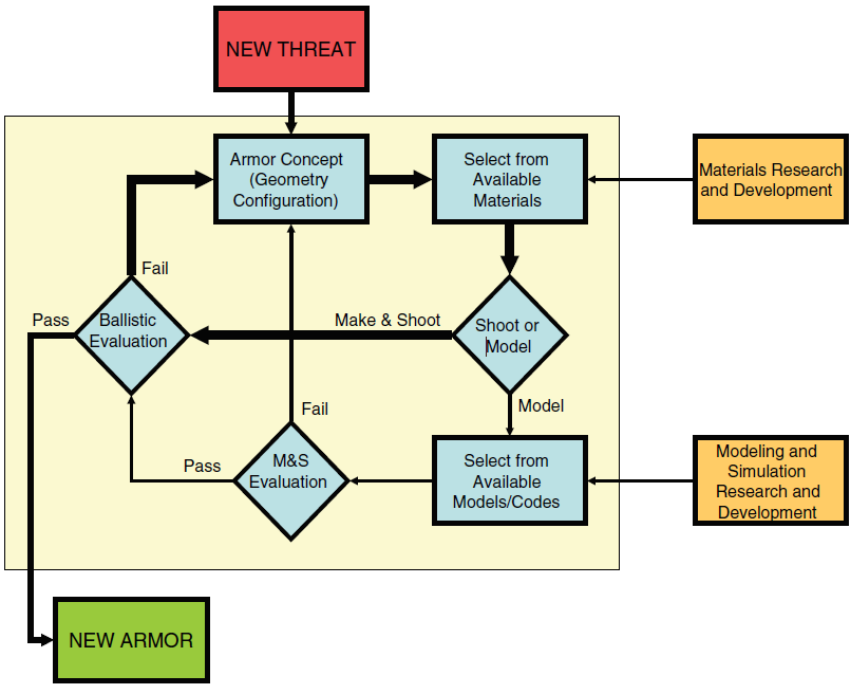

Figure 2.1. New armor design steps [4]

There are various international ballistic test standards to measure the ballistic protection level of armors. The mostly used ballistic test standards are National Institute of Justice (NIJ) for personnel armors and Standardization Agreement (STANAG-4569) for Logistic and Light Armored Vehicles [2, 4, 17].

2.1.1. Ballistic Performance and Armor System Testing

Ballistic performance of an armor material is affected by several factors. Material itself is a big factor in determining the ballistic performance. However, external factors are also efficient in performance determination [1,2,4].

The weight of the material directly affects the total mass of the system. It is aimed to have the same ballistic performance with lighter materials. Nevertheless, light materials for vehicle protection might be very heavy for personnel protection. So, a term called "areal density" is used to address the weight property of armor systems. Areal density is the weight per unit area of the armor required to provide protection against a specific ammunition and can be simply expressed as a multiplication the depth of penetration of a specific projectile with the density of the armor material. To understand whether the armor system is lighter in weight or not, a comparison of areal densities of armor materials with the areal density of rolled homogenous armor steel (RHA) is done. When the ratio is found to be two, it means new armor material has the same ballistic protection level at the half weight of the RHA [4, 13].

$$Mass\ Effectiveness = \frac{A_{d(RHA)}}{A_{d\ Armor\ Material}}$$

Other material dependent ballistic performance determination factors are hardness, fracture toughness, modulus of elasticity, tensile and bending strength, and porosity. The hardness of armor material must be higher than the projectile. A material with high hardness is favorable since hard material can deform projectile nose when it hits

the armor material. Furthermore, when the armor material is broken upon impact, the projectile will further be abraded by armor material while it passes through it. The armor material must be durable and withstand the tensile stresses when collision of projectile occurs. Fracture toughness is another important material parameter on protecting the system against threats. The higher the fracture toughness, the better the ballistic performance. Modulus of elasticity of the material also has a great effect on ballistic properties. A high modulus of elasticity materials will have a smaller strain for a given stress compared to a material that have relatively lower modulus of elasticity and this brings into a faster increase in stresses of projectile and the material. Sonic velocity in materials are direct proportional with the square root of modulus of elasticity. The higher the modulus of elasticity, the higher the sonic speed and thus the load can be spread over the wider region in armor materials [4, 13, 18].

Projectile geometry and velocity are two significant factors in ballistic efficiency of armor materials. In projectile geometry, diameter, mass and tip geometry of a specific projectile are three main factors. In a study conducted by Naik and Doshi [19], ballistic limit increased with increasing projectile diameter at constant weight and nose geometry of projectile. And ballistic limit decreased with increasing projectile weight at constant diameter and geometry of the projectile [1, 19]. The projectile velocity is also very important. The reaction of ballistic armors to threats is different according to the velocity of that threat. At relatively low velocities (<700 m/s) the penetration resistance of a material is governed by the dynamic deformation mechanisms within the projectile and target. At very high velocities (>5000 m/s) the material exhibit liquid behavior. At middle level velocities which is the range of most military weapons work, (700-5000 m/s), hydrodynamic effects dominate and the penetration response becomes controlled by only the density of the impacted material to determine efficiency [12].

As it can be seen, not only inherent properties of materials affect the ballistic performance, but also projectile geometry, velocity, material and weight have critical effects in ballistic performance. It can be concluded from this information that there

is not only one armor material solution for all ballistic protection. Because of this reason, there are various material types used in the armors to meet different mission requirements.

Standardization of tests and processes is very important. It is true in ballistic armors as well. There are several standard test methods for ballistic testing. Among all ballistic test standards, two widely used test standards are NIJ 0101.06 and STANAG 4569. Test methods are shown in Table 2.1 and Table 2.2 [4, 17].

Table 2.1. NIJ 0101.06 Ballistic test standard [4]

Protection Level	Projectile	Weight (g)	Velocity
Type IIA	9 mm (FMJ RN)	8	373 ± 9.1
	.40 S&W	11.7	352 ± 9.1
Type II	9 mm FMJ RN	8	398 ± 9.1
	.357 Magnum JPS	10.2	436 ± 9.1
Type IIIA	.357 SIG FMJ FN	8.1	448 ± 9.1
	.44 Magnum SJHP	15.6	436 ± 9.1
Type III (Rifles)	7.62 mm FMJ M80	9.6	847 ± 9.1
Type IV (AP Rifle)	.30 caliber AP bullet (M2 AP)	10.8	878 ± 9.1

Figure 2.2 shows ammunitions that are used in ballistic test of armor materials. As it can be seen, various size and shape ammunitions are used to determine ballistic protection levels of armor materials.

Figure 2.2. Ballistic test ammunitions [19]

STANAG 4569 /AEP 55 Volume 1 defines kinetic energy threats and fragments that are generated from detonation of an artillery shell or fragmenting improvised explosive devices. Table 2.2. shows kinetic energy threats and artillery threats with their level of ballistic protection. As mentioned earlier, there is no only one armor material which can protect systems or people from all threats coming from outside. Thus, different armor materials are being studied for different area of utilization.

Table 2.2 STANAG 4569 / AEP 55 Volume 1 Ballistic Test Standard [17]

Level	Kinetic Energy Threat				Artillery Threat (FPS 20 mm)		
	Ammunitions	Velocity (m/s)	Azimuth	Elev.	Velocity (m/s)	Azimuth	Elev.
1	7.62 mm x 51 NATO Ball	833	0-360 °	0°-30°	520	0-360 °	0-18 °
	5.56 mm x 45 NATO SS109	900	0-360 °	0°-30°	520	0-360 °	0-18 °
	5.56 mm x 45 M193	937	0-360 °	0°-30°	520	0-360 °	0-18 °
2	7.62 mm x 39 API BZ	695	0-360 °	0°-30°	630	0-360 °	0-22 °
3	7.62 mm x 54R B32 API	854	0-360 °	0°-30°	770	0-360 °	0-30 °
	7.62 mm x 51 AP (WC core)	930	0-360 °	0°-30°	770	0-360 °	0-30 °
4	14.5 mm x 114 API/B32	911	0-360 °	0°	960	0-360 °	0-90 °
5	25 mm x 137 APDS-T. PMB073	1258	± 30 °	0°	960	0-360 °	0-90 °

2.1.2. Ballistic Impact Mechanism of Materials

As it was mentioned in previous title, there is not a specific material which can meet the required protection level. Thus, there are various kinds of ballistic applications with very different kinds of materials. These armor materials can be a rolled homogeneous armor steel and they can be very high engineered advanced material with respect to their application areas and usage aims. Therefore, understanding the ballistic impact mechanism of armor materials is very significant.

When a projectile hits on armor material perforation occurs in three steps. These are impact, penetration and exit as can be seen in Figure 2.3. When impact velocity is very low than ballistic limit, the projectile forms a crater on the surface of armor material

and stay there. This is the mostly preferred situation in armor applications. In the second scenario, if velocity of impacted projectile is just smaller than the ballistic limit, penetration starts. If projectile velocity is higher than the ballistic limit of that armor material, because of the shear force of projectile plugging occurs and projectile completely perforate the material and exit [3].

Perforation (%) - impact velocity graph is an important graph for ballistic materials. In the safe case, ballistic limit should be smaller than the half of impact velocity V_{50}. After the point of V_{90}, fully penetration starts and it can cause some vitals problems for ballistic armor [3].

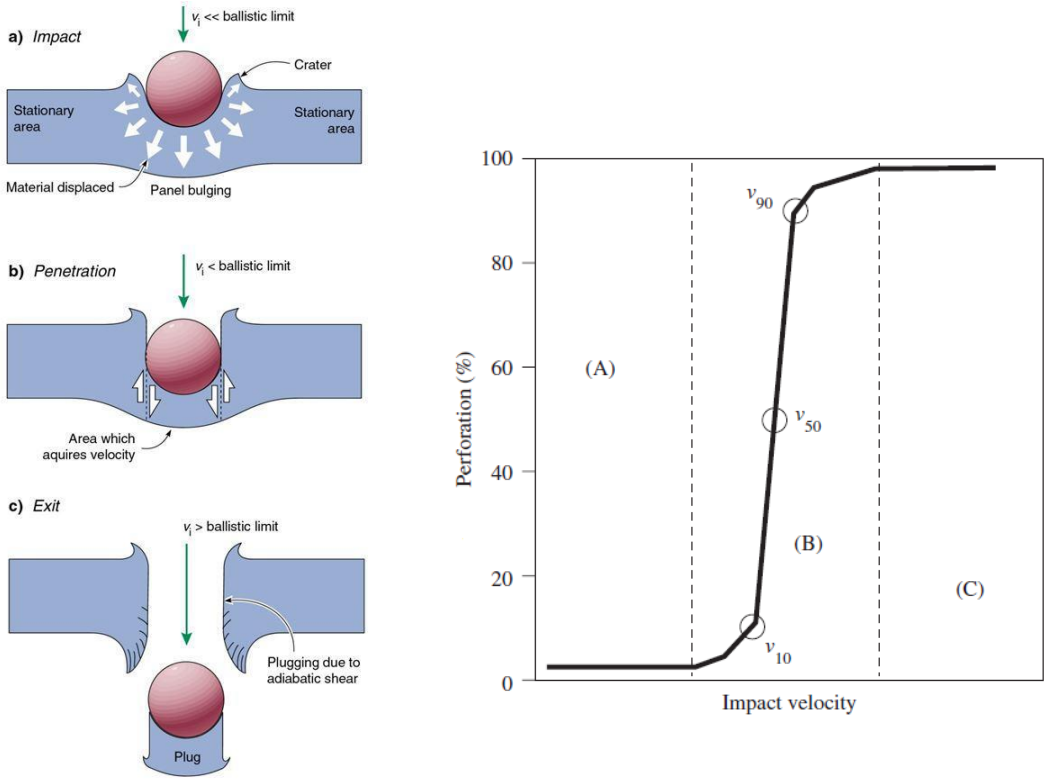

Figure 2.3. Steps in ballistic impact and impact velocity – perforation % graph [3]

2.1.2.1. Ballistic Impact Mechanism of Metals

Metals are commonly used materials in ballistic applications. They have some significant properties that make them suitable for ballistic armor materials. They are cheaper than other materials and metals can be joint with each other by welding, brazing and some other processes. Secondary and post processing can be done to metals like heat treatment to make their mechanical properties better. Metals can be used more than one time. they have multihit capacity, a projectile can hit on metals more than one time. One disadvantage of mostly used metallic materials is their relatively higher density compared to fibers and ceramic materials [3].

According to Yungwirth and his co-workers, ductility is a significant parameter for ballistic metals. As it can be seen in Figure 2.4., the ductility of metal should be balanced. If metal has low ductility, it shows brittle fracture behaviors like ceramic materials. On the other side, if metallic material has high ductility, projectile penetrates whole material and exits. Therefore, moderate ductile metals should be chosen [30].

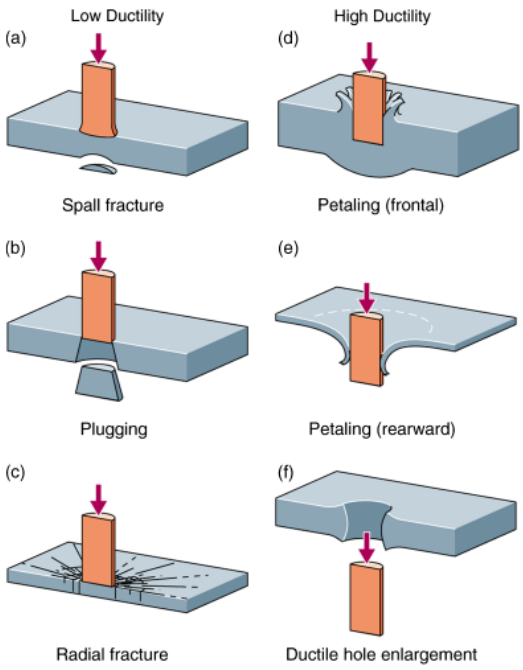

Figure 2.4. Ballistic impact mechanism of metals [3]

2.1.2.2. Ballistic Impact Mechanism of Ceramics

Ceramic materials have some good properties which makes them useful in armor applications. Ceramic materials have low density and correspondingly have low weight. Ceramics are hard and have high elastic modulus values. Moreover, they have high compressive strength. Figure 2.5. shows ballistic impact mechanism of ceramic materials. When a projectile hit on the surface of a ceramic material, many cracks forms and the kinetic energy of the projectile is transferred to material in the form of cracks. This is the main impact mechanism of ceramic materials. Also, these cracks that are fractured from ceramic material will deform the projectile since they are very hard and have high compressive strength [3,31]

Ceramic materials have mainly two disadvantages. One disadvantage is that their stress-strain values are only in elastic region which means they cannot be deformed plastically. The other disadvantage is that they do not have a multihit capacity. However, this drawback can be overcomed by statistics because of the fact that it is really hard to hit a material from the same point in a battlefield statistically. [3,35]

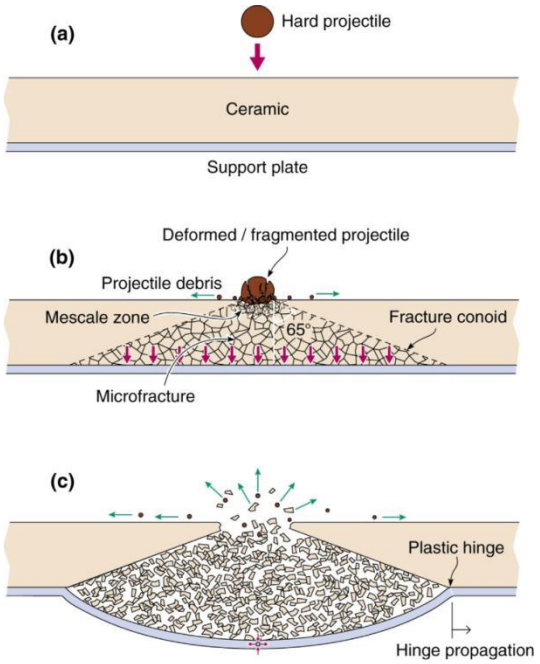

Figure 2.5. Ballistic impact mechanism of ceramic materials [4]

2.1.2.3. Ballistic Impact Mechanism of Fibers

Fibers are another mostly preferred form of materials in ballistic armor applications. Fibers from carbon, aramid and glass are used usually with polymer matrix materials. These fibers can also be used with metal matrix materials. Fibers have many advantages that make useful them in armors. They have very low densities compared to metals and ceramics. Moreover, they have high elastic modulus so that they can absorb energy. When a projectile hit on it, there will be a high stress on the tip of the projectile and this stress will be spread over the fiber to a wide area and this energy will be completely absorbed. This is the main impact mechanism of fibers (see Figure 2.6.) [3,32].

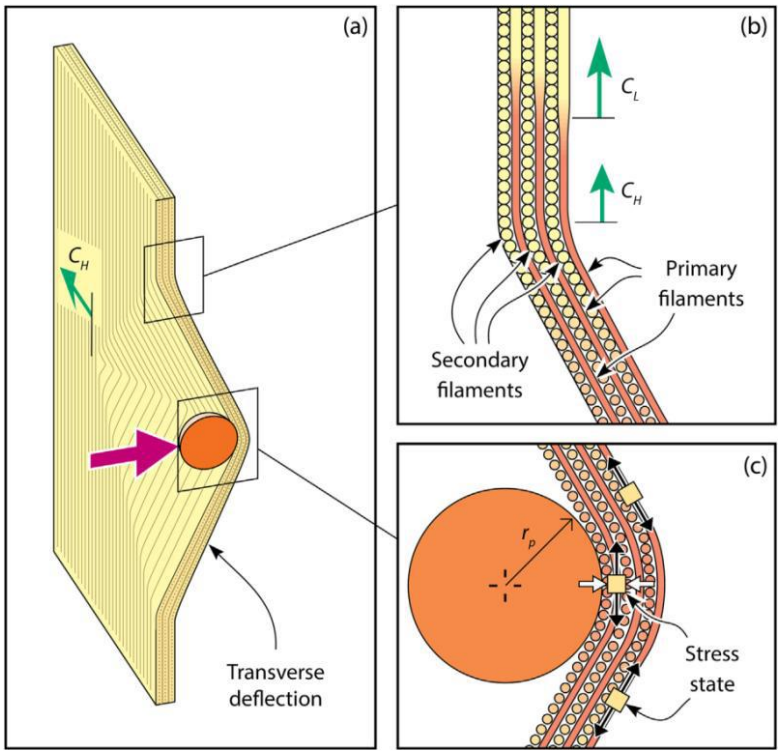

Figure 2.6. Ballistic impact mechanism of fibers [3]

One drawback of fibers and fiber reinforced composite materials is their high production cost.

2.2. Functionally Graded Materials

In most engineering applications, expectations from materials are generally conflicted. An application might necessitate the usage of a material that is both hard and ductile. Any material in its pure state is available to meet this need. Thus, combining a metal with another metal in molten state called “conventional alloying” can serve to requirements. However, because of thermodynamic equilibrium limits, there is a limit in solubility of metals in between each other. In addition to this, when combination of two different material that have very high difference in melting point conventional alloying is not a suitable method. Another production method called “Powder Metallurgy” is a method that materials in powder state come together with powder pressing and sintering processes. Parts that are produced with powder metallurgy techniques have great properties like improved wear characteristics and having near net shape, wide composition range, et cetera. Despite the great properties of powder metallurgy parts, there are some deficiencies. Complex shape parts cannot be produced easily, and fully dense structure achievement is hard. Consequently, mechanical properties decrease [8].

An advanced class of materials called “composite materials” are another form of materials that have exceptional properties. Composite materials are made of two or more materials with distinct physical and chemical properties. Thus, producing a material with similar or better properties and lighter in weight is possible. Like all materials have some deficiency, composite materials do have some inadequacy. Composite materials fail under extreme service conditions. In a high temperature and temperature cycling conditions when two materials with dissimilar thermal expansions is used, they will fail due to different thermal expansion values of these materials. To eliminate this problem, in 1980s in a hypersonic space vehicle project, researchers in japan encountered with a problem requiring a thermal barrier where outside temperature was 2000K and inner temperature 1000K and this gradient was in 10 mm thick material. And they came up with Functionally Graded Materials (FGM) [8].

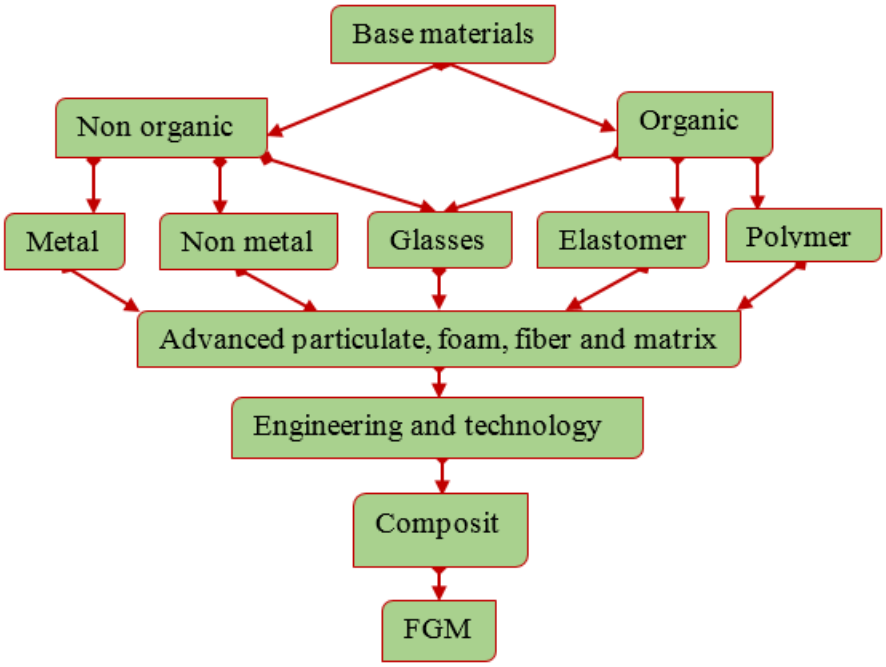

Figure 2.7. Modern material evolution as for FGM [7]

FGMs is a novel material that have different properties throughout its structure. Having varying property is provided by its gradual change in chemical composition, porosity level, phase distribution and microstructure. Thus, mechanical, electrical, thermal and magnetic properties differ in particular regions of this materials so that these materials can be used in many different areas [6-9, 20]. Figure 2.8. shows different forms of FGMs. This gradual change can be in the fraction level of one of the constituents through one direction of the material, orientation of one constituent may change through one direction or orientation can change and different size of constituent can be used in different regions. Thus, there will be a property change in one direction thanks to this structure change in this direction [21].

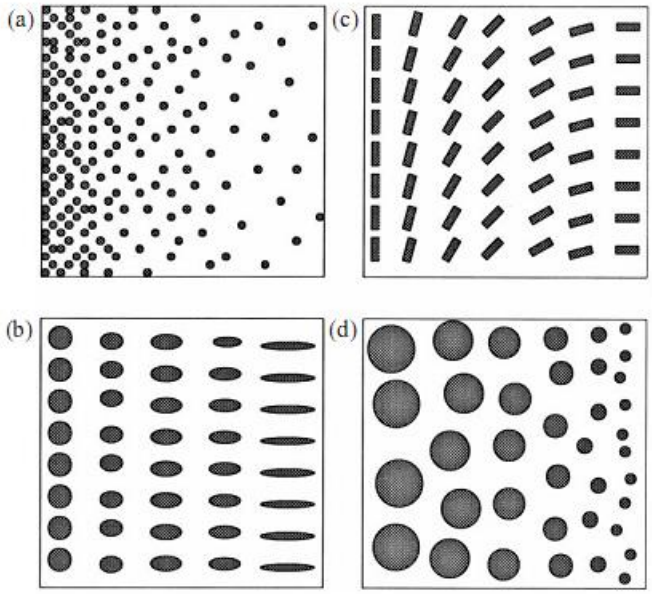

Figure 2.8. Different gradient types in FGM (a) fraction, (b) shape, (c) orientation (d) size [21]

The change in the structure can be either continuous or stepwise (See Figure 2.9.). In continuous structure change, there is a gradual change in composition and microstructure in one direction. In stepwise graded structure, this change occurs sharply, and the structure is composed of multilayers with interfaces in between each separate layer. Each type of graded structures serves different purposes [22].

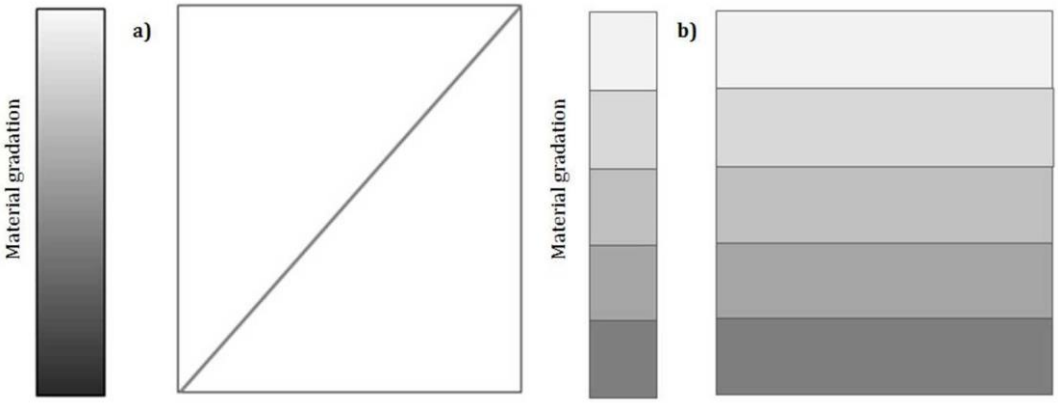

Figure 2.9. (a) Continuous structure change, (b) Stepwise structure change [22]

The significant characteristics of the FGM made them to be favorable material in almost every area of application:

In the aerospace industry: rocket engine components, heat exchange panels, turbine wheels, turbine blade coatings, nose caps and space shuttles are produced.

In automobile industry, it is still limited because of its relatively high cost of production, engine cylinder liners for diesel engine pistons, for leaf springs, spark plugs, combustion chambers, flywheels, racing car brakes.

In biomedical, human body has natural FGMs which are bones and teeth. When these parts are damaged, they can be replaced with artificial FGMs. Implants with porosity graded structures are produced.

In defense industry, FGMs offer great advantage to inhibit crack propagation when a projectile hit on it.

In energy industry, they are used in inner wall of nuclear reactors, thermo-electric converter for energy conversion, solar panel and solar cells, tubes and pressure vessels, turbine blade coatings and for thermal barrier coatings.

In electrical and electronics industries, they are used in thermal-shielding elements in the micro-electronics, in semiconductors, for insulators, and to produce sensors.

In marine implementations, FGMs are used in the propeller shaft, sonar domes, composite piping system and the diving cylinders.

In opto-electronics, they are used in optical fiber materials, the lens, and grinsh lasers, solar cells, magnetic storage media and in the production of semiconductors.

In sport equipment used in tennis rackets, golf clubs and skis. [6,7]

As it can be seen from usage areas, due to FGMs' wide variety range of properties, they find many application areas and it is indispensable that their usage will

continually increase with developing technology and decreasing in production cost. Figure 2.10. shows areas of application.

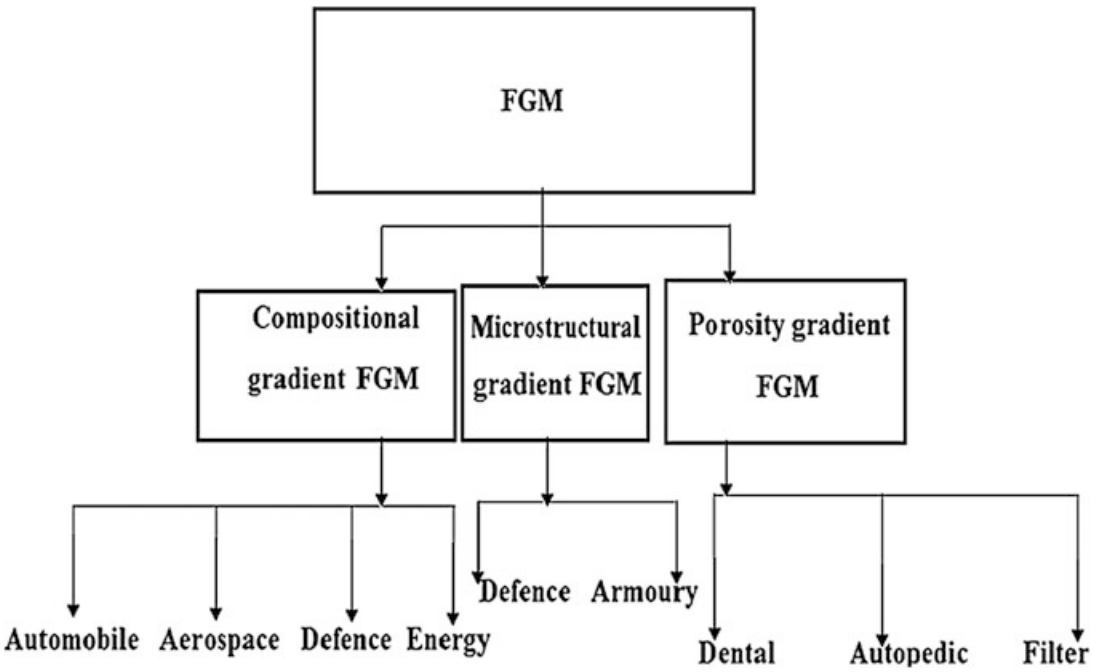

Figure 2.10. Application areas of FGMs [6-7]

2.2.1. Production Methods of Functionally Graded Materials

FGMs are mainly grouped into two categories in accordance with their thickness [6]. These are:

1. Bulk FGMs
2. Thin FGMs

Thin FGMs are generally thin sections and coatings. They are produced by vapor deposition techniques (Physical Vapor Deposition (PVD) and Chemical Vapor Deposition (CVD)), Plasma Spraying, Self-propagating High Temperature Synthesis (SHS) [20].

Bulk FGMs are relatively thick layers and materials that can be produced by several producing techniques. Producing techniques for bulk FGMs can be grouped into liquid state processes and solid-state processes. Since in this study bulk FGM layers from ceramics and aluminum matrix composite materials were produced with liquid state processes, bulk FGMs liquid production techniques related to production of this material type will be explained in the following section.

2.2.1.1. Squeeze Casting

Squeeze casting is a casting method in which solidification of metal or metal matrix composite parts occurs under applied pressure in a metal die. It can be said that it is a combination of die forging and permanent mold casting. Figure 2.11. shows steps in squeeze casting. The cast parts that are produced with squeeze casting can be used readily in service or only minor post processing may require. Thus, this process is regarded as near or near net shape processing technique [5, 11].

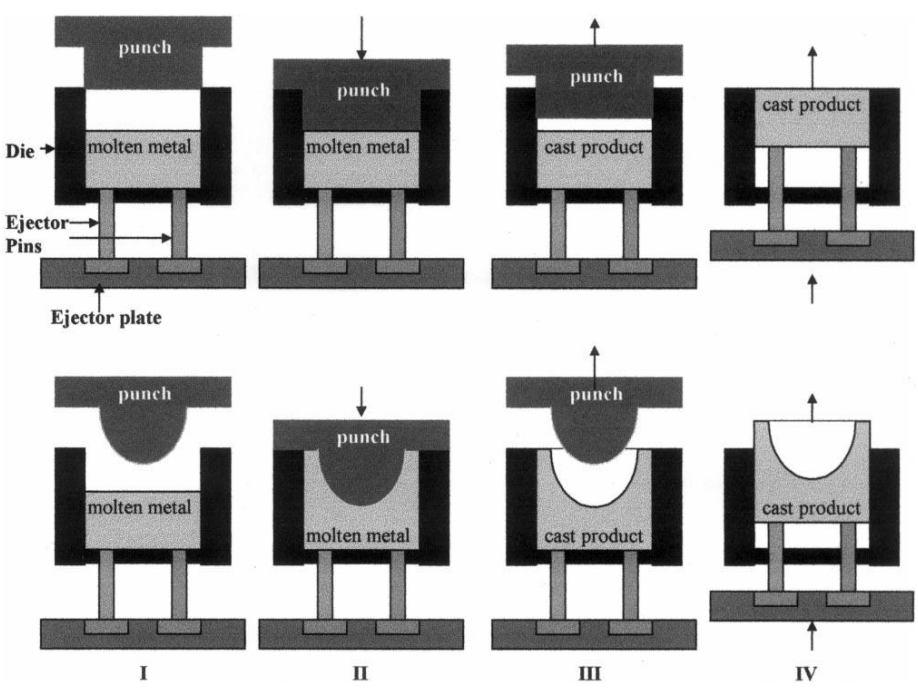

Figure 2.11. Process steps in squeeze casting [5]

The squeeze casting process occurs in four steps. These steps are:

1. A pre-determined amount of liquid metal is poured onto the lower die.
2. Upper punch squeezes the liquid metal until solidification of the metal takes place.
3. When the complete solidification occurs, the upper punch is drawn to the its initial level.
4. Finally, casted part is ejected by ejection pins [11]

The squeeze casting process is mainly grouped into two with respect to application of pressure. The pressure can be applied either directly onto metal that are being solidified or exerted through a feeding metal. These methods are called direct and indirect squeeze casting. if pressure is directly applied on solidifying metal, the process is called direct squeeze casting. if pressure is applied on a feed metal then the process is called as indirect squeeze casting. Schematic view of these two processes can be seen in Figure 2.12.

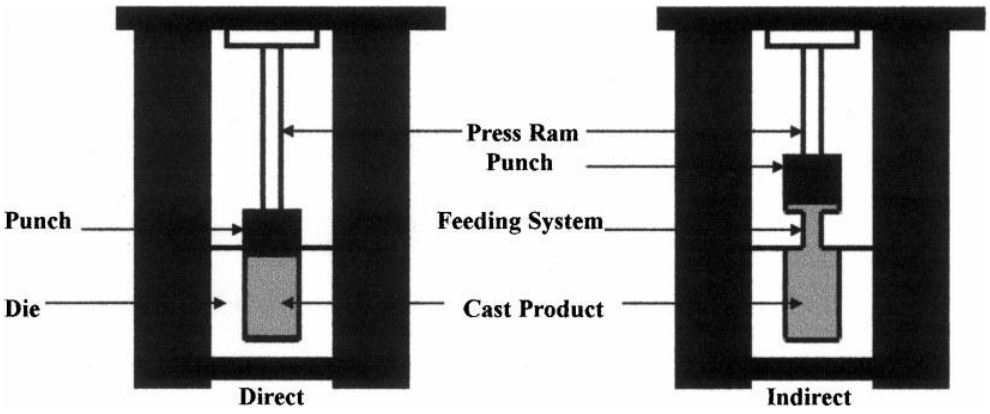

Figure 2.12. Direct and indirect squeeze casting processes [5]

Further classification with respect to squeeze casting equipment can be done. Direct squeeze casting machines are grouped into according to metal movement in the die. However, indirect squeeze casting machines are grouped into four categories. These

are: vertical die closing and injection, horizontal die closing and injection, horizontal die closing and vertical injection, vertical die closing and horizontal injection. These machines are produced either designed and produced either by researchers or machine tool companies [5, 11].

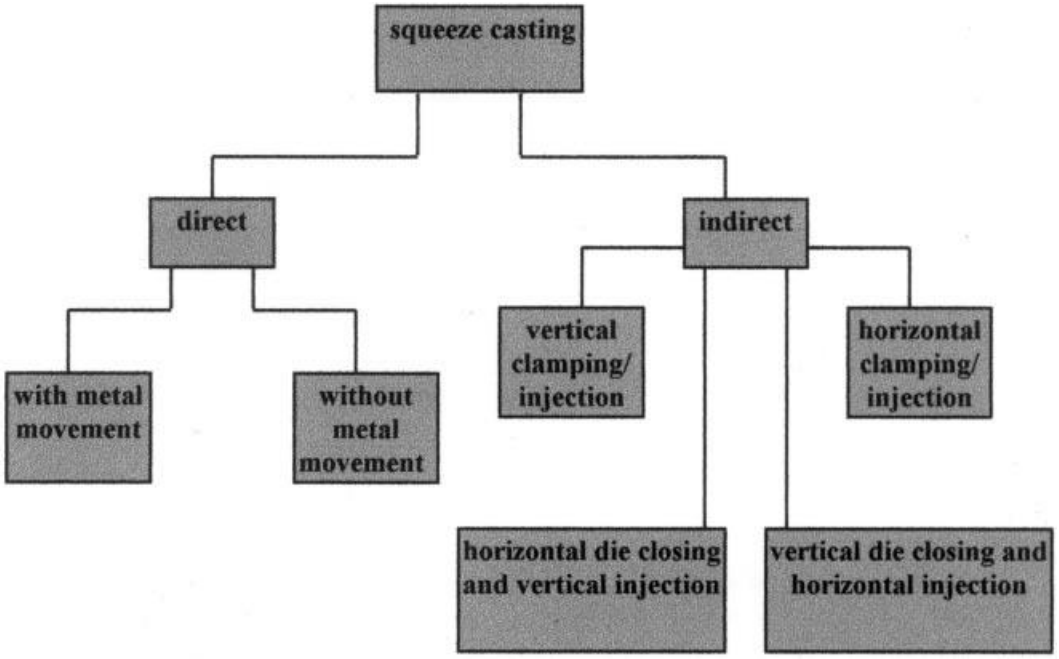

Figure 2.13 Various squeeze casting methods [5]

In squeeze casting, there are various process parameters that can directly affect the microstructure and mechanical properties of the casted parts. These are casting material, squeeze pressure, die temperature, casting temperature, die coat, time interval over which the pressure is applied [11].

The alloy being casted has a direct effect in squeeze casting process. The melting temperature of alloy affects die life. At the same time, thermal conductivity of the alloy together with heat transfer coefficient and soldering onto die material. The higher the melting temperature of the alloy, the shorter die life. Thus, in general aluminum and magnesium alloys are being used. And the composition of the alloy determines the freezing range and hence it affects the quality of the finished products [11]

Pressure is another important process parameter that can affect phase relationship of alloys being casted. This effect can be expressed with Claysius-Clapeyron equation:

$$\frac{\Delta T_f}{\Delta P} = T_f \frac{(V_l - V_s)}{\Delta H_f}$$

In the equation, T_f is the equilibrium freezing temperature, V_l and V_s specific volumes of liquid and solid, respectively, and H_f is the latent heat of fusion. When thermodynamic equation for volume (the liquid metal is taken as ideal gas in the calculations) is substituted in the equation, the effect of pressure on freezing temperature can be estimated as following equation:

$$P = P_0 \exp(\frac{-\Delta H_f}{RT_f})$$

P_0, H_f and R are constants. Thus, T_f must increase with increasing pressure. This theoretical calculation has been proved with experiment. In Figure 2.14. given below, application of approximately 150 MPa squeezing pressure increased the liquidus temperature about 9 °C and eutectic point was shifted towards higher silicon content region in an aluminum silicon binary alloy. This phenomenon improves mechanical properties and microstructures of squeeze casted parts [11].

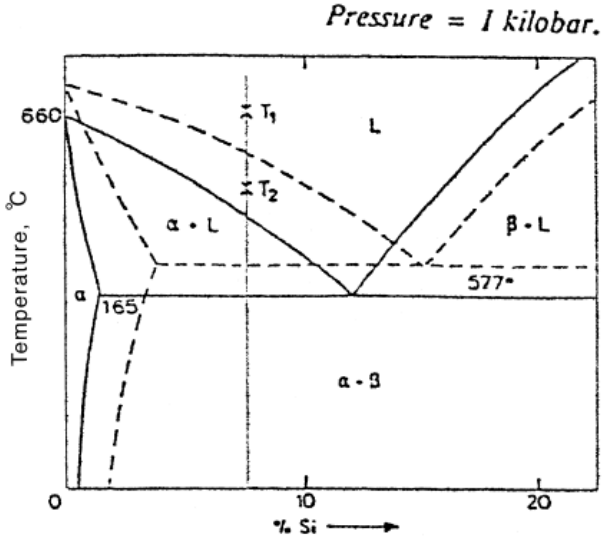

Figure 2.14. Effect of rapid cooling and pressure application on the Al-Si binary phase diagram [5]

Pressure application also improves wettability of reinforcement particles in metal matrix composite materials. And application of pressure reduces air gap in between metal and die and thus helps heat dissipation from part to die and consequently rapid solidification occurs [5]. The pressure in squeeze casting process is usually kept in between 50 and 150 MPa.

The casting and die temperature are another important parameter in squeeze casting. in the theory, the melt undercooling can occur in a most efficiently when the squeezing pressure is applied onto casting while the metal temperature is below its liquidus temperature [5] and the die temperature is generally kept at 250-300 ° C [11].

The general advantages of the squeeze casting process can be summarized in below:

1. Since the solidification occurs under applied pressure, the cast part has minimum or no gas porosity and shrinkage porosity.
2. Parts that are produced with this technique are near net or net in shape. This eliminates the material wastage. (no runners, gates, feeders and shrinkage compensating units are required).
3. Since solidification occurs under applied pressure, the castability of the alloy is little or no concern. Both wrought and casting alloys can be casted using this process.
4. Parts have exceptional surface finish with fine grained structure.
5. Superior mechanical properties can be obtained.
6. Parts have almost no porosity and segregation.
7. Non-equilibrium phases can be obtained thanks to applied pressure.
8. Both metal and metal matrix composites can be produced.
9. Preform infiltration process can be done. This provides having composite materials with high ceramic content in the structure [5, 11].

The disadvantages of this technique are cost and die wear due to high temperature and pressure. However, in mass production and high-quality product needs, these disadvantages can be eliminated [5,11].

2.2.1.2. Melt Infiltration Technique

Melt infiltration technique is a liquid state processing in which metal matrix composites can be produced. In this technique, a preformed ceramic material is infiltrated by liquid metal. If ceramic preforms are produced in a graded form and infiltrated with liquid metal, FGMs can be successfully produced. The production of functionally graded aluminum matrix composite materials with using this process can be done in two steps. The first step is the production of ceramic preforms. And the second step is infiltration of that ceramic preforms with liquid metal. Ceramic preforms can be produced with various techniques. The simplest and easiest way is sintering of coarse ceramic powders or incomplete sintering of fine ceramic powders. Another way to produce ceramic preforms is foam replication method. In this process a ceramic slurry is coated onto a porous polymeric material with open cell structure and firing out of polymeric material leaves a porous ceramic preform. Addition of pore forming agents into ceramic powder is another way to produce a porous ceramic preforms. Pore forming agent materials can be wax, starch, carbon fiber, et cetera. The porosity in ceramic preform structure can be altered by changing the amount of pore forming agents. After ceramic preform is produced, the second step in melt infiltration process is infiltration of liquid phase into ceramic preform [22].

Due to non-wetting nature of most liquid metals on ceramic materials, it is generally not possible to infiltrate the ceramic materials with liquid metals without application of an external pressure. The pressure can be applied using an inert gas (gas infiltration), a direct contact with a squeezing ram or vacuum application so that infiltration process takes place [22].

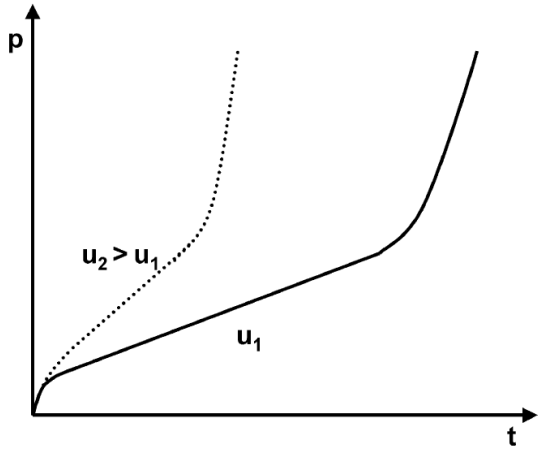

Figure 2.15. Pressure increase during squeeze casting for two melt velocities [22]

Figure 2.15. shows infiltration time and pressure in infiltration process with two different infiltration speeds where v_2 is higher than v_1. As it can be seen in figure there are three distinctive region in a metal infiltration process. In the first region starting of infiltration process occurs until capillary thereshold pressure is reached. In the beginning, a thereshold pressure should be reached to start the infiltration. This pressure can be calculated using capillary law:

$$P_0 = \frac{\sigma_{lv}}{r_{hydraulic}} cos\theta$$

σ_{lv} is the liquid vapor surface tension of the melt, θ is the contact angle and $r_{hydraulic}$ is the hydraulic radius. When threshold pressure is reached, the liquid metal infiltrates into capillaries of the preform. After the complete penetration, a small increase in pressure occurs due to filling of micropores in the structure [22]. Figure 2.16. shows a complete infiltration process of ceramic preforms using gas pressure infiltration process [7].

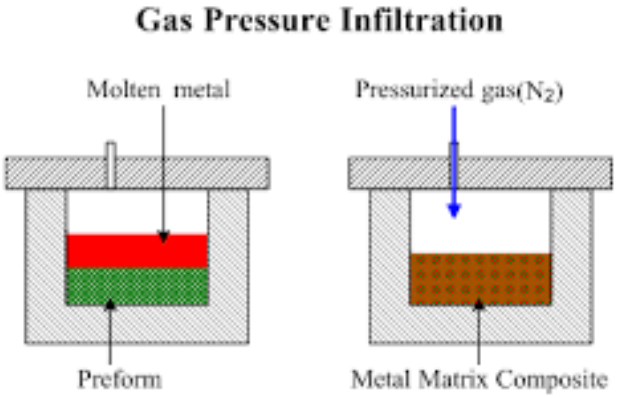

Figure 2.16 Gas infiltration process

2.2.1.3. Stir Casting

In stir casting process, reinforcement particles are added into liquid metal and stirred with a stirrer screw. The process is very useful for metal matrix production and it is a cost-effective production method for composite production since the system does not use advanced equipment. Figure 2.17. shows a schematic view of the stir casting process [7].

The reinforcement particles can be added into liquid metal with several methods. These methods are:

1. Reinforcement particles can be incorporated into matrix alloy through a feeding system using an inert gas.
2. The particles can be added during pouring the liquid metal into die.
3. A piston can push the particles in liquid metal.
4. The particles can be sprayed with liquid metal onto a substrate.
5. The particles can be distributed in the matrix with vortex [7, 23, 24].

The stirring speed, casting temperature, stirring time, and stirrer geometry have effect on the efficiency of the process. And distribution of reinforcement phase should be homogeneous throughout the structure to have better mechanical properties in finished products.

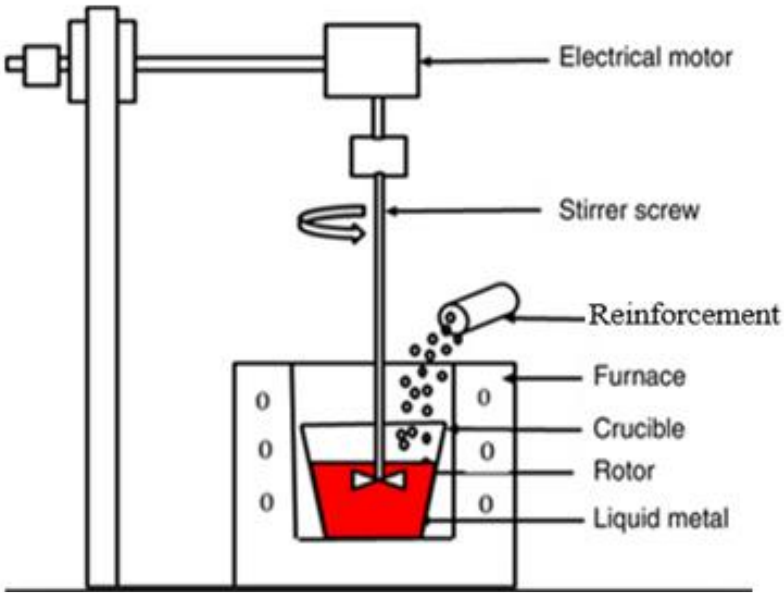

Figure 2.17. Melt stirring process

2.3. Armor Studies

2.3.1. Related Studies in the Literature

In the literature, there are many armor studies with many different materials and processing routes. Ceramics, metals and composite materials are widely used in ballistic armor production. Among all materials, studies that were conducted only on metal matrix composite materials will be presented here.

Kalemtaş et al. studied ballistic properties of boron carbide (B_4C) infiltrated with an aluminum alloy without pressure. They used two different particle size of B_4C as coarse and fine and they examined the effect of heat treatment on the properties of infiltrated ceramic preforms. They observed an increase in hardness and compression strength values with heat treatment. In ballistic tests conforming to MIL-STD-6621, infiltrated composites which were subjected to 48 hours heat treatment at 700 °C and 11.5 mm thick composite material with 10 mm thick E-glass composite backing layer provided level 4 ballistic protection [37].

Senthilvelan et al. produced metal matrix composites (MMCs) by stir casting process followed hot rolling using AA7075 as matrix material and B_4C, Al_2O_3 and SiC as reinforcement materials. They were compared mechanical properties of 10 wt. % reinforced composites with each other and with no reinforced added matrix alloy. Microhardness (HV 0.5) results were obtained as 96, 120.5, 112.3 and 138 for 0 wt.% reinforced, 10 wt. % SiC reinforced, 10 wt % Al_2O_3 and 10 wt.% B_4C composites, respectively. Tensile strengths were measured as 125 MPa, 182 MPa, 235 MPa and 304 MPa for 0 wt.% reinforced, 10 wt. % SiC reinforced, 10 wt % Al_2O_3 and 10 wt.% B_4C composites, respectively. And finally, elongation % were measured as 6.86, 3.2, 3.33, 4.33 for 0 wt.% reinforced, 10 wt. % SiC reinforced, 10 wt % Al_2O_3 and 10 wt.% B_4C composites, respectively [38].

Yılmaz and Kalkanlı synthesized and characterized SiC reinforced AA 7075 matrix composite materials with 10-15-20-25-30 wt. % reinforcement level of SiC. They used stir casting followed by squeeze casting methods and they did T6 heat treatment to some samples to see the effect of heat treatment on the mechanical properties of samples. They observed a homogeneous distribution of reinforcement phase in matrix alloy. The maximum average flexure strength and tensile strength were observed from T6 heat treated 10 wt.% reinforced MMCs as 580 MPa and 340 MPa, respectively. Effect of different aging heat treatment durations on hardness values showed that 24 hours aging at 120 °C gives maximum hardness value. And hardness increased with increasing amount of the reinforcement particles [39].

Ubeyli et al. investigated the ballistic performance of B_4C reinforced AA7075 based FGMs. They were produced FGMs with hot pressing. Two group of FGMs were produced with respect to amount of reinforcement particles in middle and top layers. In both FGM AA7075 was used without any reinforcement as backing layer. In the first FGM 10 wt.% and 20 wt.% B_4C was used in middle and top layers, respectively. In the second FGM 20 wt.% and 40 wt. % B_4C was used in middle and top layers, respectively. They measured hardness values of different layers for different aging hours (in heat treatment). They also did ballistic test using 7.62 mm AP. And they

reported that ballistic tests of the produced samples were failed. And they concluded that more than 25 mm thickness of this armor material is needed or harder material with increasing ceramic content in the structure is needed to have better ballistic protection against given projectile [40].

In a study conducted by Kalkanlı et al. alumina, silicon carbide and boron carbide ceramic materials were used to produce ceramic preforms which they were then infiltrated with AA7075 alloy. They used both pressure and pressureless melt infiltration processes to produce melt infiltrated preforms. They achieved 85% ceramic phase containing composites. They also studied effect of solutionizing temperature on hardness of AA7075 materials and maximum hardness values were obtained from 475 °C solutionizing temperature with 120 °C, 24 hours aging temperature and time, respectively. They achieced the maximum average hardness value from melt infiltrated alumina preforms that were sintered at 1450 °C as 550 HB [41].

Demir et al. investigated the ballistic performance of some aluminum alloys: AA 7075, AA 5083 and AISI 4140 steel against 7.62 mm AP projectile. And they did some heat treatments to AA7075 and AISI 4140 to see the effect of hardness and strength on their ballistic performance. The best ballistic performance obtained from AA7075-T651 with areal density of > 85 kg/m^2. They also reported that 25 % reduction in the weight of armor is provided with AA7075-T651 compared to RHA of 380 HB [42].

2.3.2. Aim / Motivation of the Study

Defense industry needs advanced materials solutions for better ballistic protection against various threats and expectations from armor materials are: having a multihit capacity, having a low weight to keep the overall mass minimum, high penetration resistance to different threats and being relatively cost effective.

This study aims to develop aluminum matrix composite materials ballistic layers for functionally graded materials using squeeze casting for vehicle protection.

As it can be seen in the literature review, alumina, boron carbide and silicon carbide were used in the production of ballistic protective ceramic and metal matrix composite (MMC) material armors. In this study, olivine, a naturally occurring silicate mineral, will be used first time in the literature to produce MMCs. Olivine is widely used in casting mold. It has high deposit in the earth crust and its production does not necessitate advanced engineering processes and equipment like used in the production of advanced engineering ceramics. It has relatively high hardness (6.5-7 mohs') and very cheap material more than 10 times cheaper than alumina ceramics. All these properties of olivine makes it an interesting raw material to be used in ballistic armor studies.

Most of literature studies use powder metallurgy processes to produce high ceramic content MMCs. However, in this study, melt infiltration process will be used in infiltration process of ceramic preforms to produce high ceramic content MMCs.

AA7075 aluminum alloy has been used by many researchers to produce high strength components. Thus, it is aimed to have superior mechanical properties with using AA7075 as a matrix material in composite production.

CHAPTER 3

EXPERIMENTAL PROCEDURE

In this chapter, experimental procedures used during this study were showed and explained with details. During experiments, various methods were used in order to comprehensively understand and characterize the properties of materials. Raw materials of ceramics (olivine and alumina) and matrix alloy (AA7075 aluminum alloy) which were used in the experiments are explained. Production technique of ceramic materials and metal matrix composite materials are given. Also, characterization methods and equipments used in experiments are given in this chapter. Figure 3.1. shows steps of experimental procedures which were employed in this study. Experiments, testing and characterization of composites were done mainly at 3 different facilities. While ceramic pellet preparation (mixing, drying, and pressing), composite sample preparation (metallography), optical microscopy, scanning electron microscopy examinations, density measurements and studies were done at Materials Development Laboratory, ASELSAN Inc., preform production (mixing, drying, pressing, sintering) and sintering of pellets, melting and melt infiltration by squeeze casting of composites, composite backing production from aluminum matrix composite material, heat treatments were done at Foundry, Metal, Processing and Automotive Materials Laboratory METU, X-Ray Diffractions were done at X-Ray Diffraction Laboratory-METU and UNAM-Bilkent, mechanical testing of samples were done at Mechanical Testing Laboratory - METU, and radiographic examinations were done at Welding Technology and Non-Destructive Testing Center) at Metallurgical and Materials Engineering, METU.

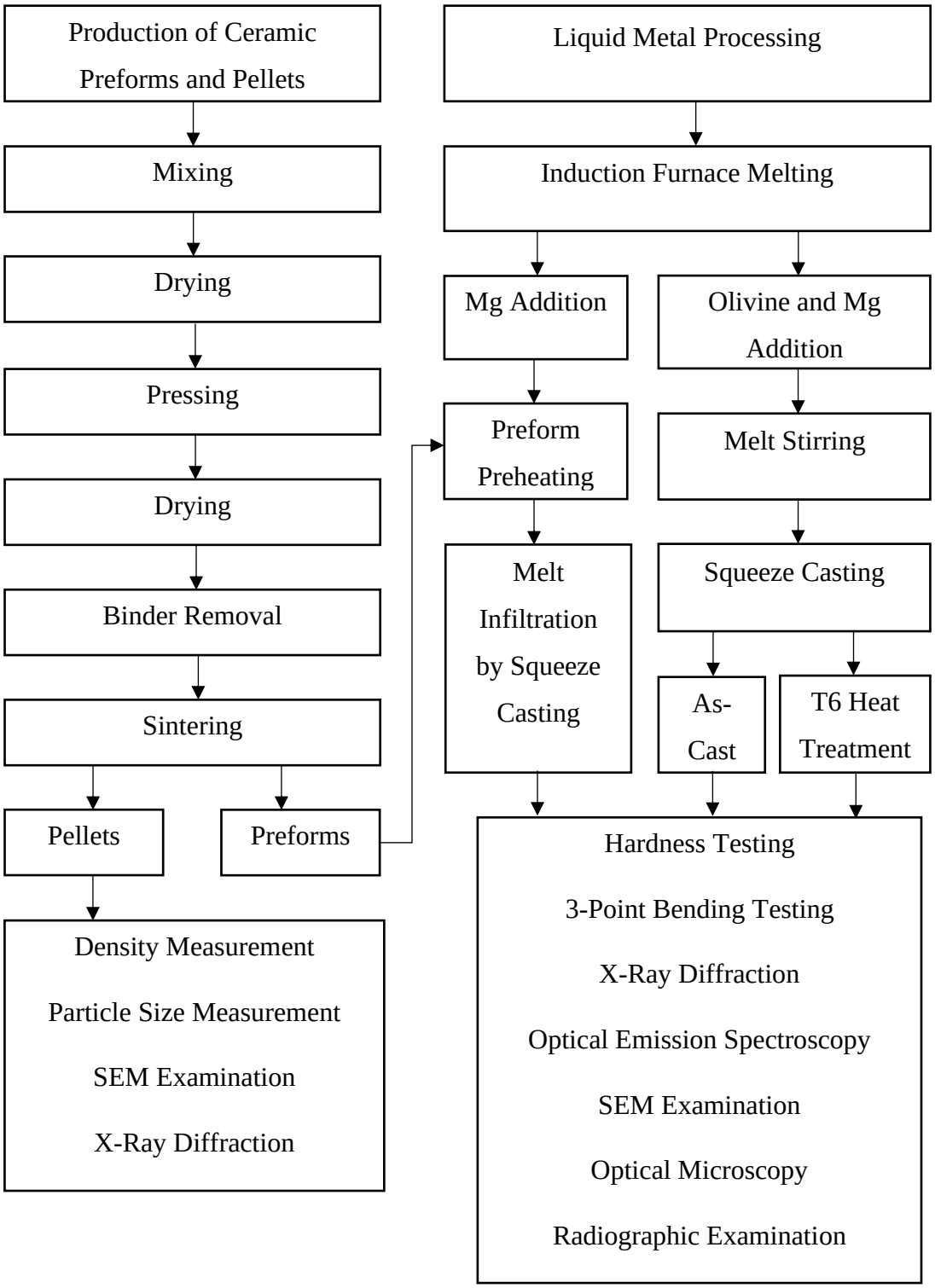

Figure 3.1. Experimental Methodology

3.1. Materials

In this study, as it can be seen in Figure 3.1. two main processing routes were employed. Olivine and alumina were used for ceramic pellet production and for ceramic preform production. Olivine was also used in the reinforcement of metal matrix composite material. High strength aluminum alloy AA7075 was used as matrix alloy for metal matrix composite (MMC's) developed in this work.

3.1.1. Olivine and Alumina

In the experiments olivine and alumina materials were used for pellet production and for reinforcement phase of MMC's studied. Figure 3.2. shows olivine and alumina samples which were used in the experiments.

Figure 3.2. Fine olivine (left), coarse olivine (middle) and alumina (right)

Olivine was procured from Eryas Olivine Mining Corporation. Two different average particle size olivine was taken. It was aimed to have bimodal size in pellet and preform mixtures. These particles were called as coarse and fine. In the experiments, effect of particle size on sintering process and porosity gradient were investigated. In Figure 3.2. coarse and fine olivine materials can be seen. Their average particle size was

measured using Malvern-Mastersizer 2000 device. Coarse olivine has an average particle size of 437 μm and fine olivine has an average particle size of 16 μm. Some of its physical and chemical properties are given in Table 3.1. and Table 3.2., respectively.

Table 3.1. Properties of olivine sample

Property	**Value**
Appearance	Grayish-green Particles
Grain Shape	Angular
Melting Temperature	1750 °C
Specific Gravity	3.2 g/cm^3
Bulk Density	1.9 g/cm^3
Solubility in Water	Negligible
pH	8-8.5
Hardness (Mohs)	6.5-7
Moisture	Less than 0.1%

Table 3.2. Chemical composition of olivine

MgO	SiO_2	Fe_2O_3	Al_2O_3	Na_2O	Cr_2O_3	NiO
46-49	41-43	7-9.5	>0.35	>0.05	>0.29	>0.2

Alumina was provided from Eti Alüminyum Inc. Macro scale image of alumina can be seen in Figure 3.2. Its mean particle size is 60 μm. It has more than 80.4% alpha alumina having 99.68% purity. Chemical analysis of alumina which was used in experiments can be seen in Table 3.3.

Table 3.3. Chemical composition of alumina

Al_2O_3	Fe_2O_3	SiO_2	Na_2O	CaO	TiO_2	V_2O_5	ZnO	Ga_2O_3
99.68	0.007	0.011	0.21	0.005	0.0007	0.0007	0.0037	0.009

3.1.2. AA7075 Aluminum Alloy

High strength aluminum wrought alloy AA7075 was used as matrix material for composite production and as an infiltrate metal during infiltration process. AA7075 aluminum alloy materials were purchased from Rutaş Co. Ltd. (see in Figure 3.3.). Its superior specific properties make it very attractive matrix material for metal matrix composite production. It has alloying elements zinc, copper and magnesium. Magnesium has a positive effect in wetting of reinforcement materials. Table 3.4. shows a range of chemical composition of AA7075 aluminum alloy.

Table 3.4. Chemical composition of AA7075 aluminum alloy

Zn	Mg	Cu	Cr	Si	Ti	Fe	Al
5.1-6.1	2.1-2.9	1.2-2	0.18-0.28	0-0.4	0-0.2	0-0.5	Balance

Figure 3.3. AA7075 samples

3.2. Production of Ceramic Pellets and Preforms

As it was mentioned earlier, alumina and olivine materials were used in the production of pellets and preforms. In the production of ceramic specimens conventional ceramic processing route was used. Firstly, slurries were prepared. The slurries were composed of ceramic particles, an organic binder (PVA), a mixing media ethyl alcohol and glucose solution as a binder. The ingredients were mixed well until a homogenous mixture was obtained. After complete mixture was obtained, the slurries left to lose its water and alcohol content to have good mechanical properties just after pressure application. When compositions had low moisture content, they were pressed with hydraulic press. After pressing, green ceramic pellets and preforms were acquired. As a final step for production of ceramic pellets and preforms, sintering process was done. In the following titles, a detailed information of ceramic processing will be given.

3.2.1. Pellet Preparation

In pellet production, different composition of slurries was prepared. For olivine samples, two different size olivine particles were mixed with 1.5 wt. % PVA and 30 vol. % ethyl alcohol. Olivine mixture was prepared by 10 wt. % change in between coarse and fine particles. In addition to different particle size olivine mixtures, these mixtures were sintered at five different sintering temperature starting from 1200 °C to 1400 °C by 50 °C temperature change. A list of olivine bimodal particle size ratio and sintering temperatures can be seen in Table 3.5.

Table 3.5. Sintering temperature and bimodal particle size ratio

Sintering Temperature (°C)	Particle Size Distribution (Coarse % / Fine %)				
1200	100/0	90/10	80/20	70/30	60/40
1250	100/0	90/10	80/20	70/30	60/40
1300	100/0	90/10	80/20	70/30	60/40
1350	100/0	90/10	80/20	70/30	60/40
1400	100/0	90/10	80/20	70/30	60/40

In the production of alumina pellets, similar slurry preparation procedures were used. In alumina samples, a various amount of aluminum alloy powder was added to improve green strength. It was also aimed to decrease the sintering temperature of alumina pellets by adding metal powders in it. Powders were added 2, 4 and 6 wt. % of alumina particles. Like olivine samples, they were sintered at different temperatures. Table 3.6. shows mixtures and sintering temperatures of alumina samples.

Table 3.6. Sintering temperature and mixing

Sintering Temperature (°C)	wt. % Metal Powder			
1200	0	2	4	6
1250	0	2	4	6
1300	0	2	4	6
1350	0	2	4	6
1400	0	2	4	6

After slurries were prepared, they were dried in a drying oven. Nuve FN400 dying oven having a maximum working temperature 250 °C was used in drying processes.

When all ceramic mixtures were dried, they were prepared for pressing. Before making pressing process, dried ceramic particles were humidified with water and glucose (sugar) solution. 15 vol. % water-crystal sugar solution was added (100 ml distilled water + 21 grams crystal sugar). The aim of this addition was both to increase green ceramic strength after pressing and to humidify the powders prior to pressing.

In pressing process, a cylindrical die which has an inner diameter of 13 mm was used (see Figure 3.4. a.)). when die was filled with humidified ceramic particulates, 1500 kg load was applied using PIKE Technologies Crush IR 10 tons load capacity hand press. The equipment can be seen in Figure 3.4. b.)

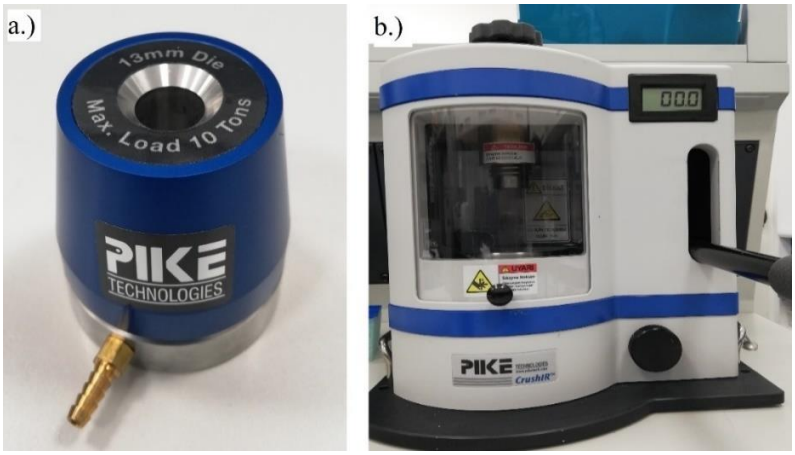

Figure 3.4. a.) Pressing mold used in pellet production, b.) hand press equipment

At the end of pressing, pellets were grouped and prepared for sintering process. Sintering process was done in two stages, these are binder removal step and sintering step. During in these steps temperature was kept constant. A heating rate 10 °C/min was selected. 600 °C was chosen for binder removal and sintering temperature was kept at 1200-1250-1300-1350 and 1400 °C for each of pellet groups and duration time at sintering temperature was selected as 75 minutes. Figure 3.5. shows a graph of different time and sintering temperature regimes that were used in the sintering processes.

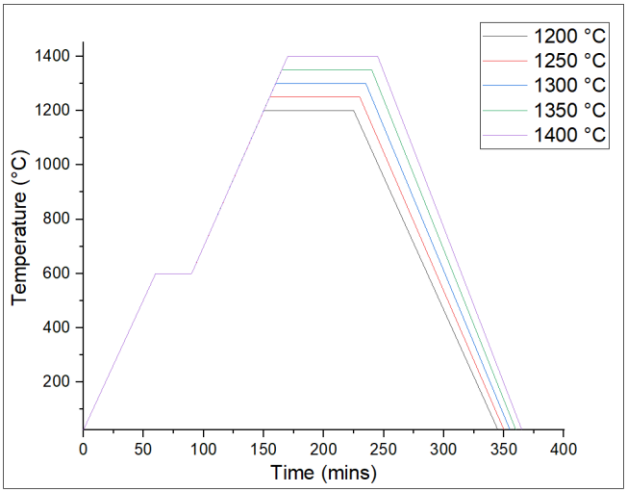

Figure 3.5. Time and temperature graph for different sintering temperatures

In sintering process, Protherm PLF 150/5 shuttle type kiln was used. The inner volume of the kiln is 5 liters and maximum continuous working temperature is 1450 °C. After sintering process, ceramic pellets were taken out of the kiln and they were prepared for density measurements and characterization. Sintered pellets can be seen in Figure 3.6. and 3.7.

Figure 3.6. Sintered olivine pellets

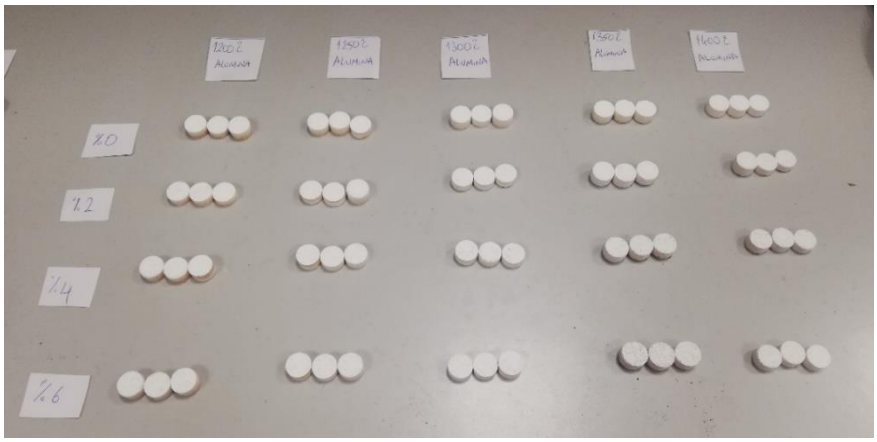

Figure 3.7. Sintered alumina pellets

3.2.2. Preform Preparation

Like pellet production, preforms were mixed with binders and mixing medium and they were dried, and glucose solution was added prior to pressing. Since preforms were used for metal infiltration and infiltrated preforms were characterized by three point bend testing, pressing was done in three-point bend sample mold of squeeze casting machine. three-D design of the representative mold can be seen in Figure 3.8. The mold was made from H-13 hot work tool steel and heat treated to have good mechanical properties and dimensional stability at high temperature operations.

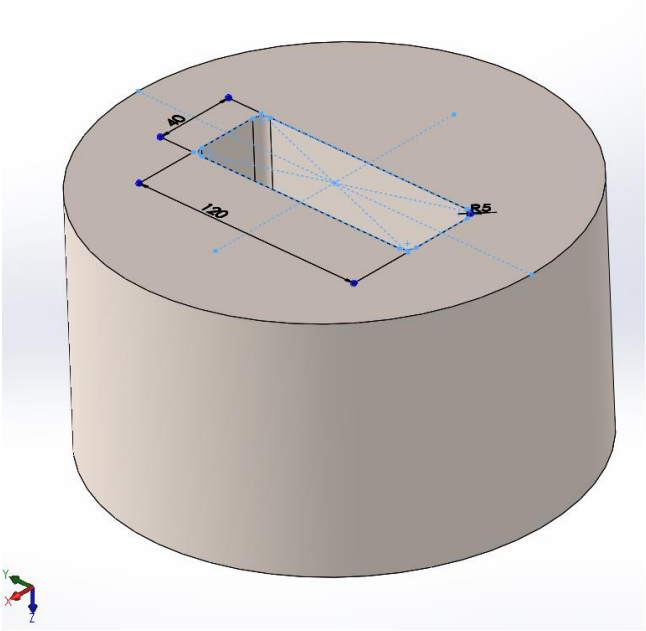

Figure 3.8. Metal die used in preform pressing

In alumina preforms 0.5 wt. % cu added zinc stearate and 0.5 wt. % aluminum alloy powder were added and they were mixed well until having a homogeneous mixture. The preforms were pressed and sintered at 1300 °C, 1350 °C, 1400 °C. In olivine samples 80/20 (coarse/fine) mixtures were sintered at 1250 °C, 1300 °C and 1350 °C and it was aimed to investigate sintering temperature on preform structures.

90/10, 80/20, 70/30, 60/40, 50/50 (coarse/fine) olivine mixtures were sintered at a constant temperature (1300 °C) to investigate the effect of particle size distribution on preform structures after sintering and infiltration. Figure 3.9. and Figure 3.10. shows sintered olivine and alumina preforms, respectively.

Figure 3.9. Sintered olivine preforms for pressure infiltration casting and three point bend testing

Figure 3.10. Sintered alumina preforms in resistance furnace

3.3. Induction Furnace Melting and Composite Preparation

AA 7075 aluminum alloys were melted in induction furnace at Foundry, Metal Processing and Automotive Materials laboratory, Metallurgical and Materials Engineering Department, METU. The induction furnace equipment was produced by Ajax Magnethermic Corp. (see Figure 3.11.). In this induction furnace, the heating by induction method occurs when an electrically conductive material is placed in varying magnetic field. It is a rapid form of heating in which current is induced directly into the part being heated. Resistance to electrical current flow of material causes heat and this heat leads to melting of the material. This technique is good for aluminum alloy and metal matrix composite production because the magnetic field formed in the system causes directional forces and it is desirable to circulate the alloy so that a homogenous mixture can be obtained.

Figure 3.11. Induction melting furnace used for alloy preparation and melting

AA7075 aluminum alloys were weighed and their chemical compositions were determined using optical emission spectrometer. In induction furnace, metals were melted and their temperature were measured using k-type nickel-chromium thermocouple with regular intervals during casting process.

In composite production, olivine was used as reinforcement material. 5-7.5-10 wt. % olivine was added. Olivine was dried at 105 °C to eliminate any moisture entrapping by liquid metal. In every different reinforcement amount, a new liquid metal was prepared. When liquid metal temperature reached to a level just over the liquidus temperature of the alloy (>635 °C), olivine particles were added in liquid metal and temperature of the liquid metal was decreased to a level of partial liquid and partial solid state which is so called semi solid state (a temperature range in between liquidus and solidus temperature). In this state, olivine was fed into matrix by melt stirring method. Figure 3.12. shows composite production using melt stirring process with graphite rods.

Figure 3.12. Melt stirring with graphite rods during alloy preparation

After olivine was added into liquid metal, magnesium as AZ91 (magnesium alloy which has aluminum and zinc as main alloying elements) alloy was added into liquid metal to increase wettability of olivine particles by liquid metal. The amount of total AZ91 addition was about 1.5 - 2 wt. % of total liquid metal weight. Magnesium was added in two stage. First addition was done 5 minutes later of olivine addition at 615 °C. An improvement in wettability was achieved after magnesium addition. Temperature of melt was risen above liquidus temperature of the melt. Throughout all the process the melt was continuously stirred mechanically with graphite rods. It was expected to further improvement in wettability by adding additional magnesium. So, the liquid metal temperature again decreased to 615°C and AZ91 was added. A good mixture was obtained after addition of more magnesium. The overall process took about 30 minutes to completely wet the olivine particles. When composite material was ready to cast, it was transferred to squeeze casting machine. The process is presented in the following title.

3.4. Squeeze Casting and Melt Infiltration

For experiments, vertical squeeze casting machine having 100 tons pressing capacity was used (Figure 3.13.).

Figure 3.13. Squeeze casting machine

Die assembly of the machine was specially designed for three-point flexural test samples. It was made of H-13 hot work tool steel. Figure 3.14.a and Figure 3.14.b. shows the 3D design of mold and punch assembly and three- point flexural test sample, respectively. The sample has 120 mm length, 40 mm width and approximately 10 mm thickness. The thickness of sample can be changed thanks to adjustable lower punch level in z direction.

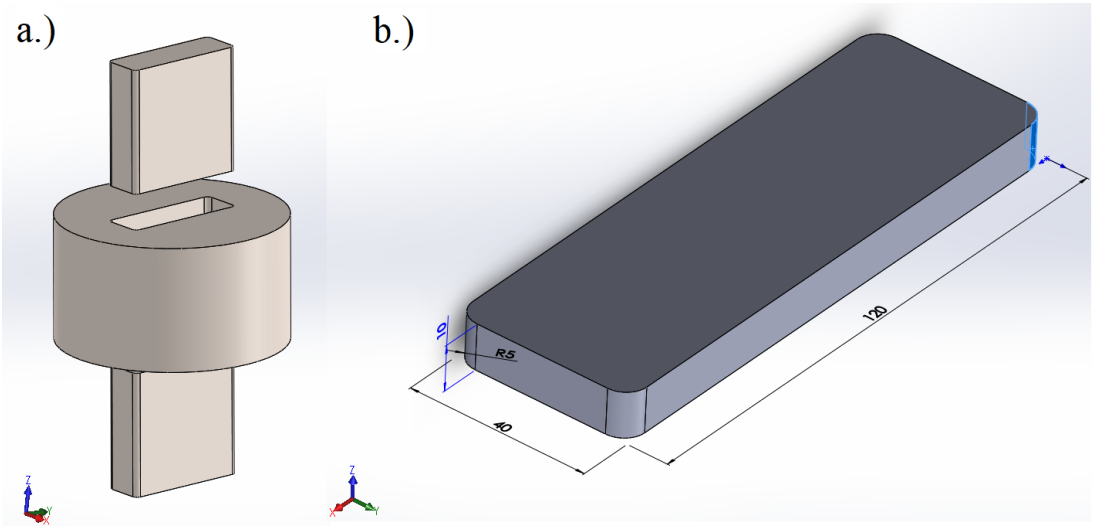

Figure 3.14. a.) 3D design of squeeze casting mold punch assembly b.) Three-point flexural sample

Aluminum matrix olivine reinforced composites were squeeze casted by a squeeze caster (Figure 3.13.). During melt infiltration, 50 tons pressure was applied onto preheated hot preform samples. A photo of composite samples can be seen in Figure 3.15. From each different reinforcement composites, 3 samples were taken for T6 heat treatment to investigate effect of heat treatment on hardness and flexural strength properties of samples.

Figure 3.15 Metal matrix composite samples after squeeze casting

Similarly, metal infiltration to preheated ceramic preforms which were pressed and sintered at various sintering temperatures, was done by squeeze casting. Process steps can be summarized as following:

1. AA7075 aluminum alloys were melted in induction furnace.
2. When the metal was melted, 1 wt. % magnesium (AZ91 alloy) was added to improve wettability at semi solid temperature range.
3. The liquid metal was stabilized at 700 °C.
4. Ceramic preforms were heated to 1000 °C in an electrical resistance muffle furnace and kept at this temperature for approximately 1 hour.
5. The mold was preheated to about 150 °C using gas torch and the mold temperature was measured using a optical pyrometer.
6. Ceramic preforms with alumina based thermal papers (thermal paper was used to prevent excessive temperature decrease) were placed in lower die half.
7. The liquid metal was poured and die punch squeezed until complete infiltration and solidification took place.
8. Finally, infiltrated parts were ejected, taken out of the die and cooled down.

In Figure 3.16. given below, melt infiltration processing steps are given one by one.

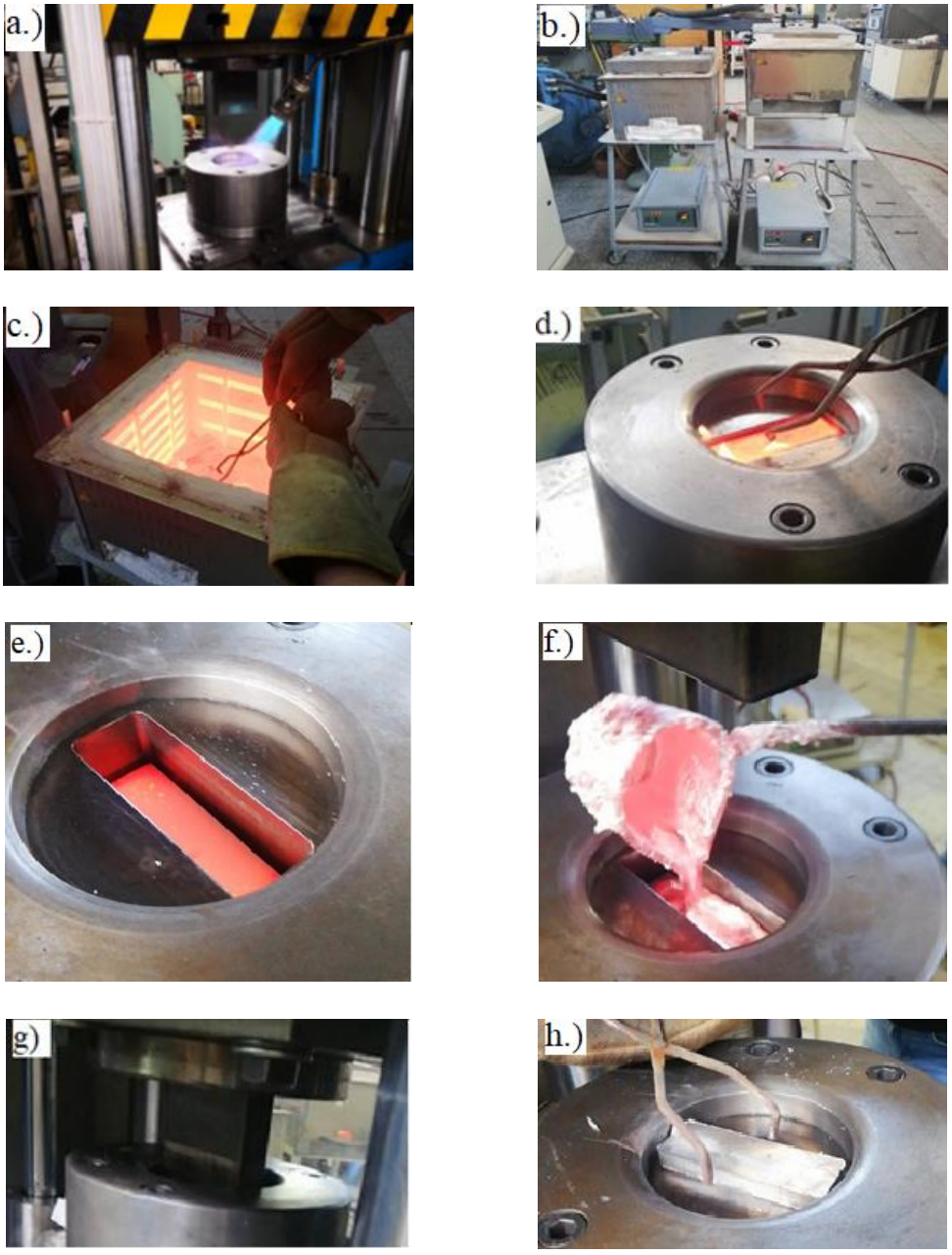

Figure 3.16. Steps in pressure melt infiltration technique a.) Mold preheating, b.) Preform preheating c.) 1000 °C preheated preforms in muffle furnace d.) Placement preheated preforms onto lower die of squeeze casting equipment, e.) Preheated preform in the lower die, f.) liquid AA7075 pouring onto preform, g.) squeezing by upper mold, h.) Ejection of infiltrated composite from die

Figure 3.17. Optical pyrometer used to read die temperature

Figure 3.18. Melt infiltrated samples after casting

After squeeze casting of olivine reinforced 5-7.5-10 wt.% composites and melt infiltrated preform composites were produced in accordance with given procedures, some of olivine reinforced composite materials were T6 heat treated to compare hardness and 3 point flexural strength properties of as cast and heat-treated conditions.

3.5. T6 Heat Treatment

T6 heat treatment was applied to some of olivine reinforced composite materials. Other samples were left in as cast condition. T6 heat treatment is a process of treating materials with different temperatures. The general process can be divided into three steps. These steps are solution heat treatment, quenching and artificial aging. Firstly, the composite materials were put into an electrical resistance muffle furnace,

previously used in the preform preheating (see Figure 3.20.a.) and heated to solutionizing temperature. After solutionizing, samples were quenched in water.

Figure 3.19. MMC samples in muffle furnace for solutionizing heat treatment

And they were taken to another furnace to do artificial aging treatment. In Figure 3.20. b. aging furnace can be seen.

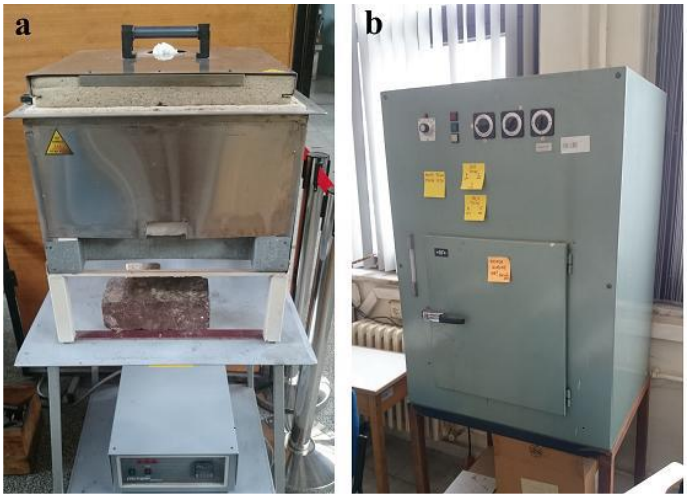

Figure 3.20. T6 heat treatment furnaces a.) Muffle b) Electrical resistance furnaces

Solutionizing and artificial aging temperatures and times were determined from ASM Metals Heat Treatments Handbook and Durmaz's master thesis studies. According to Durmaz's studies [3], maximum hardness values were obtained at 475 °C solutionizing temperature and 90 minutes duration and 120 °C artificial aging temperature and 24 hours duration. In this study, 65 minutes duration at 475 °C solutionizing temperature and 24 hours duration at 120 °C artificial aging temperature was determined according to ASM Metal Handbook [33] for the thickness of materials that were used in this study. Figure 3.21. shows solutionizing, quenching and artificial aging steps with relevant temperature and time scale.

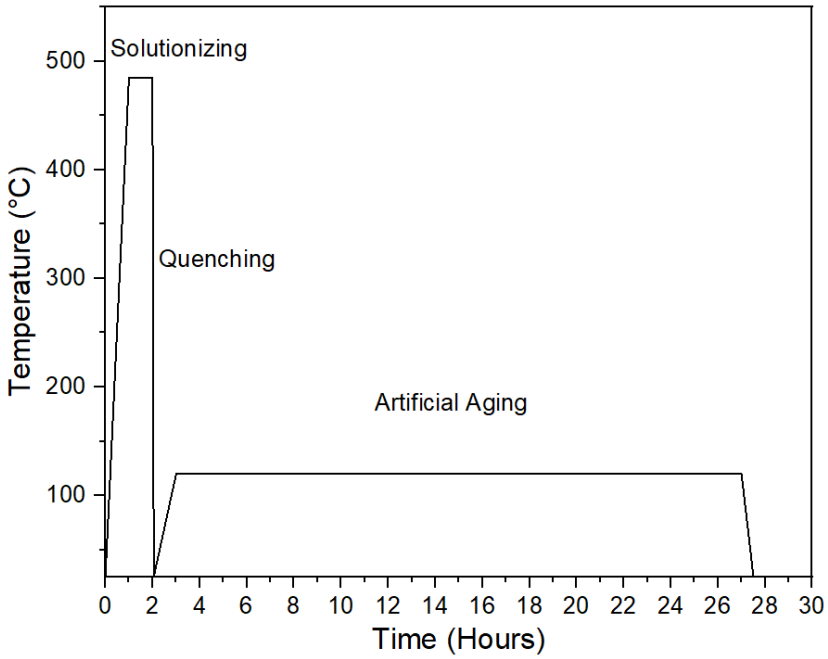

Figure 3.21. Time and temperature for solutionizing and aging

3.6. Mechanical Testing

After experiments, samples were mechanically tested to investigate their mechanical properties. Hardness testing and three-point bend test were done. It is aimed to observe hardness values since hardness is an essential performance merit in ballistic protection and three-point bend test is significant to examine material under ballistic impact conditions. Even though three-point bend test has a quasi-static loading mode while in ballistic impact, material's deformation mechanisms work dynamically, it is proposed that a better three-point flexure strength gives better ballistic protection under bullet impact.

3.6.1. 3-Point Flexure Testing

In flexure tests, squeeze casted AA7075 matrix olivine reinforced composites, olivine and alumina ceramic preform infiltrated AA7075 matrix composites were tested. For three-point bend testing, 2 different testing machines were used. These are Instron 5582 electromechanical testing machine that can apply 100 KN force and Mares hydraulic tensile testing machine that can apply 500 KN force were used with three-point bend testing apparatus.

In testing apparatus, 2 supporting pins and 1 loading pin were used. The distance in between 2 supporting pins were kept 100 mm (span length) Total length of samples were 120 mm and width of samples were 40 mm. 1 mm/min strain rate was applied during testing. Flexure strength and flexure strain were calculated using following formulas:

$$\sigma_{flex} = \frac{3PL}{2BT^2}$$

$$e = \frac{6ST}{L^2}$$

Where σ_{flex} and e are flexure strength and flexure strain, respectively. P, L, B, T, S are maximum load applied by the machine at fracture, span length, width, thickness and deflection, respectively.

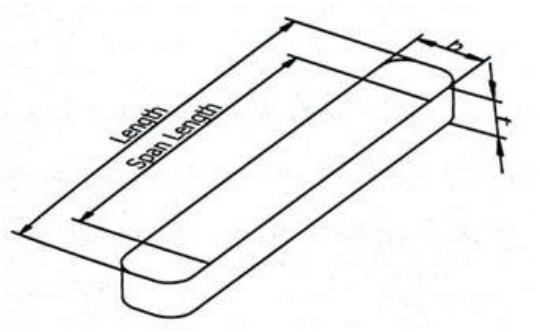

Figure 3.22. Three-point bending sample

3.6.2. Hardness Testing

Universal Emco M4U-025 hardness testing machine was used in hardness measurement tests. Hardness testing was done per ASTM E-10 -01 (Standard Test Method for Brinell Hardness of Metallic Materials) [34]. A tungsten carbide indenter ball having a ball diameter of 2.5 mm was used and 62.5 kgs load was applied for composite materials and 187.5 kgs load was applied for infiltrated preforms. For alumina preforms sintered at 1300 °C and 1350 °C, microhardness tester was used.

3.7. Characterization Techniques

Various characterization techniques were used in order to investigate the microstructure, chemical compositions, phases, and some physical properties like density and particle size. For this reason, optical emission spectroscopy was used to determine chemical composition of used AA7075 alloys. Metallography was done to prepare samples for optical and scanning electron microscope examinations. In optical

microscope size and distribution of reinforcement particles and microstructure were observed and with SEM characterization chemical composition was determined using Energy Dispersive Spectrometry (EDS) detector and matrix-reinforcement interface morphology was investigated. X-Ray Diffraction analysis was used to determine phases in materials and radiographic examination was used to see distribution of reinforcement particles in composite samples. Density measurements of pellets were done to investigate the effect of sintering temperature and initial ceramic ingredients on sintering behavior and porosity of the structure. All these techniques, samples and used equipment will be presented in this section.

3.7.1. Optical Emission Spectrometer Analysis

Optical emission spectrometer equipment is useful for chemical composition determination of metallic materials. In an argon protective atmosphere, electrical energy is applied onto sample through an electrode. This energy causes vaporization of atoms on the sample surface. These vaporized atoms become in an energy state called “discharge plasma”, Each element has a unique spectral emission, this spectral energy emitted from sample surface is detected by detectors and their type and amount is calculated by wt. % [29].

WAS Foundry Master optical emission spectrometer was used to determine the chemical composition of AA7075 samples. The measurements were taken before and after casting and chemical composition of used alloys were determined.

3.7.2. Metallography

Olivine reinforced AA7075 matrix composite materials and AA7075 infiltrated olivine – alumina preforms were prepared for optical and scanning electron microscopy examinations. Samples were taken after three-point bend test and their fracture surfaces and one flat surface were cut using Metkon Metacut 251 Abrasive Cutter.

After cutting operation completed, metal infiltrated samples were grinded using grinding papers with different numbers starting from 320 to 1200 (320 – 600 - 800 - 1200). For olivine reinforced AA7075 composites after cutting with Metkon Metacut 251 Abrasive Cutter, Leica EM TXP sample preparation device was used to grind and to polish the samples. In metallographic preparation of ceramic and composite materials, it is not possible to apply etching process because these materials have some different properties. So, they were examined after grinding and polishing steps without any etching operation.

3.7.3. Optical Microscopy

Olivine reinforced composite materials were characterized under optical microscopy examination. Nikon Eclipse MA200 which is an inverted materials microscope was used in optical microscopy observations. 100X magnifications was used to see details in microstructure. It was aimed to find out the distribution of reinforcement material in metal matrix. Both, heat treated and as-cast specimens were examined. Moreover, ImageJ image analyzer software was used to calculate vol.% of ceramic particles in melt infiltrated preform composite materials.

3.7.4. Scanning Electron Microscopy

Scanning electron microscopy was used to get more detailed images from samples. SEM analyses was done in all samples. AA7075 samples were analyzed with SEM both in as-cast and T6 heat treated conditions in order to see microstructural change, phases in aluminum matrix and chemical composition observations. Olivine, alumina and Aluminum alloy particles were examined using SEM to examine their particle size and shape and their elemental composition. Olivine reinforced AA7075 matrix composite materials were investigated both as-cast and T6 heat treated conditions to see phases, chemical composition and reinforcement distribution in alloy matrix. Ceramic pellets were examined to see microstructural change as a result of applying different sintering temperature (for olivine and alumina), using different particle size (for olivine) and using different additive amount (for alumina). And finally, metal

infiltrated ceramic preforms were examined to observe interface in between ceramic preform and metal matrix, wettability and infiltration performance.

Prior to SEM analysis of ceramic particles and ceramic pellets were coated with carbon to have a conductive surface and thus to eliminate possibility of surface charging. For this purpose, Safematic - CCU010 Carbon Coating Unit was used. Samples were coated with carbon to about 10 nm.

In SEM observations Phenom XL SEM equipment was used. All images were taken with Back Scattered Electron (BSE) detector. Energy Dispersive X-Ray Spectroscopy (EDS) was used in elemental analysis studies. Images were taken with various magnifications (500, 1000, 2000, 4000x).

3.7.5. Radiographic Examination

Radiographic examination is a non-destructive testing method which is widely used in welding and casting industry. It is a very useful technique to observe any discontinuity inside the material. Any discontinuity or irregularity within the material like segregation, inclusions and porosities can be seen with the help of this technique.

In this study, it was aimed to observe olivine particle distribution inside the matrix AA7075 alloy. Since it is possible to observe the material completely, a general information about distribution of particles would be acquired. GE – MF 42 -200 KeV X-Ray tube was used. 60 KV with 3mA current was applied for 45 seconds exposure time.

3.7.6. X-Ray Diffraction

X-Ray Diffraction analysis of olivine reinforced composite materials, olivine and alumina particles, and ceramic pellets were done to investigate phases in the materials. D8 Advance Bruker having a 40 KV and 40 mA capacity equipment was used in the experiments. Cu-K_α radiation was used for diffraction. XRD of Composite materials and alumina pellets were taken in the range of 20-100° and at a speed of 2°/min. For olivine the range was kept in between 10-80° and the scanning speed was 4°/min.

3.8. Density Measurement

Density is a critical physical property of materials. Since it was aimed to infiltrate ceramic pellets, open porosity is an essential parameter for this study. Ceramic pellets were sintered at various temperature and various composition (alumina ceramics). Thus, determination of density of these samples will give information about their physical properties. Mass of samples were determined using a precision balance with four decimal digits.

After sintering process took place, Archimedes' technique was used to determine the density of sintered pellets. three different weight measurements were done. First of all, dry weight of the pellets was calculated. And then, suspended weight was calculated. Suspended weight was measured of pellets by immersing the pellet in distilled water and the value is read just after the immersion. Finally, saturated weight was calculated. Pellets were immersed in water and put into vacuum vessel at -0.8 bar. All open porosities in samples were filled with distilled water thanks to applied vacuum. The vacuum process took 2 hours. After vacuum application, surfaces of samples were wiped with a wet cloth and their weight was measured immediately. Weight measurements and Archimedes' technique was done with Precisa model XB 220A equipment (See in Figure 3.24.) and vacuum was applied with the equipment given in Figure 3.23. Bulk density of pellets were calculated using given formula: [36]

$$d_{bulk} = \frac{Wdry}{W_{Sat} - W_{Susp}} \sum d_{liquid}$$

Where, d_{bulk} is the bulk density of sample, d_{liquid} is the density of saturating/suspending liquid, W_{dry} is the dry weight, W_{susp} is the suspended weight and W_{sat} is the saturated weight.

After the bulk densities of samples were calculated, relative density of ceramics were calculated using the given formula below: [36]

$$Relative\ to\ theoretical\ density = \frac{d_{bulk}}{d_{theoretical}}$$

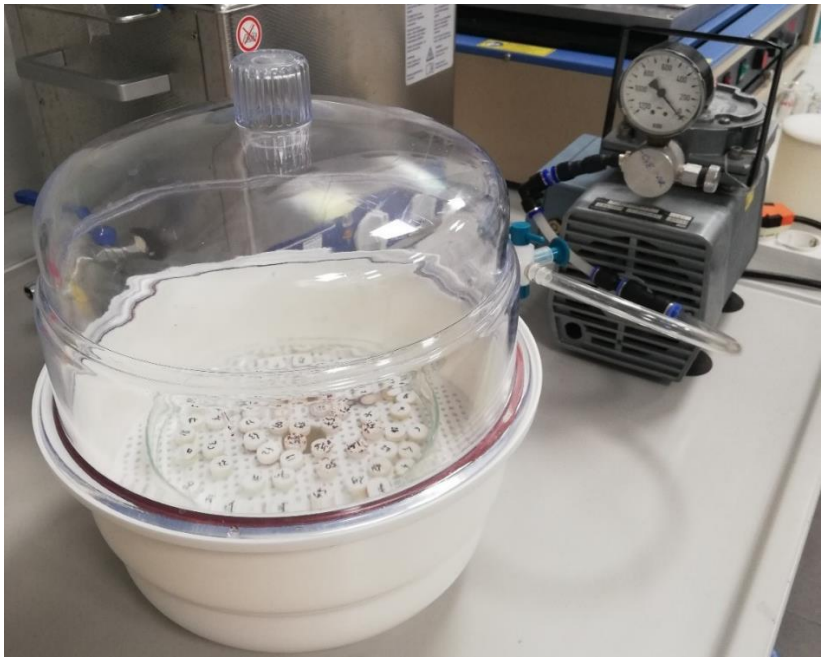

Figure 3.23 Vacuum chamber set-up

Figure 3.24. Archimedes density measurement

CHAPTER 4

RESULTS AND DISCUSSION

In this chapter, results of characterization and tests that were obtained from samples during this study are given. Results are divided into three groups with respect to materials. Firstly, results of ceramic pellet production are given. Secondly, results of metal matrix composite production are showed and finally results of melt infiltration process are presented.

4.1. Ceramic Pellet Production

In ceramic pellet production, olivine and alumina were used for pellet preparation. It is a well-known fact that initial material structure and properties directly affect the final product properties. Thus, particles were characterized physically and microstructurally. In following titles, Particle size measurement of ceramic powders, density measurement, SEM examination and XRD results of ceramic pellets are given.

4.1.1. Particle Size Measurement

Particle size measurement of olivine (coarse and fine) and alumina were done with Malvern 2000 Master-sizer equipment. The mean particle size (d_{50}) of alumina, coarse olivine and fine olivine was found to be 59 μm, 437 μm and 16 μm, respectively. Figure 4.1. shows particle size distributions of alumina and olivine samples.

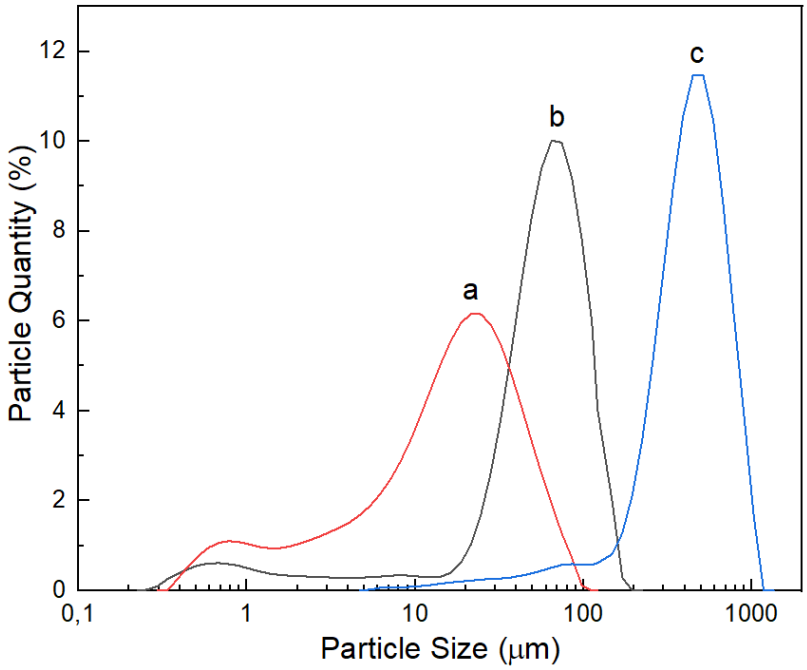

Figure 4.1. Particle size distribution of a.) fine olivine, b.) alumina and c.) coarse olivine

4.1.2. SEM Examination

SEM examination was done for initial ceramic particles of alumina and olivine (coarse and fine olivine) as received and ceramic pellet samples after sintering process. It was aimed to see particle shape and size with SEM examination for particle materials and EDS analysis was done to determine chemical composition of initial powders. Ceramic particles and pellets were coated with carbon to prevent occurrence of electrostatic charge on sample surface. In alumina particle sample only aluminum and oxygen were determined clearly which match up with supplier's analysis certificate. In olivine particle sample magnesium, oxygen, iron, silicon was observed with EDS analysis. Carbon peaks coming from coated surface was eliminated in EDS graphs. SEM images and EDS analysis results can be seen in figures given below. It can be clearly seen from SEM images that alumina particles have relatively spherical and olivine particles have angular shape.

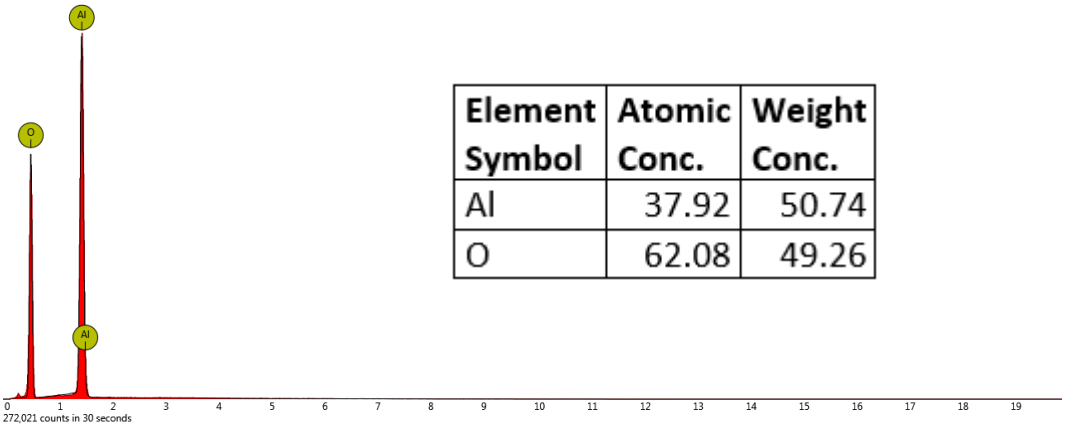

Element Symbol	Atomic Conc.	Weight Conc.
Al	37.92	50.74
O	62.08	49.26

Figure 4.2. EDS graph of alumina sample

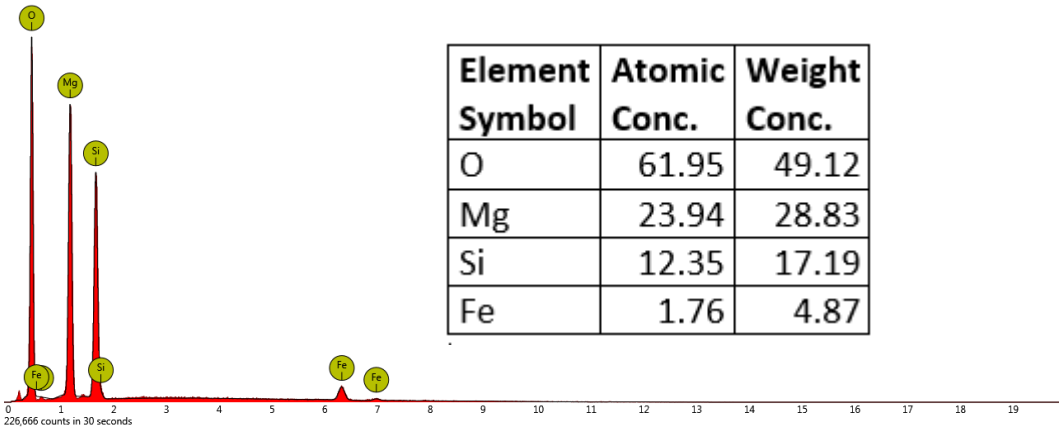

Element Symbol	Atomic Conc.	Weight Conc.
O	61.95	49.12
Mg	23.94	28.83
Si	12.35	17.19
Fe	1.76	4.87

Figure 4.3. EDS graph of coarse olivine sample

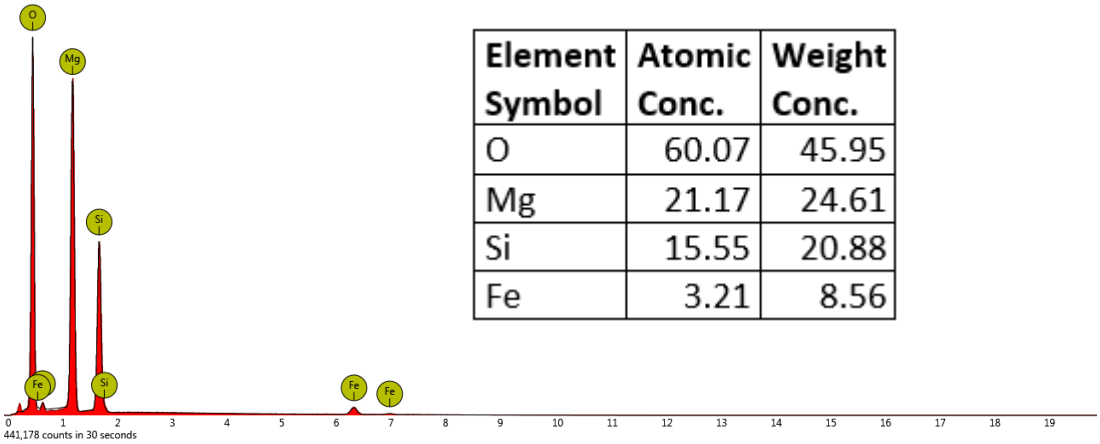

Element Symbol	Atomic Conc.	Weight Conc.
O	60.07	45.95
Mg	21.17	24.61
Si	15.55	20.88
Fe	3.21	8.56

Figure 4.4. EDS graph of fine olivine sample

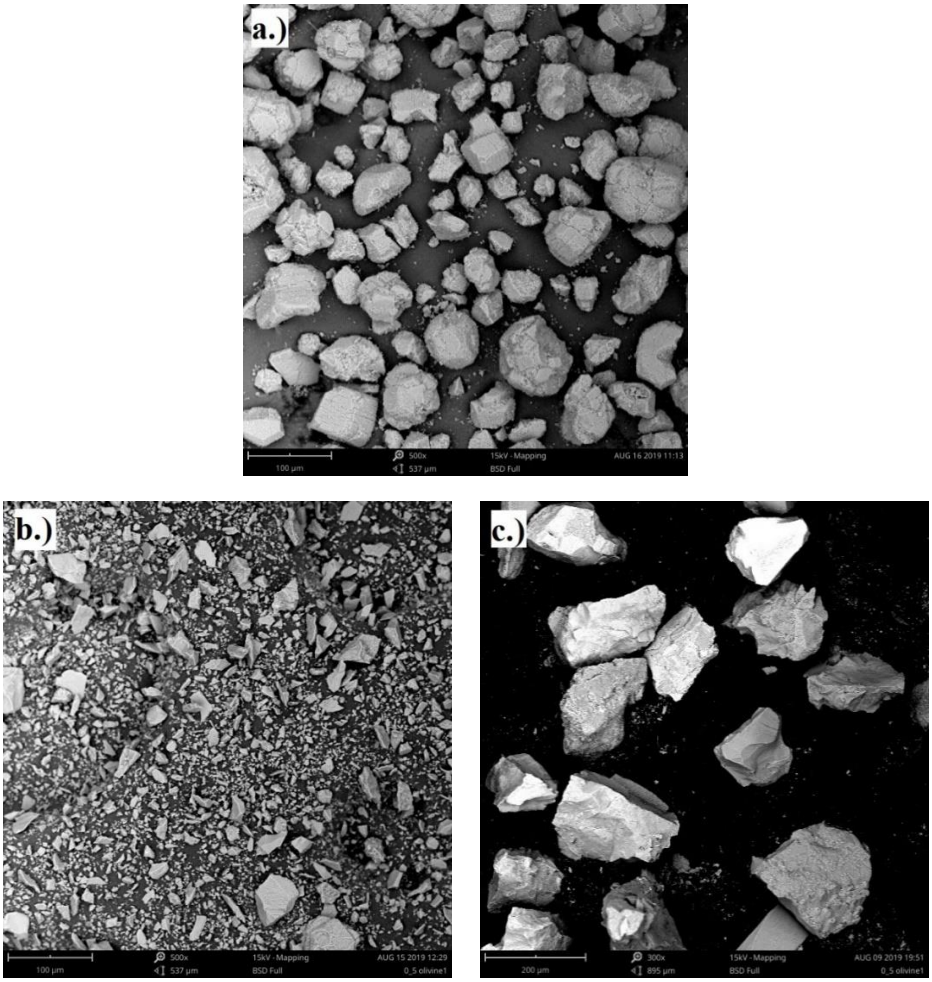

Figure 4.5. SEM images of ceramic particles a.) alumina, b.) fine olivine, c.) coarse olivine

SEM imaging was also done for alumina pellets which were sintered at 1200-1250-1300-1350 and 1400 °C (see figure 4.6.). SEM images showed that there is no shrinkage or sintering sign until 1400 °C. From this point of view, sintering temperature should be higher than 1350 °C and sintering time should be longer than 75 minutes.

Since this study aimed to infiltrate porous ceramics with liquid metal to produce high ceramic content metal matrix composite materials, a controlled porous microstructure is convenient to meet the given purpose.

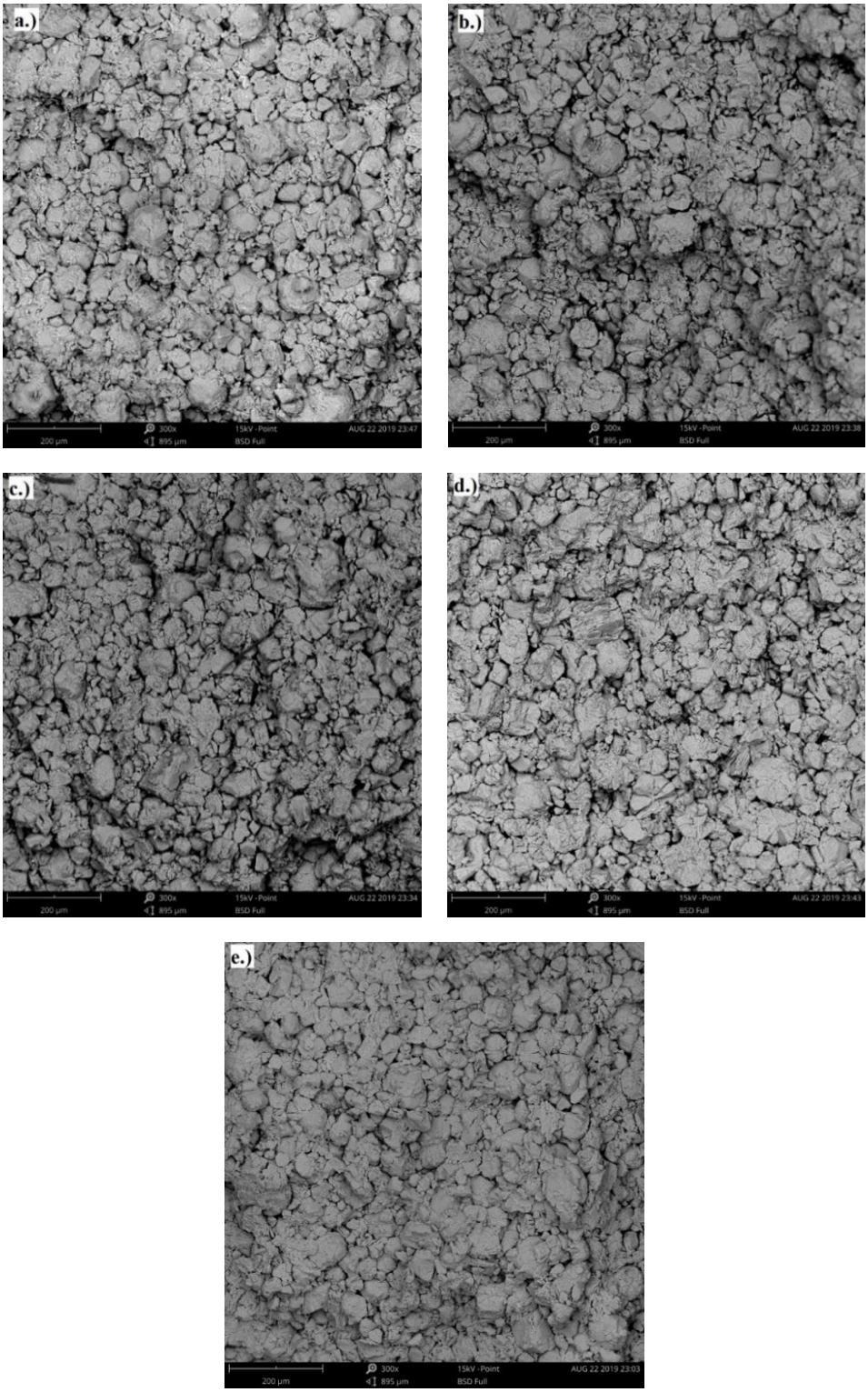

Figure 4.6. SEM images of alumina pellets sintered at a.) 1200 °C, b.) 1250 °C, c.) 1300 °C, d.) 1350 °C, e.) 1400 °C

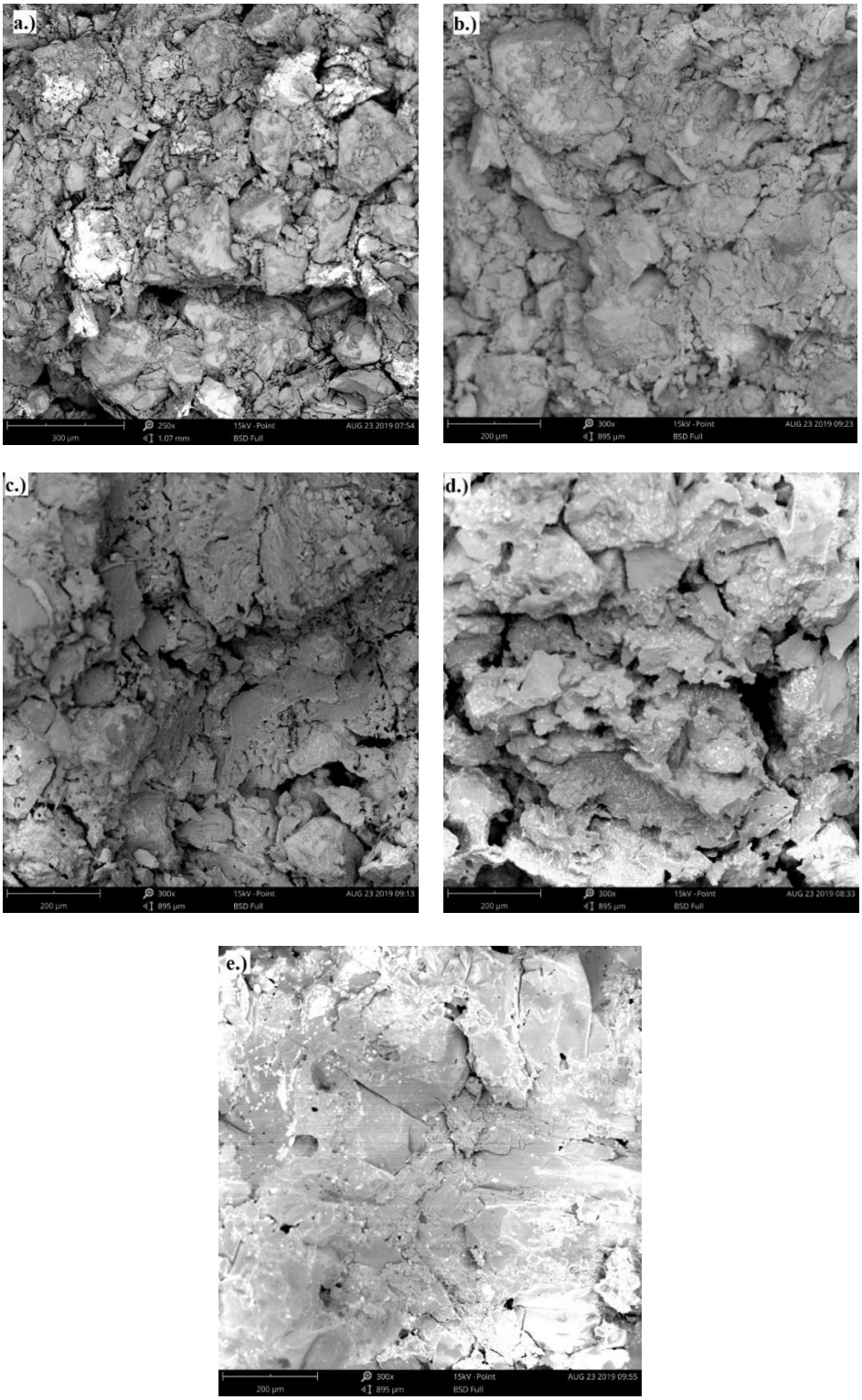

Figure 4.7. SEM images of 80/20 olivine samples

sintered at a.) 1200 °C, b.) 1250 °C, c.) 1300 °C, d.) 1350 °C, e.) 1400 °C

SEM imaging of olivine pellets composed of 80/20 (coarse / fine) bimodal particle size and sintered at 1200-1250-1300-1350-1400 °C was also done (see Figure 4.7.). As it can be seen clearly in Figure 4.7. sintering of pellets started at 1300 °C. At 1400 °C particles get much closer to each other.

4.1.3. Density Measurement

Density measurement of ceramic pellets were done to examine the density change with sintering temperature, different amount of metal addition (for alumina pellets) and having different particle size (for olivine pellets) in the structure.

Relative to theoretical density (3.97 g/cm^3 for α-Al_2O_3) density measurement results for alumina pellets can be seen in Table 4.1. From given table, it can be observed that there is no clear change in density up to sintering temperature 1400 °C. Metal addition to ceramic particles decreased the pellet density due to forming internal and external cracks in the ceramic pellets. These cracks can be clearly seen even with naked eyes (See Figure 4.8.). The reason for crack formation in ceramic pellets can be explained with having different thermal expansion of metal phase and ceramic phase. During heating and cooling, expansion and contraction of aluminum powder will cause pressure on the ceramic and this results in crack formation. Another reason for this occurrence can be explained with heating rate (10 °C/min) as a process parameter. Slower heating rate should be chosen to prevent crack formation in the ceramic structure.

Figure 4.8. Crack formation in ceramic pellets having high metal additive content

Table 4.1. Relative density values for alumina pellets sintered at various temperatures

	1200 °C				**1250 °C**			
	0 wt. %	**2 wt. %**	**4 wt. %**	**6 wt. %**	**0 wt. %**	**2 wt. %**	**4 wt. %**	**6 wt. %**
1	39.343	39.892	39.949	39.848	39.405	39.525	40.190	41.579
2	39.746	40.005	39.513	43.933	38.920	38.685	40.480	42.928
3	39.917	39.925	39.746	40.442	42.934	38.519	43.330	35.237
Avg.	**39.668**	**39.941**	**39.736**	**41.408**	**40.420**	**38.910**	**41.334**	**39.915**
	1300 °C				**1350 °C**			
	0 wt. %	**2 wt. %**	**4 wt. %**	**6 wt. %**	**0 wt. %**	**2 wt. %**	**4 wt. %**	**6 wt. %**
1	40.556	38.067	40.442	39.846	40.527	39.960	39.206	35.373
2	40.502	40.431	37.704	40.867	40.160	40.405	38.455	38.273
3	39.562	40.445	37.770	41.836	41.113	40.432	39.774	44.133
Avg.	**40.207**	**39.648**	**38.639**	**40.849**	**40.600**	**40.266**	**39.145**	**39.260**
			1400 °C					
			0 wt. %	**2 wt. %**	**4 wt. %**	**6 wt. %**		
1			46.243	41.984	40.038	39.247		
2			60.243	41.230	40.200	41.603		
3			51.116	42.831	40.464	38.262		
Avg.			**52.534**	**42.015**	**40.234**	**39.704**		

When Figure 4.9. is examined, the maximum relative density was obtained from alumina pellets sintered at 1400 °C with no metal addition. For pellets with 0 wt. % and 2 wt. % metal addition, almost linearly increase in relative density was observed while for 4 wt. % and 6 wt.% metal added ceramic pellets, there is not a linear behavior in relative density. And, scattering in relative density is higher in 6 wt. % ceramic pellet which originate in formation of cracks.

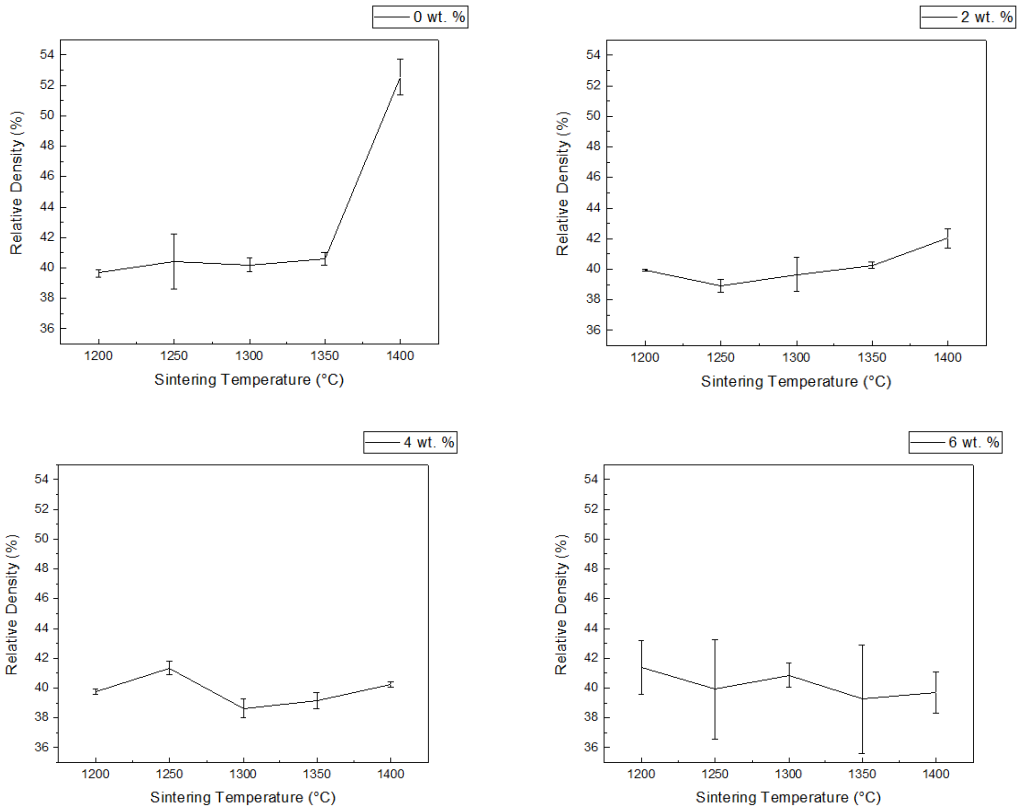

Figure 4.9. Relative density graphs for alumina pellets sintered at different temperatures with different amount of metal addition

Relative to theoretical density (3.2 g/cm^3 for olivine) measurements of olivine pellets were also done. As it was mentioned before, olivine pellet samples were produced with bimodal particle size ranging from 100/0 (100% coarse and 0% fine) to 60/40 (60% coarse and 40% fine). With density measurement, effect of sintering temperature and particle size distribution on the density of ceramic pellets was observed. Table 4.2. shows measured densities of pellets with their average values.

Table 4.2. Relative density values for olivine pellets sintered at various temperatures

	1200 °C					1250 °C				
	100/0	**90/10**	**80/20**	**70/30**	**60/40**	**100/0**	**90/10**	**80/20**	**70/30**	**60/40**
1	69.53	70.11	67.79	71.66	70.45	68.74	69.09	71.20	69.89	70.95
2	69.76	69.59	68.72	69.23	69.29	67.87	68.96	70.36	71.23	70.91
3	69.41	68.91	71.94	71.02	71.47	68.90	69.39	70.18	72.09	72.39
4	69.77	69.07	69.59	68.76	70.39	68.37	71.95	72.66	72.67	69.38
Avg.	**69.62**	**69.42**	**69.51**	**70.17**	**70.40**	**68.47**	**69.85**	**71.10**	**71.47**	**70.91**
	1300 °C					**1350 °C**				
	100/0	**90/10**	**80/20**	**70/30**	**60/40**	**100/0**	**90/10**	**80/20**	**70/30**	**60/40**
1	68.27	70.16	69.79	73.99	71.73	72.67	71.99	73.23	75.25	74.27
2	67.78	70.32	69.93	70.98	73.00	70.53	71.69	73.39	73.67	75.34
3	68.83	69.00	67.95	70.70	72.89	70.27	71.44	71.83	74.75	75.27
4	68.28	70.12	77.18	72.78	71.54	72.84	71.56	72.70	73.07	75.16
Avg.	**68.29**	**69.90**	**71.21**	**72.11**	**72.29**	**71.58**	**71.67**	**72.79**	**74.17**	**75.01**
				1400 °C						
				100/0	**90/10**	**80/20**	**70/30**	**60/40**		
			1	79.18	82.15	82.32	82.86	88.79		
			2	80.31	81.03	81.23	83.52	86.46		
			3	82.33	80.92	82.87	83.25	86.26		
			Avg.	**80.6**	**81.37**	**82.14**	**83.21**	**87.17**		

In Figure 4.12. graphs of relative densities of sintered olivine pellets with bimodal particle size were given. In graphs, there is an increase in relative density with increasing sintering temperature as expected since temperature is a driving force for sintering process. This increase in relative density is higher at temperatures above 1300 °C. Sintering behavior of olivine was expressed by Furlani et al [25,27]. According to them, hematite phase in olivine melts into liquid phase and its quantity increases with temperature and this results in densification by liquid phase sintering.

When the effect of particle size ratio is examined (see Figure 4.10.), it is seen that pellets have higher relative density with increasing finer particles amount. Since finer particles have more surface area to catalyze sintering reactions, sintering process can take place at lower temperature and in shorter time. Furthermore, finer particles can fill the gaps in between coarse particles so packed green density increases when bimodal size ceramic particles are used in ceramic pellets [28].

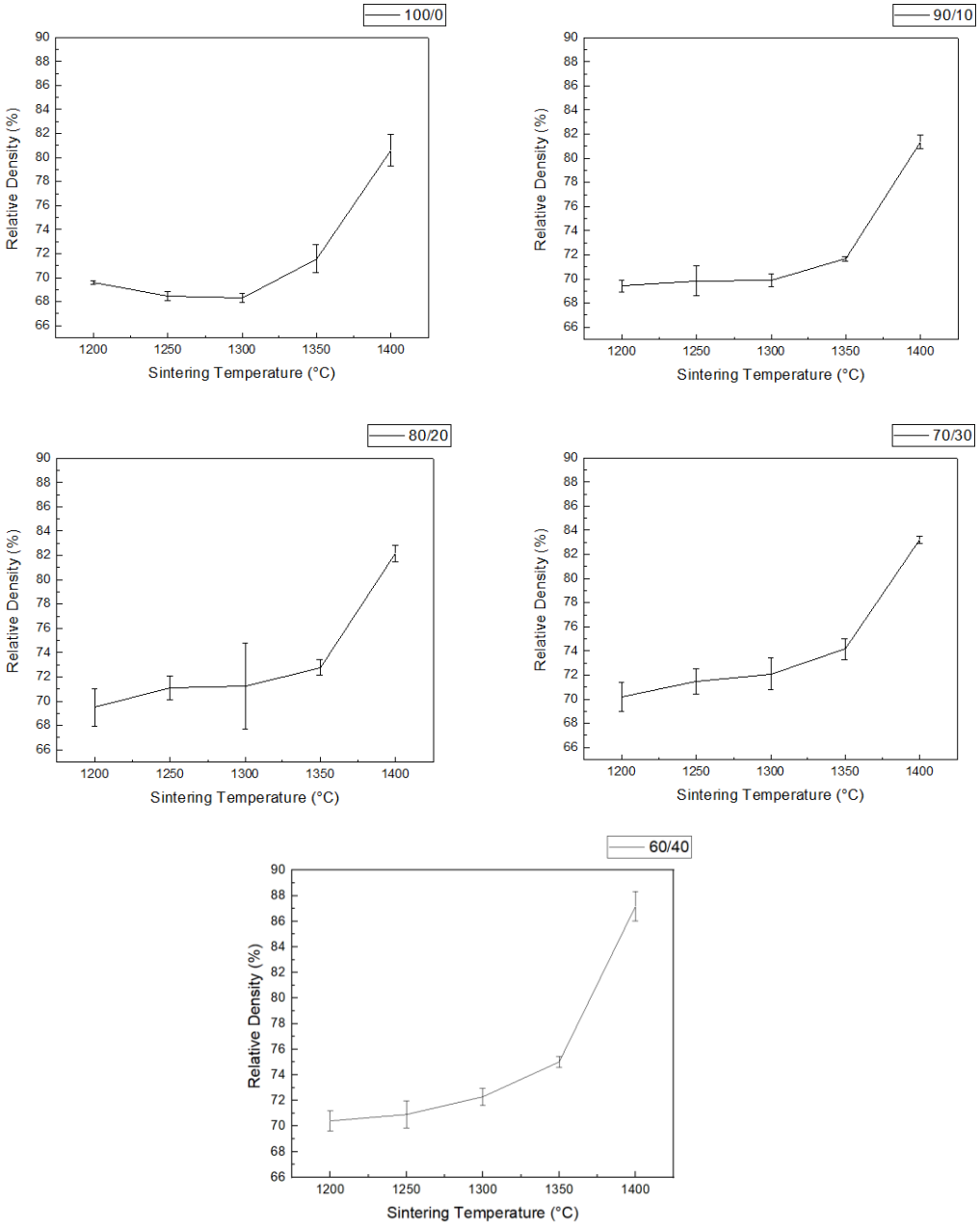

Figure 4.10. Relative density graphs for olivine pellets sintered at different temperatures with different particle size ratio

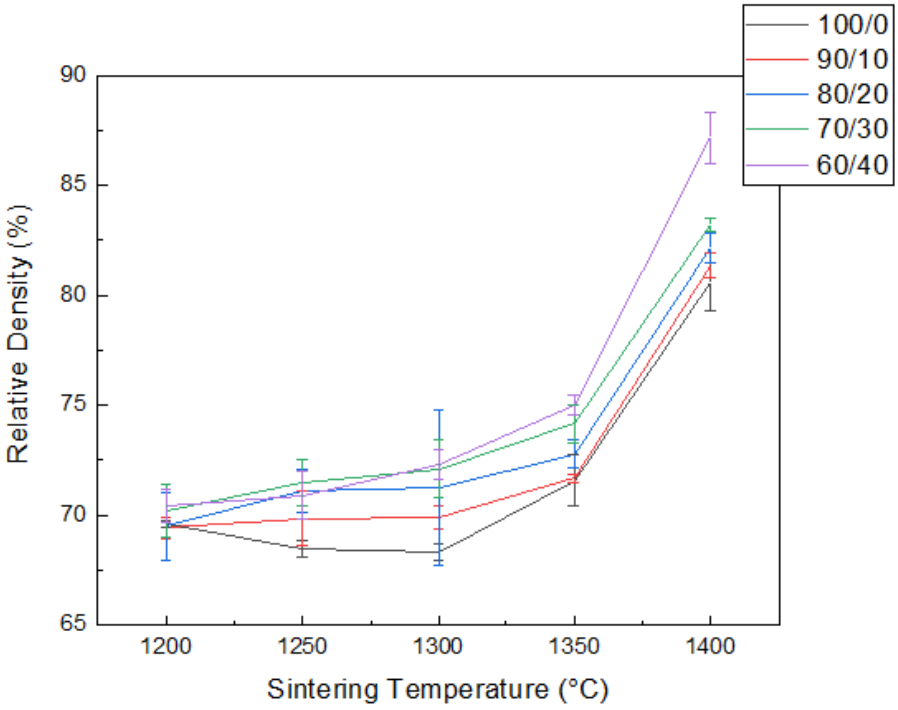

Figure 4.11. Particle size effect on relative density values of olivine pellets sintered at different temperatures

4.1.4. X-Ray Diffraction

XRD examination of ceramic pellets were done to see phases in different sintering processes. Firstly, alumina pellets without metal addition and sintered at different temperatures were characterized with XRD. No phase change or shifting in peaks were observed with changing sintering temperature. The reason for not observing any change in phase and shifting can be explained with the used alumina. The alumina used in alumina pellets is alpha alumina with rhombohedral crystal structure. (PDF (Powder Diffraction File) - 01-082-1467). Since alpha alumina is the most stable form of alumina, no change was observed. Alpha alumina gives 2θ peaks at 25.58°, 35.15°, 37.78°, 43.36°, 52.55°, 57.5°, 61.3°, 66.52°, 68.2°. Figure 4.12. shows XRD graph for alumina pellets without metal addition and sintered at different temperatures.

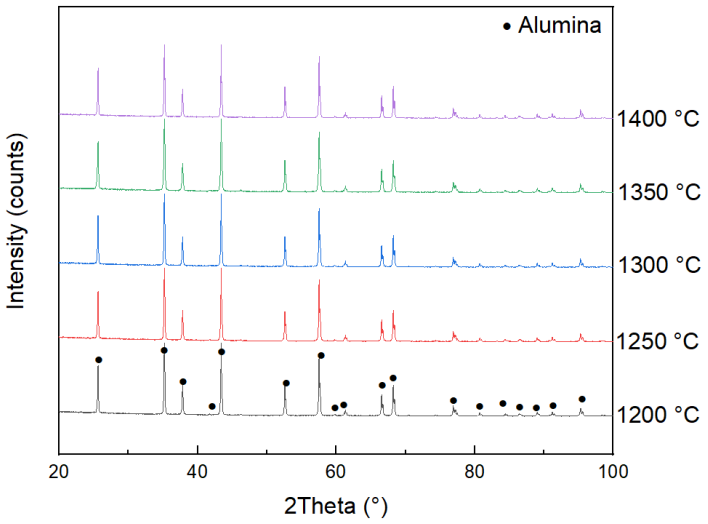

Figure 4.12. XRD graph of alumina pellets sintered at different temperatures

XRD analysis was also done for alumina pellets with different amount of metal addition. In addition to alumina peaks, aluminum peaks can be seen (see Figure 4.13.). aluminum gives peak at 38.5°, 44.76°, 78.31°. These peaks can be seen when metal addition ratio is 6 wt. %. However, peaks were reduced in intensity and disappeared towards 0 wt. % metal addition.

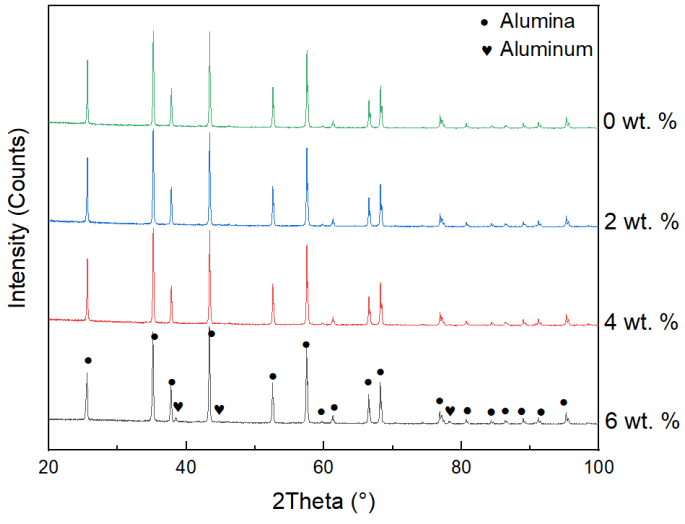

Figure 4.13. XRD graph of alumina pellets (with different metal ratios) sintered at 1300 °C

Similarly, XRD analysis was done to olivine samples. Forsterite (Mg_2SiO_4) (PDF-00-004-0769) mineral with orthorhombic crystal structure, enstatite ($Mg_2(Si_2O_6)$) (PDF-01-086-0430) mineral with orthorhombic crystal structure and hematite (Fe_2O_3) (PDF-01-077-9927) mineral with rhombohedral crystal structure was seen in XRD. Pellets sintered at 1200 °C showed enstatite peaks at 19.4°, 28.3°, 31.07°, 36°, 40-45°, forsterite peaks at 17.34°, 22.9°, 25.5°, 32.32°, 35.7°, 36.53°, 40°, 41.76°, 52.29°, 57.99°, and 62.77°. Hematite peaks at 24.14°, 33.13°, 35.63°, 54.03°, 62.42°, 71.85°. With increasing sintering temperature hematite phase was disappeared due to melting of this phase which mentioned in density measurement title.

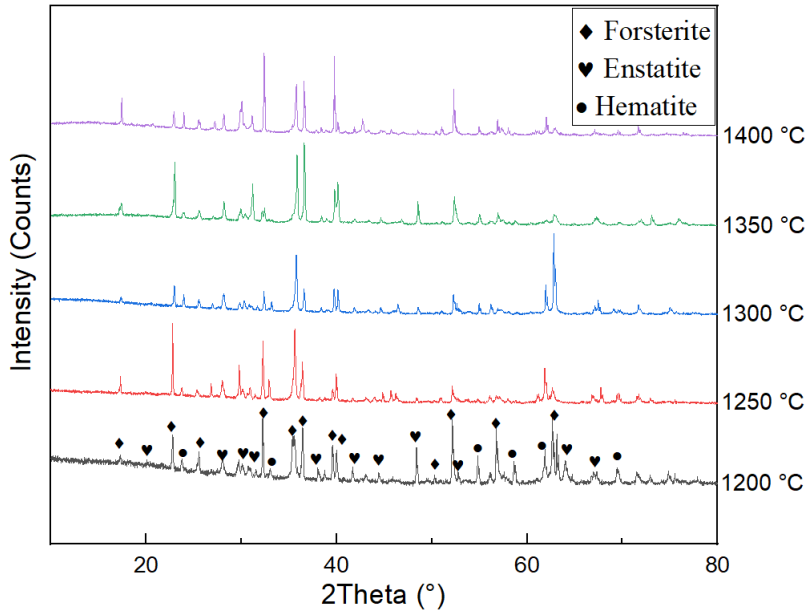

Figure 4.14. XRD graph of olivine pellets (80/20) sintered at different temperatures

4.2. Metal Matrix Composite Production

In metal matrix composite production, as it was mentioned earlier, AA7075 aluminum alloy is used as matrix material and olivine particles were used in the reinforcement phase. Olivine was added 5-7.5 and 10 wt.% of total composite composition.

In this section, firstly optical emission spectroscopy results of initial matrix alloy are given. After that, heat treatment results are presented. Hardness measurement, three-point bend test, optical microscopy, SEM analyses, and XRD were done for both heat-treated and as-cast samples. The effect of heat treatment and different amount of reinforcement particles on mechanical properties were compared.

4.2.1. Optical Emission Spectroscopy

Optical emission spectroscopy of as received aluminum alloys were done to check alloy composition. Three measurements were taken from sample and results can be seen in Table 4.3. The chemical composition of as received alloy is in the range of specifications for AA 7075 aluminum alloys.

Table 4.3. Spectral analysis of as received AA7075 alloys

Spectral Analysis Results (Element %)				
	#1	#2	#3	**Avg.**
Al	87.8	87.9	87.9	**87.87**
Si	0.18	0.16	0.19	**0.18**
Fe	0.49	0.46	0.49	**0.48**
Cu	1.7	1.78	1.75	**1.74**
Mg	2.3	2.44	2.49	**2.41**
Mn	0.84	0.75	0.86	**0.82**
Zn	5.88	5.77	5.78	**5.81**
Cr	0.05	0.05	0.05	**0.05**
Ni	0.23	0.23	0.28	**0.25**
Ti	0.05	0.05	0.05	**0.05**

4.2.2. Mechanical Test Results

4.2.2.1. Hardness Measurement

Hardness measurements of metal matrix composite materials were done. measurements were taken before heat treatment (as-cast) and after heat treatment

process. Hardness measurements were taken from ten points for each sample. It was seen a scattering in hardness values since the material is inherently heterogenous with reinforcement phase and matrix phase. All hardness values were given in Table 4.4 and Table 4.5.

Table 4.4. Hardness values of as-cast metal matrix composite materials

As-cast (HB 2.5/62.5)			
	AA7075- 5 wt. % Olivine	**AA7075- 7.5 wt. % Olivine**	**AA7075- 10 wt. % Olivine**
1	91.4	86.1	112
2	102	95.9	100
3	103	123	129
4	78.6	102	129
5	95.5	143	113
6	75.7	151	123
7	76.3	130	126
8	116	125	128
9	123	80.9	107
10	122	82.9	119
Avg.	**98.35**	**111.98**	**118.6**

Table 4.5. Hardness values of T6 heat treated metal matrix composite materials

T6 Heat Treated (HB 2.5/62.5)			
	AA7075- 5 wt. % Olivine	**AA7075- 7.5 wt. % Olivine**	**AA7075- 10 wt. % Olivine**
1	136	147	169
2	147	174	161
3	111	179	157
4	108	156	158
5	144	109	155
6	146	169	147
7	152	161	145
8	163	130	183
9	165	135	152
10	151	152	161
Avg.	**142.3**	**151.2**	**158.8**

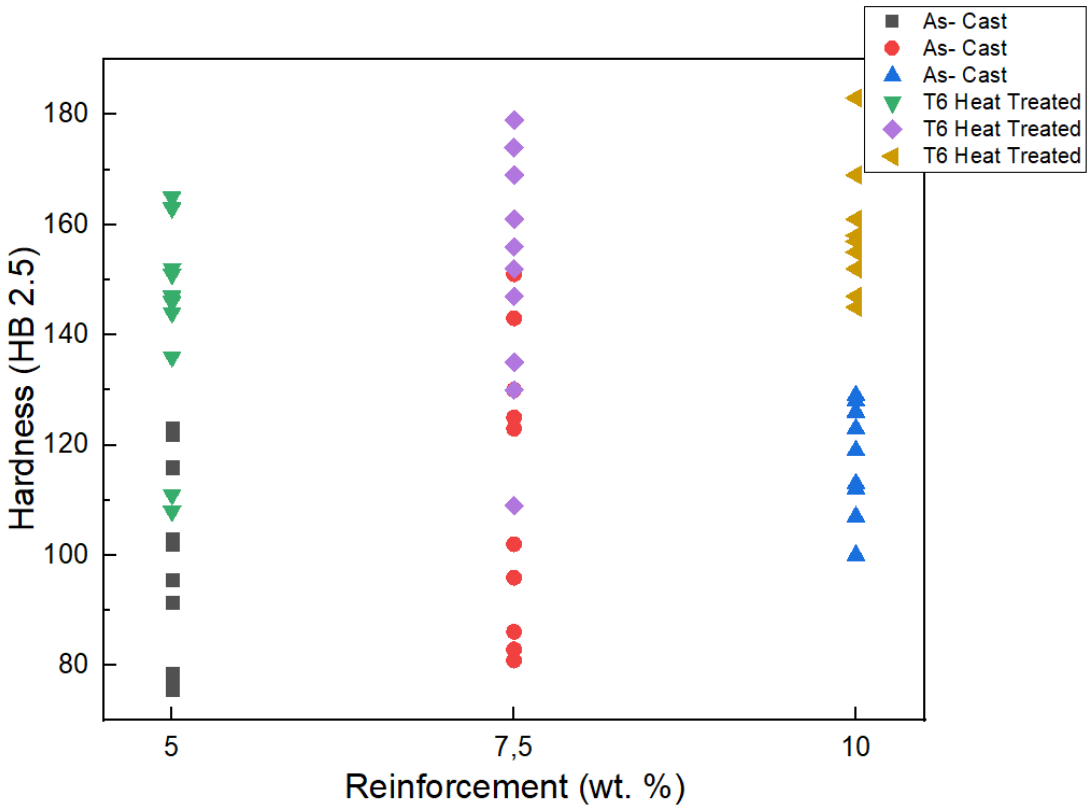

Figure 4.15. Brinell hardness values comparison graph of as-cast and T6 heat treated samples

Figure 4.15. shows all Brinell hardness (ball diameter of 2.5 mm with applied load 62.5 kg) values of metal matrix composite materials. As It can be seen clearly, there is an increase in hardness with increasing olivine reinforcement for both as-cast and T6 heat treated samples. In addition to this, hardness values of all compositions (5 wt. % - 7.5 wt. % - 10 wt. %) increased with T6 heat treatment and hardness values were reached up to 183 HB.

4.2.2.2. 3-Point Flexure Testing

After hardness testing, three-point bend testing was applied to metal matrix composite materials. Since fracture behaviors and flexure strength values are important for

ballistic applications, this test was applied to observe mechanical performance of materials developed.

The samples that were produced with squeeze casting method were machined with milling machine to have a flat and clean surface without scratches.

Figure 4.16. and Figure 4.17. shows flexure stress and flexure strain graphs for as-cast composite materials and T6-heat treated composite materials, respectively. According to the test data of samples, flexure strength decreases with increasing reinforcement level in both as-cast and T6 heat-treated condition. This can be explained in two way. Firstly, with increasing reinforcement level, homogenous distribution of reinforcement particles in alloy matrix materials becomes difficult. Reinforcement phase acts as a discontinuity in matrix phase and forms localized internal stress regions. When agglomeration of this reinforcement phase occurs, internal stress regions increases locally and ductility of matrix material cannot bear the applied load much, and consequently fracture occurs. Another reason for decrement in flexure strength can be explained with shape of reinforcement materials. As it can be seen in Figure 4.5. olivine reinforcement material has an angular shape. Edges and sharp tips give notch effect to the material. As it is known from fracture mechanics that notched regions, for example porosity, are stress raisers in materials and they lead to degradation of mechanical properties of materials developed.

Maximum strength values were obtained from samples with 5 wt. % olivine reinforced AA7075 aluminum alloy matrix composite materials in both as-cast and heat-treated conditions. An improvement in flexure strength was achieved with T6 heat treatment . An improvement in flexure strength was achieved with T6 heat treatment. Average strength value of as cast sample compared with of 5wt.% reinforced one increased 45% in T6 heat treated samples.

Four samples were tested for each reinforcement level in as-cast samples while three samples were tested for each reinforcement level in T6 - heat treated samples. See Figure 4.16. and Figure 4.17., respectively.

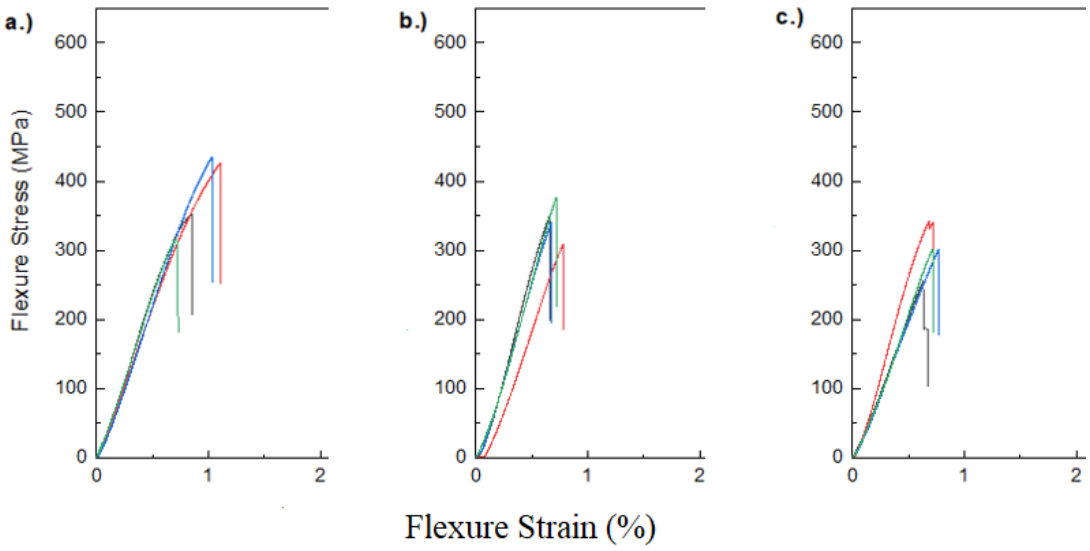

Figure 4.16. Flexure stress- Flexure strain diagram comparison of as-cast metal matrix composites a.) 5 wt. % b.) 7.5 wt. % and c.) 10 wt. %

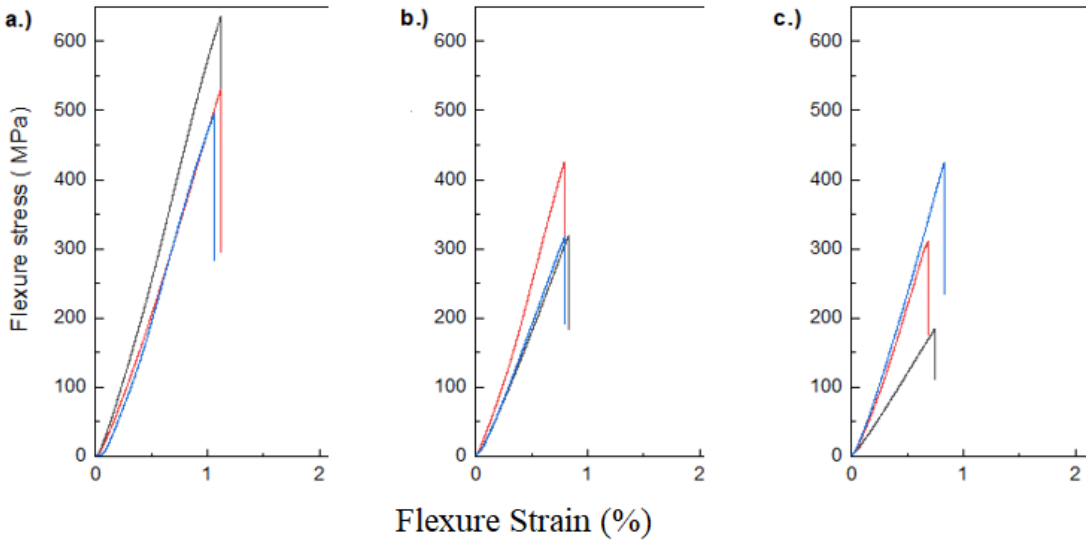

Figure 4.17. Flexure stress- Flexure strain diagram comparison of T6 heat treated metal matrix composites a.) 5 wt. % b.) 7.5 wt. % and c.) 10 wt. %

Toughness is another important material property for ballistic applications. A high toughness is required to absorb and to dissipate the residual energy of projectile after impact. It can be said from flexure stress – flexure strain graphs that flexure strain is somewhat 1% for all samples. As the flexure strength increases, the area under the curve increases (at constant flexure strain value). Thus, toughness increases. From this point of view, toughness is higher in 5 wt.% olivine added composite materials. And, T6 heat treatment has a little positive effect on flexure strain values for these samples.

4.2.3. Optical Microscopy

Optical microscopy examination of metal matrix composite materials were done to observe distribution of reinforcement particles in metal matrix. Images were taken with 100x for T6 heat treated samples. In Figure 4.18. 100x images of T6 heat treated and having 5 wt. %, 7.5 wt. % and 10 wt.% olivine reinforcement metal matrix composite materials taken with optical microscope can be seen. It can be said that relatively homogeneous distribution of reinforcement phase was obtained. However, with increasing reinforcement level and even in 5 wt. % composite material, agglomeration of particles was observed possibly due to agglomerate formation and density difference in between matrix alloy (2.8 g/cm^3) and olivine particles (3.2 g/cm^3).

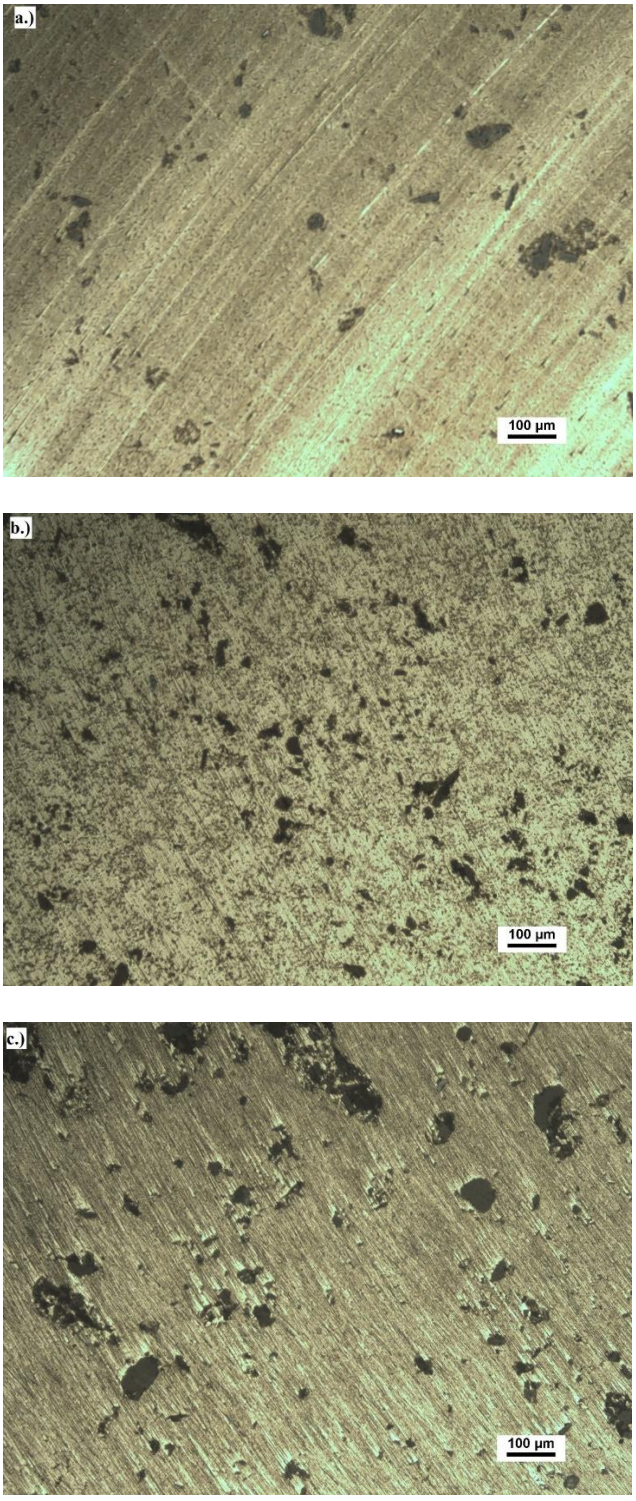

Figure 4.18. 100X Optical microscope images of a.) 5 wt. %, b.) 7.5 wt.% and c.) 10 wt.% olivine reinforced composite materials

4.2.4. SEM Analysis

SEM analysis of composite materials were done to see microstructure in detail. Figure 4.19-4.21 shows SEM images of 5 – 7.5 – 10 wt % olivine reinforced composite materials, respectively. In the figures, both as-cast and T6 heat treated microstructures were given. In as-cast structure dendritic solidification can be seen. After T6 heat treatment, dendritic structure disappeared, and relatively globular grains formed.

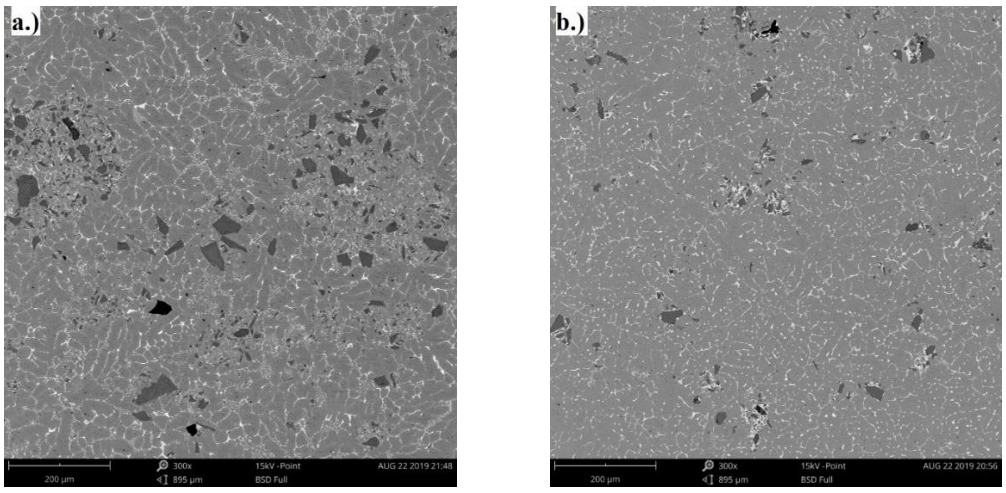

Figure 4.19. SEM images of 5 wt.% olivine reinforced composite materials a.) as-cast, b.) T6 heat treated

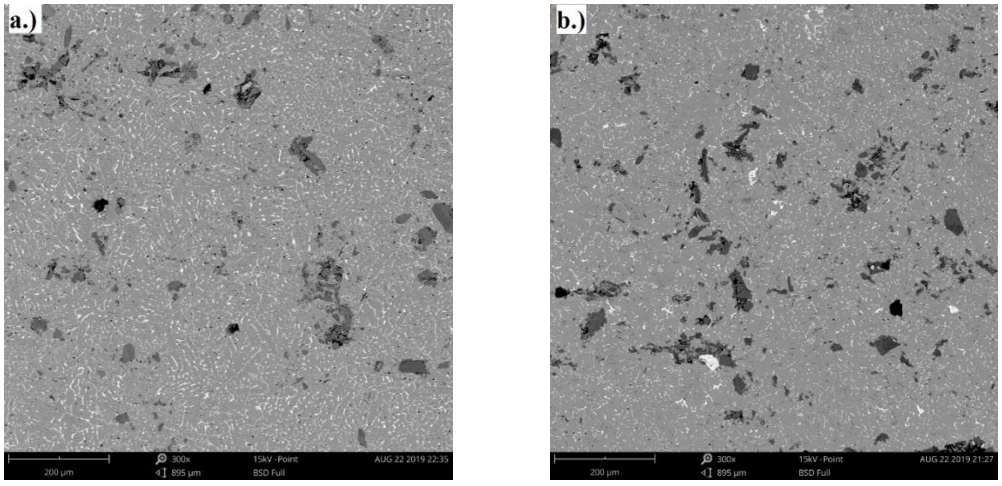

Figure 4.20. SEM images of 7.5 wt.% olivine reinforced composite materials a.) as-cast, b.) T6 heat treated

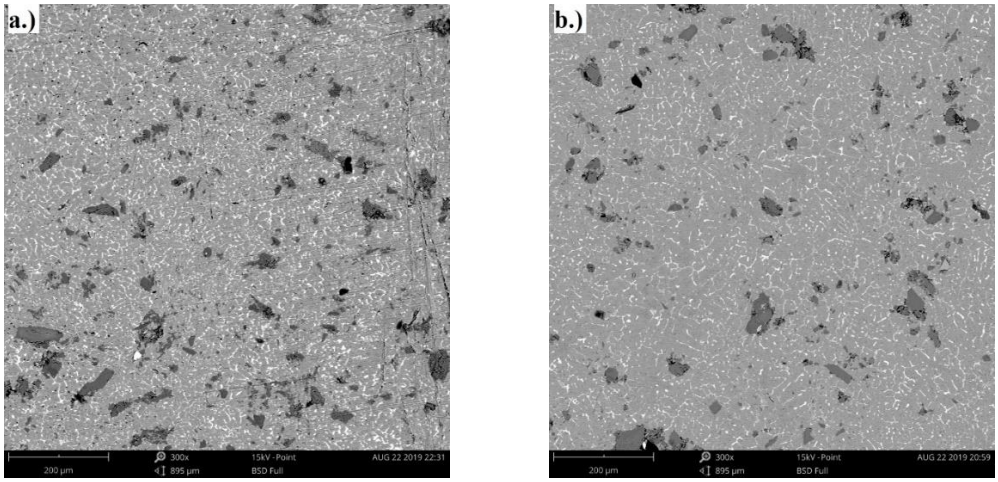

Figure 4.21. SEM images of 10 wt.% olivine reinforced composite materials a.) as-cast, b.) T6 heat treated

Wettability is one of the most important property in composite material production. In production step of olivine reinforced composites, magnesium was added into liquid metal to increase wettability. Figure 4.22. shows olivine particles in the matrix. It can be seen that there is a good wettability of reinforcement since there is no sign of discontinuity in the matrix-reinforcement interface.

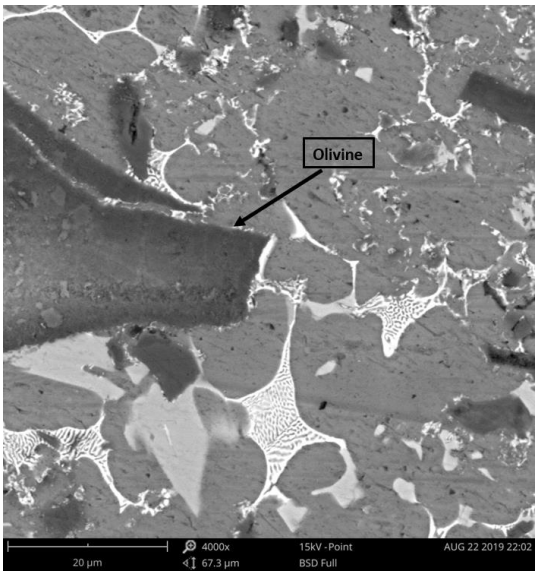

Figure 4.22. Reinforcement particle – Matrix alloy interface

Phases in the matrix alloys was also examined. Al_3Fe and AlMgZn phases were observed in the matrix alloy (see Figure 4.23.).

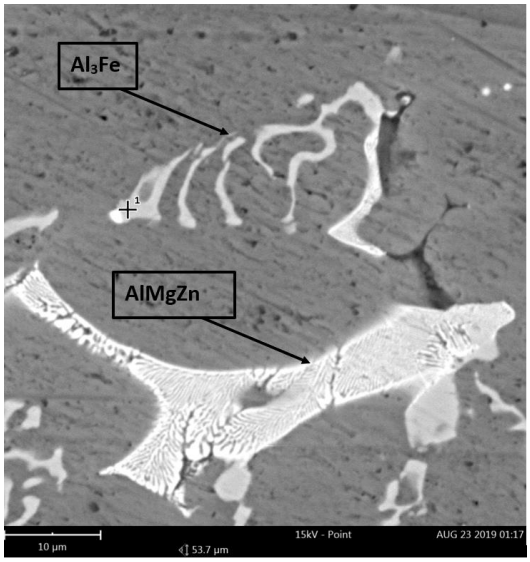

Figure 4.23. Al_3Fe and AlMgZn Phases in Matrix alloy

EDS analysis of Al_3Fe and AlMgZn can be seen in Figure 4.24. and Figure 4.25., respectively.

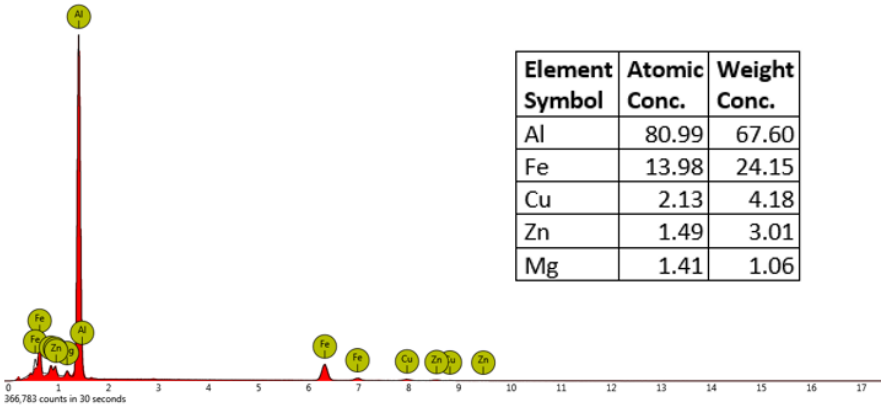

Element Symbol	Atomic Conc.	Weight Conc.
Al	80.99	67.60
Fe	13.98	24.15
Cu	2.13	4.18
Zn	1.49	3.01
Mg	1.41	1.06

Figure 4.24. EDS analysis of Al_3Fe phase in aluminum matrix

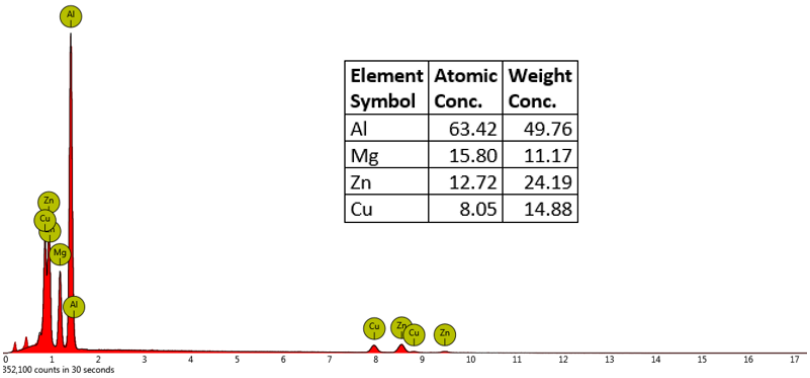

Element Symbol	Atomic Conc.	Weight Conc.
Al	63.42	49.76
Mg	15.80	11.17
Zn	12.72	24.19
Cu	8.05	14.88

Figure 4.25. EDS analysis of AlMgZn phase in aluminum matrix

It was expected to increase mechanical properties with T6 heat treatment. As it is known that the increase in mechanical properties occurs with formation of precipitates in the alloy matrix. When both as-cast and T6 heat treated samples were examined, precipitates were only observed in samples that were T6 heat treated, as expected. Figure 4.26. shows a precipitate that formed during aging step in T6 heat treatment. Precipitates are too fine (order of nanometers thick) that their chemical composition could not be detected by SEM. However, it is most probably $MgZn_2$ precipitates which forms during T6 heat treatment of AA7075 alloys.

Figure 4.26. SEM image of precipitate that formed during aging step in T6 heat treatment

4.2.5. X-Ray Diffraction

XRD examination was done for as-cast and T6 heat-treated metal matrix composite materials to observe present phases in materials. In all XRD analysis graphs, mainly pure aluminum peaks were observed. Aluminum (PDF-00-004-0787) peaks were taken at 38.47°, 44.74°, 65.13°, 78.23°, 82.43°, 99.08°, 112.04°, and 116.57°. In heat-treated samples, it was expected to see $MgZn_2$ (PDF–00–034-0457) peaks at 40.3° in XRD diffractometer. However, in addition to $MgZn_2$, the structure has olivine reinforcement which its chemical formulation is (Mg, Fe)SiO_4 and gives peak at 41.58°. Their peaks are so close and very tiny that makes identification very hard. Other peaks of olivine (PDF-00-002-1343) can be seen at 32.29°, 35.59° and 52.23°. But their existance is clear at 10 wt.% sample compared to 7.5 wt.% and 5 wt.% samples. Figure 4.27. shows XRD graphs for heat treated samples and Figure 4.28. shows XRD graphs of as cast samples.

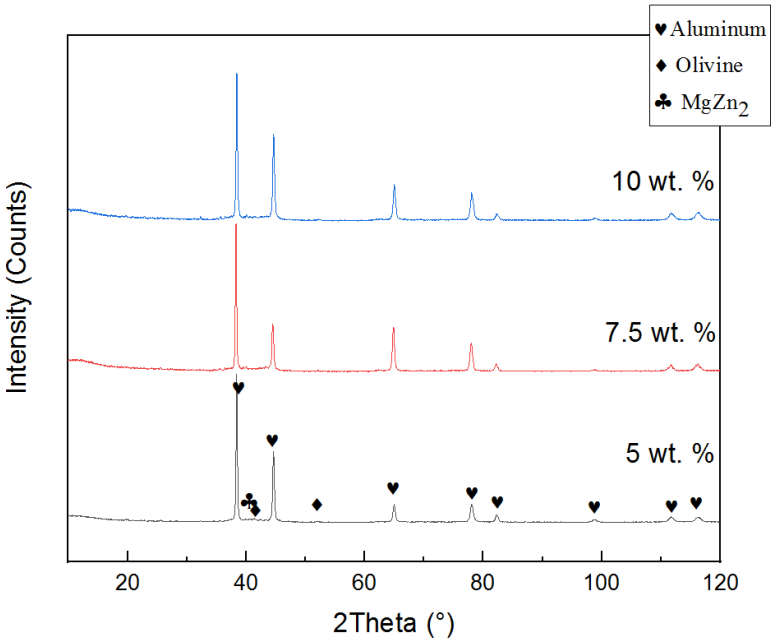

Figure 4.27. XRD graphs of T6 heat-treated samples with changing reinforcement levels

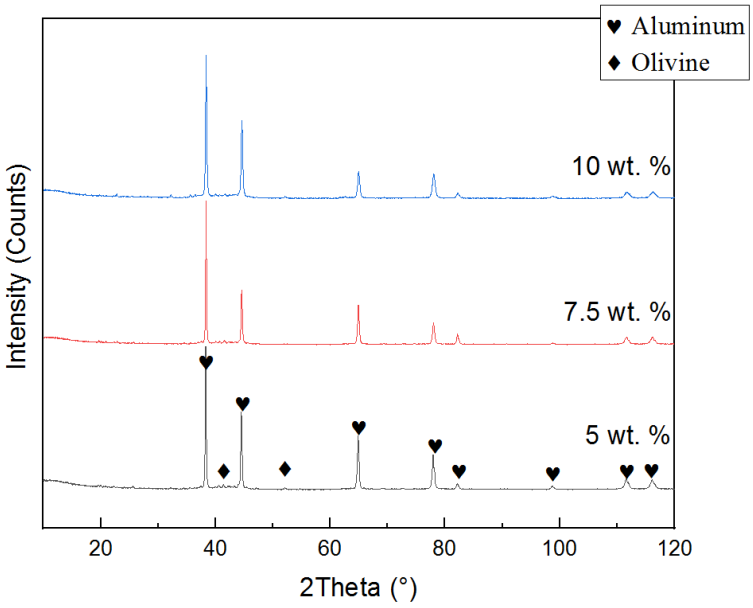

Figure 4.28. XRD graphs of as-cast samples with changing reinforcement levels

4.2.6. Radiographic Examination

Two samples from each reinforcement level was taken and they examined with X-Rays using radiographic non-destructive testing method. This technique is useful for bulk materials testing to see discontinuities inside the material. It was aimed to see olivine reinforcement distribution inside the matrix alloy. Figure 4.29. shows radiographic image of samples with different reinforcement levels. As it is known that x-rays pass through the sample and react with film that is placed behind of the sample. When there are different density particles for example olivine (3.2 gr/cm^3) and porosity (0 gr/cm^3) inside the aluminum (2.7 gr/cm^3) sample, they are posed on the film differently. This occurs with contrast. Relatively denser regions are whiter in color compared to less dense regions. From Figure 4.29. it can be said olivine particles (relatively whiter regions) are almost evenly distributed in the matrix with minimum or low content of porosity in the samples.

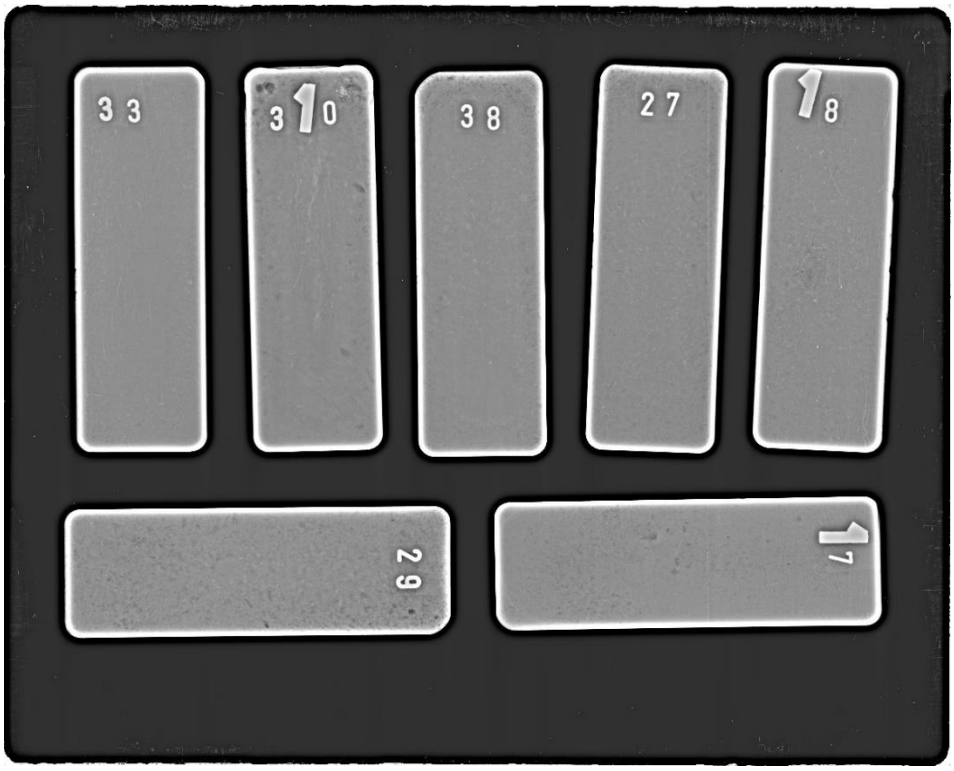

Figure 4.29. Radiographic image of metal matrix composite samples.

5 wt.% (18 and 17), 7.5 wt.% (33 and 310), 10 wt.% (27 and 29)

4.3. Melt Infiltration

4.3.1. Hardness Measurement

Hardness of metal infiltrated ceramic preforms were measured. Firstly, it was aimed to take all hardness measurements with Brinell hardness method (HB 2.5/167.5). However, hardness values could not be read by this method from alumina preforms which were sintered at 1300 °C and 1350 °C due to insufficient sintering process and thin samples (10-15 mm thick) cracked, when indenter tip stung to the surface because of high load used in Brinell method (187.5 kgs). It was also tried to decrease load to 62.5 kgs, but this time no sign of indenter tip could been observed on the screen of hardness tester. Thus, hardness measurements of alumina samples, sintered at 1300 °C and 1350 °C, were taken using microhardness tester (HV1).

Table 4.6. shows hardness values for metal infiltrated alumina ceramics and matrix alloy. All hardness measurements of metal parts and alumina infiltrated preform sintered at 1400 °C were taken using Brinell hardness (HB2.5/167.5). Micro Vickers hardness method (HV1) was used for infiltrated alumina samples sintered at 1300 °C and 1350 °C, their corresponding Brinell hardness values were also given in parenthesis for comparison.

Hardness values of melt infiltrated alumina preforms whose sintering temperature are 1300 °C, 1350 °C, and 1400 °C can be seen in Table 4.6.

Figure 4.30. shows comparison of average hardness values for these ceramic preforms. It was realized that hardness values are quite higher in infiltrated alumina ceramics sintered at 1400 °C compared to others and an average 393 HB hardness value was achieved for this sample.

Table 4.6. Brinell and Micro-Vickers hardness values of metal infiltrated alumina preforms sintered at 1300 °C, 1350 °C, and 1400 °C

Hardness						
	1300 °C		**1350 °C**		**1400 ° C**	
	Metal Region	**Ceramic Region**	**Metal Region**	**Ceramic Region**	**Metal Region**	**Ceramic Region**
1	109	167 (156)	105	313 (300)	105	422
2	115	175 (166)	113	238 (225)	111	380
3	112	178 (170)	114	235 (223)	123	351
4	117	200 (190)	110	255 (242)	123	458
5	116	180 (171)	113	243 (230)	125	371
6	105	186 (177)	108	240 (228)	119	376
Avg.	**112HB**	**181 HV1 (172 HB)**	**110HB**	**254 HV1 (241 HB)**	**117HB**	**393HB**

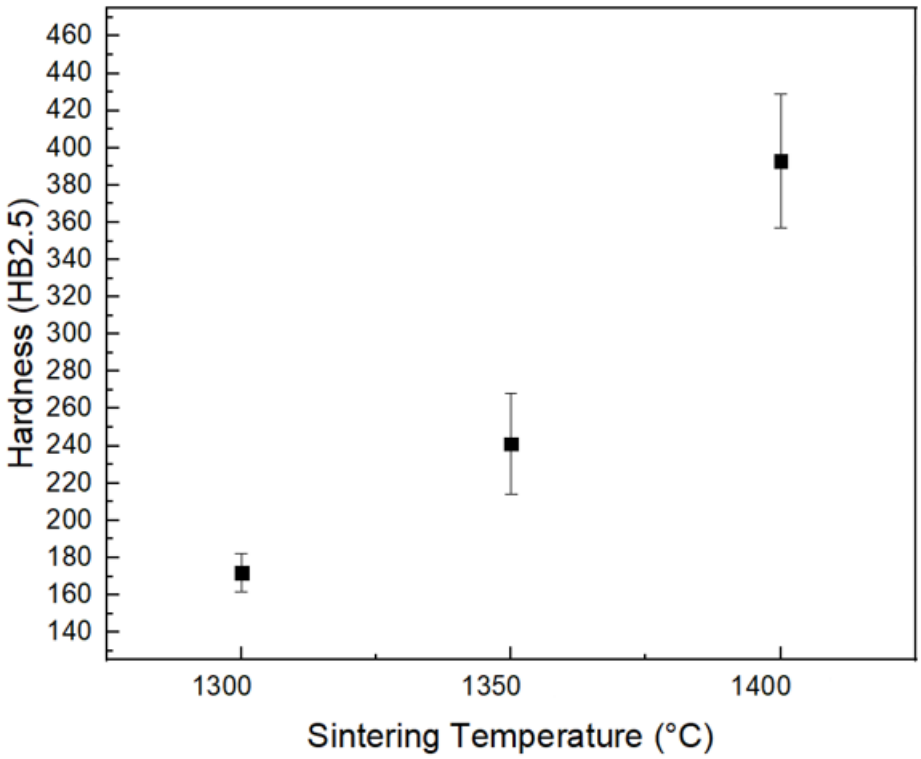

Figure 4.30. Average hardness values for melt infiltrated alumina preforms sintered at 1300 °C, 1350 °C, and 1400 °C

Hardness values of melt infiltrated 80/20 olivine preforms whose sintering temperatures are 1250 °C, 1300 °C, and 1350 °C can be seen in Table 4.7.

Figure 4.31. shows comparison of average hardness values for these ceramic preforms. It can be seen that average hardness values for 80/20 olivine preforms whose sintering temperature is 1300 ° C which is higher than that of sintered at 1250 °C and 1350 °C. This variation in hardness can be correlated with density measurement results. As it was mentioned earlier, at temperatures higher than 1300 °C, liquid phase sintering occurs in olivine samples. This glassy phase is most probably the reason for decrease in hardness. The maximum average hardness value found to be 337HB for olivine samples sintered at 1300 °C.

Table 4.7. Brinell hardness values of melt infiltrated 80/20 olivine preforms sintered at 1250 °C, 1300 °C, 1350 °C

Hardness (HB 2.5/167.5)						
	1250 °C		1300 °C		1350 ° C	
	Metal Region	Ceramic Region	Metal Region	Ceramic Region	Metal Region	Ceramic Region
1	128	279	119	305	118	244
2	125	305	124	379	134	249
3	123	308	113	316	125	226
4		334		348		239
Avg.	**125**	**306**	**119**	**337**	**126**	**240**

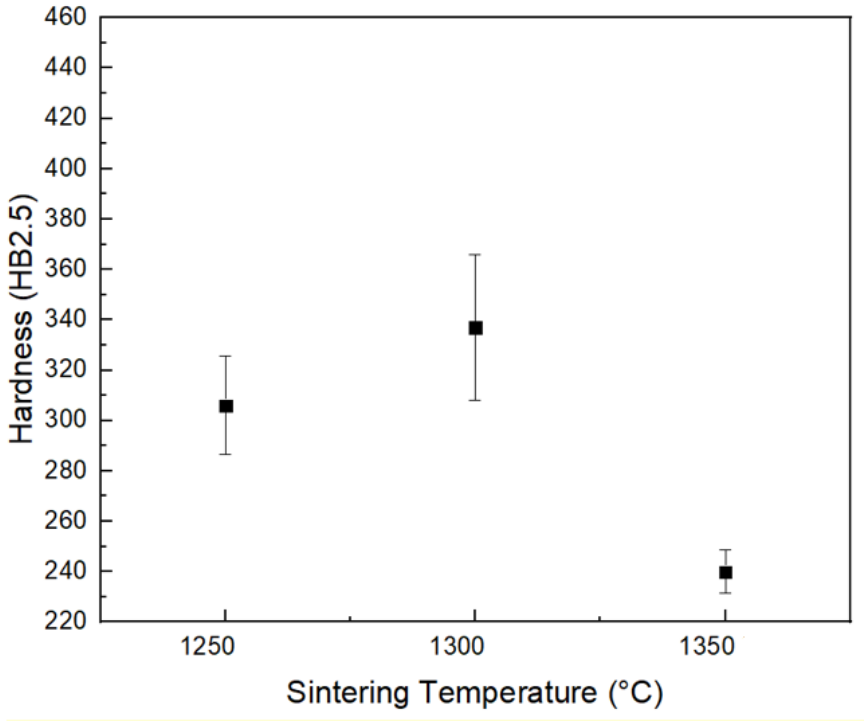

Figure 4.31. Average hardness values of melt infiltrated 80/20 olivine preforms sintered at 1250 °C, 1300 °C, 1350 °C

Hardness values of melt infiltrated olivine samples with various coarse and fine particle ratios (90/10, 80/20, 70/30, 60/40, 50/50) whose sintering temperature is 1300 °C given in Table 4.8. and comparison of average hardness value of these samples were given in Figure 4.32. Maximum average hardness value was obtained from samples with 80/20 coarse/fine particle ratio (337HB).

Table 4.8. Brinell hardness values of melt infiltrated olivine preforms whose coarse / fine particle levels are 90/10, 80/20, 70/30, 60/40, 50/50 sintered at 1300 °C,

Hardness (HB 2.5/167.5)						
	90/10		**80/20**		**70/30**	
	Metal Region	**Ceramic Region**	**Metal Region**	**Ceramic Region**	**Metal Region**	**Ceramic Region**
1	114	274	119	305	121	302
2	122	304	113	379	140	277
3	119	295	123	316	125	271
4		273		348		321
Avg.	**118**	**287**	**118**	**337**	**129**	**293**

	Hardness (HB 2.5/167.5)				
		60/40		**50/50**	
		Metal Region	**Ceramic Region**	**Metal Region**	**Ceramic Region**
	1	126	331	105	277
	2	124	308	147	195
	3	123	327	128	220
	4		319		293
	Avg.	**124**	**321**	**127**	**246**

Figure 4.33. shows average hardness values of all melt infiltrated preforms whose sintering temperatures are 1250 °C, 1300 °C, 1350 °C and 1400 °C. Among all these results, the maximum average hardness value was achieved from melt infiltrated alumina preforms (393 HB) sintered at 1400 °C and the second highest average hardness was measured for melt infiltrated 80/20 olivine preforms (337 HB).

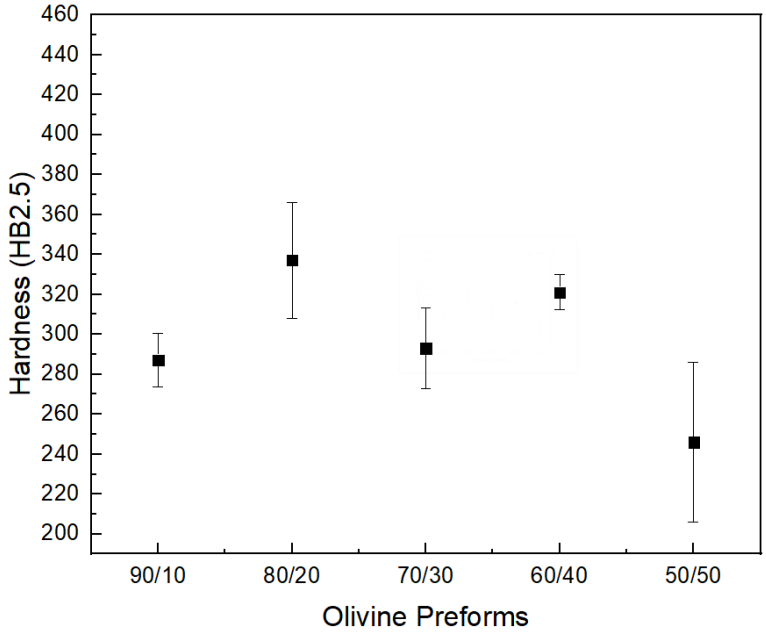

Figure 4.32. Average hardness values of melt infiltrated 80/20 olivine preforms sintered at 1250 °C, 1300 °C, 1350 °C

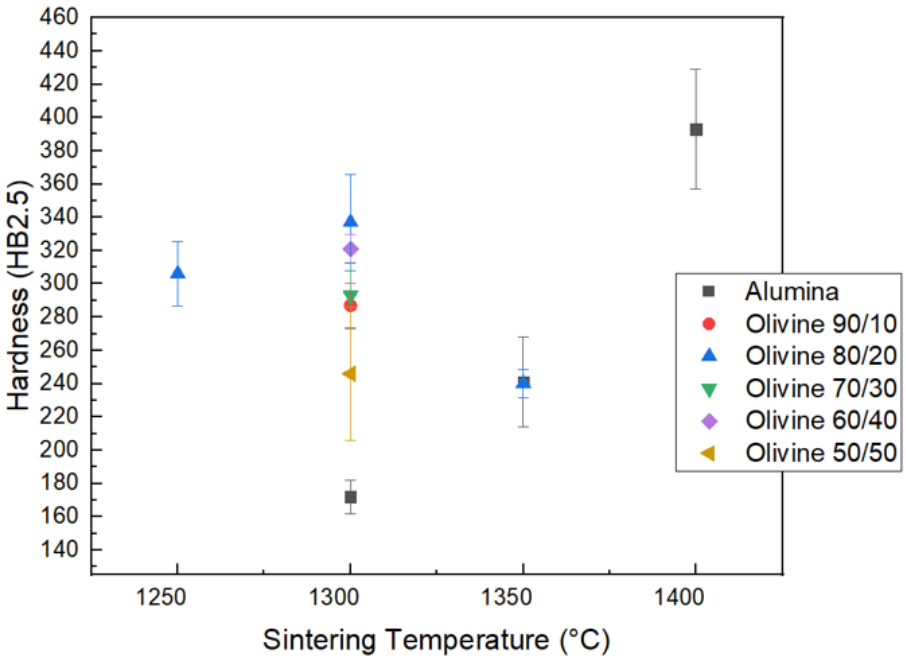

Figure 4.33. Average hardness values of melt infiltrated alumina and olivine preforms sintered at 1250 °C, 1300 °C, 1350 °C and 1400 °C.

4.3.2. 3 – Point Flexure Testing

Three-point bend testing was done to all melt infiltrated ceramic preforms to observe their flexure strength property. Firstly, melt infiltrated alumina preforms were tested. Their three-point bend test graphs can be seen in Figure 4.34. as it can be seen, flexure strength increased with increasing sintering temperature and reached up to 386 MPa for infiltrated alumina preforms sintered at 1400 °C.

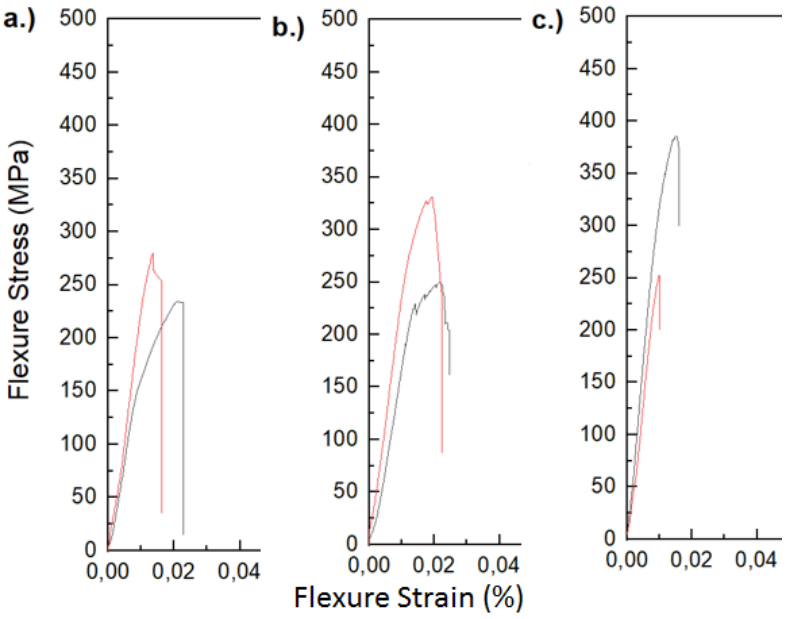

Figure 4.34. Three-point flexure stress- flexure strain graphs of melt infiltrated alumina preforms sintered at a.) 1300 °C, b.) 1350 °C, and c.) 1400 °C

3-point flexure testing was also done to melt infiltrated 80/20 olivine preforms whose sintering temperatures are 1250 °C, 1300 °C and 1350 °C. On contrary to flexure strength of alumina samples, the strength values of olivine samples decreased with increasing sintering temperatures. The reason is most probably because of formation of liquid glassy phase during sintering process.

As it can be seen in Figure 4.35. the highest flexure strength (487MPa) was achieved from samples whose sintered at 1250 °C.

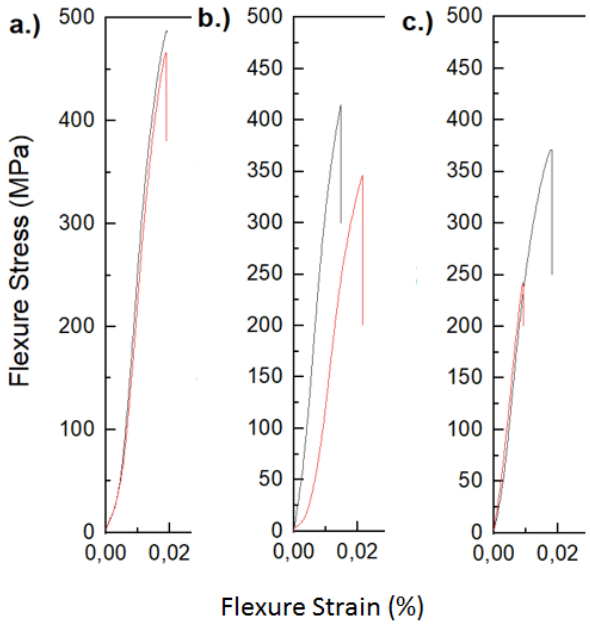

Figure 4.35. Three-point flexure stress- flexure strain graphs of melt infiltrated 80/20 olivine preforms sintered at a.) 1250 °C, b.) 1300 °C, and c.) 1350 °C

Finally, three-point flexure test was done to melt infiltrated olivine samples whose have changing coarse / fine particle ratio and sintered at 1300 °C (see Figure 4.36.). The highest flexure strength value was obtained from sample whose coarse / fine particle ratio is 90/10 (426 MPa) and the flexure strength value gradually decreased from 90/10 to 50/50. This change in flexure strength is strongly depend on the success of melt infiltration process. Preforms whose particle size ratio is 90/10 has much more open and larger porosities compared to preforms with 50/50 particle size ratio. This can be seen in density measurement results (see 4.1.3.). According to density measurements, relative to theoretical density values decreased as the fraction of coarser particles increased for constant sintering temperatures. Thus, melt infiltration

was completed successfully with preform that have 90/10 (coarse/fine) particle ratio. It can also be seen in SEM images given in following subtitle.

It is known that as the particle size in ceramic materials decrease, mechanical properties increase. However, since in this study melt infiltration into porous ceramic structures are done, the higher particle size will make the infiltration process easier and it will prevent more the formation of closed pores which are not infiltrated with metallic material and mechanical properties will increase as can be seen in Figure 4.36.

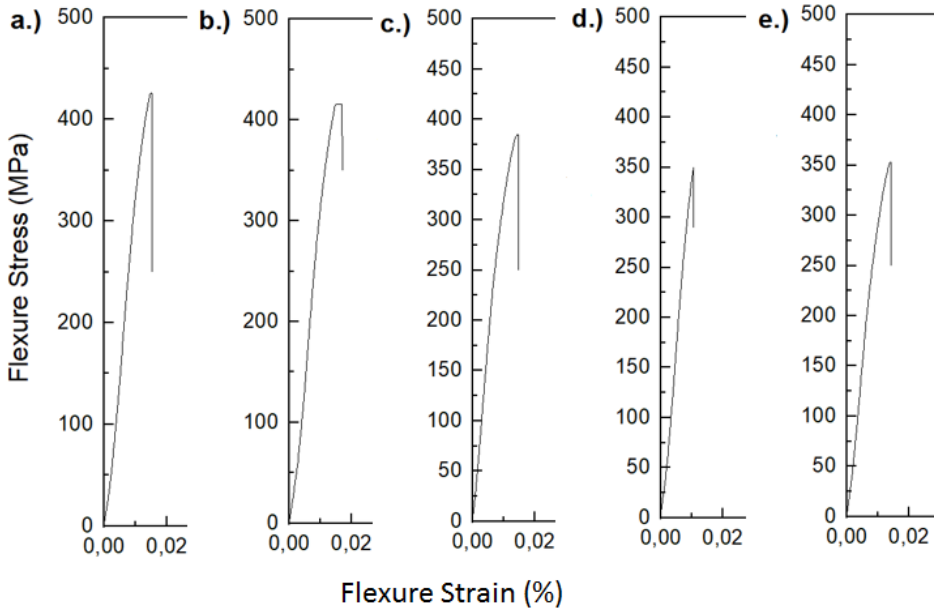

Figure 4.36. Three-point flexure stress- flexure strain graphs of melt infiltrated olivine preforms sintered at 1300 °C with changing particle size ratio a.) 90/10, b.) 80/20, c.) 70/30, d.) 60/40 and e.)50/50

For all melt infiltrated preforms, the flexure strain was found to be somewhat 0.02% which is very low strain value compared to metal matrix composite materials previously given (around 1% flexure strain). Nonetheless, in final FGM structure, starting with high ceramic content melt infiltrated ceramic material and ending with high metal content metal matrix composite material can meet the requirement for an

effective ballistic protection. A hard and relatively high strength melt infiltrated ceramic will blunt the projectile nose and a high flexure strength with relatively high toughness backing layer (MMC) will absorb and dissipate the residual energy of that projectile.

4.3.3. SEM Examination

SEM examination of melt infiltrated ceramics was done in order to observe interface in between sintered preform ceramic materials and metal matrix. In all alumina and olivine ceramics (except alumina sample sintered at 1300 °C, Figure 4.37.a and olivine sample with 70/30 particle size ratio sintered at 1300 °C, Figure 4.38.c), there is a good interface without delamination in between matrix and preforms. This means matrix alloy wet the preform thanks to applied pressure in melt infiltration squeeze casting process.

Figure 4.37. gives matrix – preform interface of alumina preforms sintered at 1300 °C, 1350 °C and 1400 °C. It can be said from images that interface of 1400 °C sintered preform has more homogenous interface structure than others. And consequently, better mechanical properties were achieved (see hardness and 3-point flexure test results.).

In both melt infiltrated ceramic preforms (alumina and olivine preforms) and metal matrix composite materials (with olivine reinforced 5 – 7.5 – 10 wt. %) there has not observed any change in the chemical composition of the matrix alloy AA 7075. This shows that olivine and alumina can be used as reinforcement material in composite production. This is one of the most critical expectation from reinforcement materials to be used in the metal matrix composite materials as a reinforcement.

In all Figures 4.37-4.39. left-hand side of images show aluminum matrix phase (brighter in color) and right-hand side part of images show infiltrated ceramic preforms (darker in color).

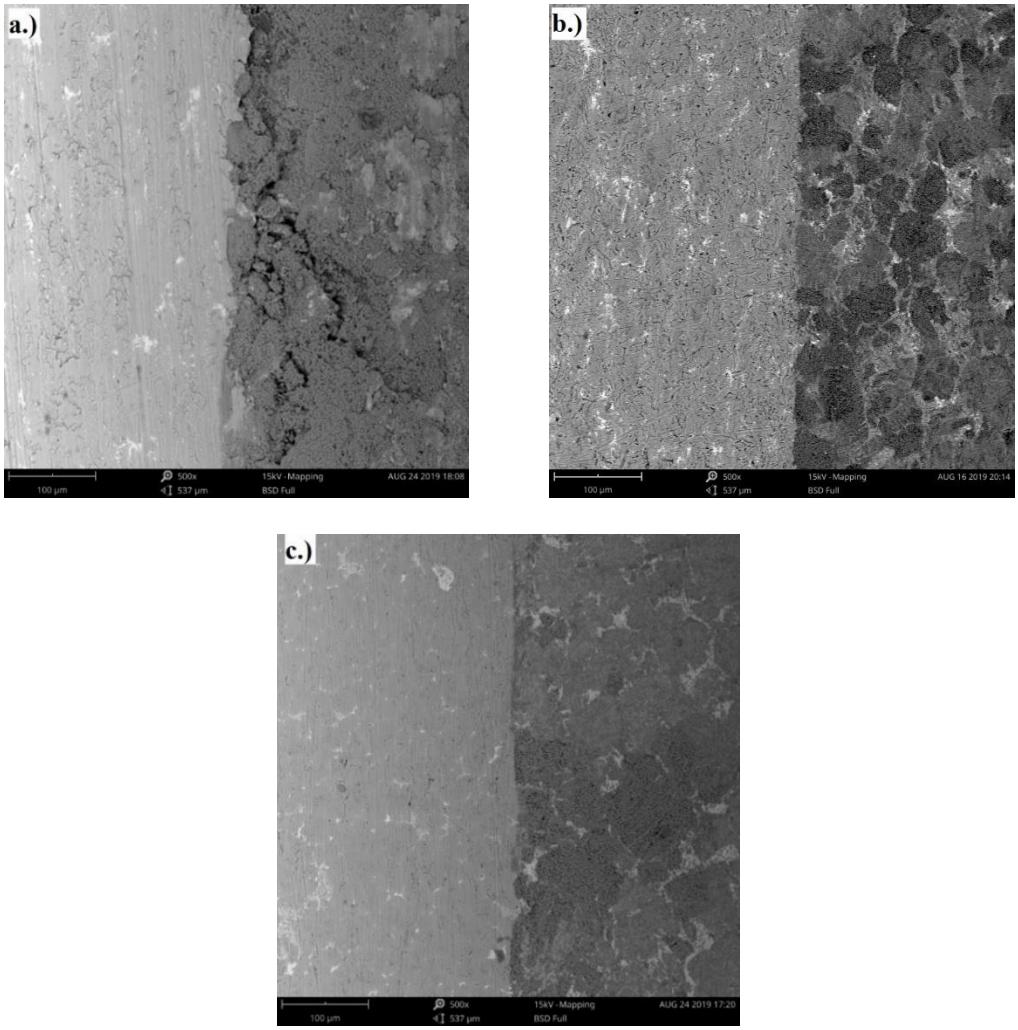

Figure 4.37. 500X SEM images of metal - ceramic preform interfaces of melt infiltrated alumina samples sintered at a.)1300 °C, b.)1350 °C, and c.)1400 °C

In Figure 4.38. metal – ceramic interfaces of melt infiltrated olivine samples with various particle size ratio and sintered at 1300 °C can be seen. As it can be concluded from SEM images in Figure 4.38., melt infiltration rate increased with increasing coarse olivine particle fraction in the preform. This led to have even metal infiltration in ceramic preform and open porosities in between particles filled better. Therefore, mechanical properties increased.

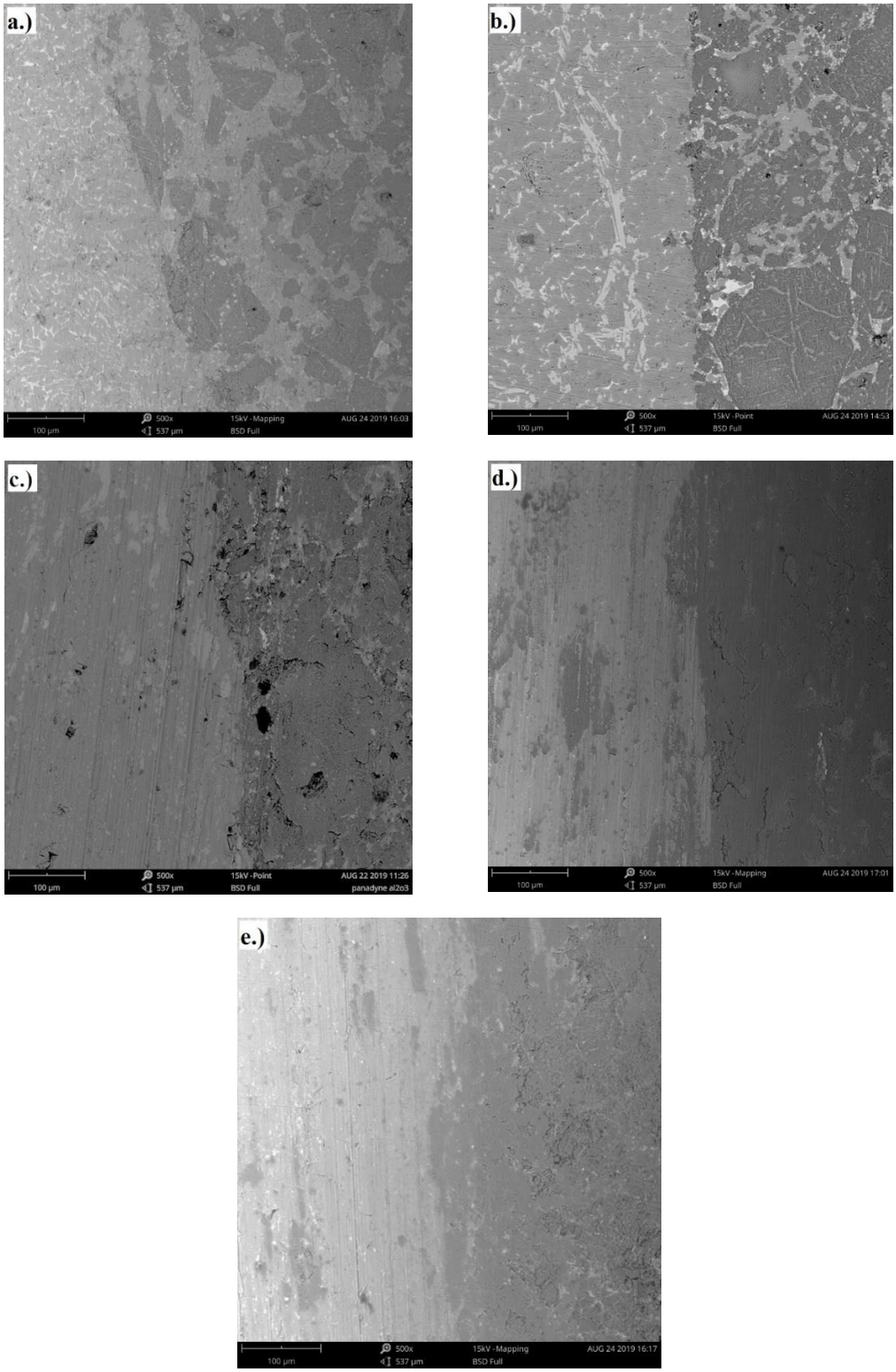

Figure 4.38. 500X SEM images of metal - ceramic preform interfaces of melt infiltrated different coarse/fine particle level olivine samples sintered at 1300 °C a.) 90/10, b.) 80/20, c.) 70/30, d.) 60/40, e.) 50/50

Lastly, Figure 4.39. shows interfaces in between ceramic and metal parts of olivine preform samples sintered at 1250 °C, 1300 °C and 1350 °C. In Appendix A, interfaces in between matrix alloy and ceramic preform were given with various magnifications (500X, 1000X, 2000X and 4000X)

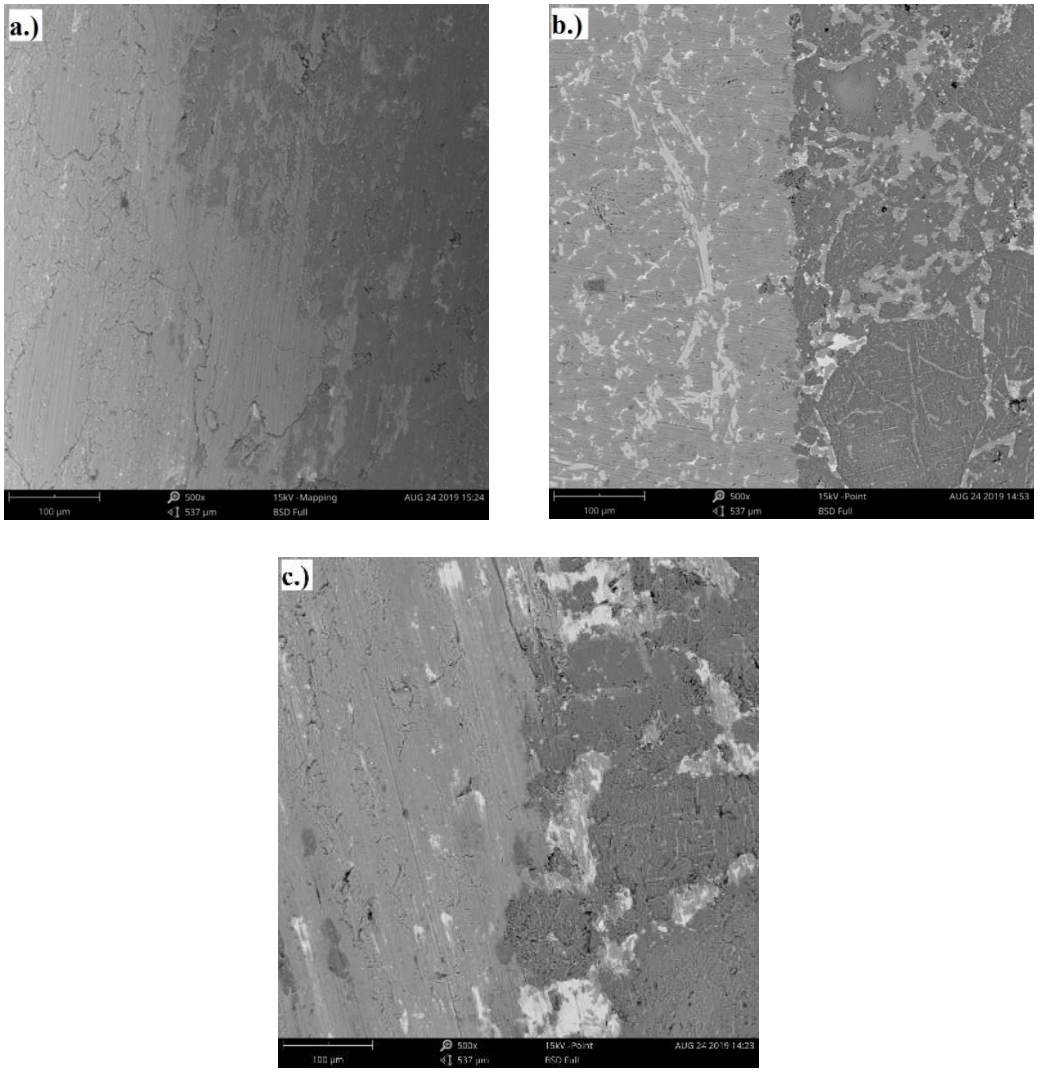

Figure 4.39. 500X SEM images of metal - ceramic preform interfaces of melt infiltrated olivine samples sintered at a.)1250 °C, b.)1300 °C, and c.)1350 °C

4.3.4. Image Analysis

Infiltrated preforms were analyzed with ImageJ- image analyzer software to measure the ceramic vol.% in infiltrated ceramic preforms. Table 4.9., Table 4.10. and Table 4.11. give alumina vol. % sintered at different temperatures, olivine vol. % with different sintering temperatures and olivine vol. % with different particle size fractions sintered at 1300 °C, respectively. Image analysis results validate the density measurement results of pellets. Images of analyzed microstructures can be seen in Appendix B.

Table 4.9. Vol. % alumina content of melt infiltrated preforms sintered at different temperatures

Sintering Temperature	1300 °C	1350 °C	1400 °C
Ceramic vol. %	60.3	76.5	87.55

Table 4.10. Vol. % olivine content of melt infiltrated preforms of 80/20 coarse/fine ratio sintered at different temperatures

Sintering Temperature	1250 °C	1300 °C	1350 °C
Ceramic vol. %	72.8	82.4	85.05

Table 4.11. Vol. olivine content of melt infiltrated preforms sintered at 1300 °C with different coarse/fine fractions

Sintering Temperature	90/10	80/20	70/30	60/40	50/50
Ceramic vol. %	77	82.4	86.4	90.11	93.15

CHAPTER 5

CONCLUSIONS

Following conclusions were drawn from results of the study:

In density measurement results of sintered pellets, an increase in density of alumina pellets was seen, when sintering temperature was 1400 °C. Addition of metal particles into alumina pellets caused crack formation and decreased the pellet density due to difference in thermal expansion coefficient and oxidation of aluminum particles at high temperatures. The maximum mean sintered pellet relative density was 52.53% from alumina pellets sintered at 1400 °C without metal addition. In olivine samples, density increase was seen at sintering temperature of 1300 °C and higher. Moreover, sintered density increased with increasing fine particle ratio. The maximum mean sintered pellet density was obtained from 60/40 samples that were sintered at 1400 °C and it is 87.17%. Density measurements has showed that it is possible to have graded ceramic structures by changing sintering temperature and mean particle size in the structure.

XRD results of sintered olivine samples showed enstatite, forsterite and hematite phases in the structure. Hematite phase started to disappear at sintering temperature above 1300 °C because of formation of glassy phase. In alumina samples, only alumina peaks were observed, and no phase change was observed with increasing sintering temperature. In metal particle added alumina samples, aluminum peaks were also observed.

Hardness measurements of metal matrix composite materials showed that hardness increased with increasing olivine content for both as cast and T6 heat treated situations. In as-cast samples the maximum mean hardness was measured from 10

wt.% olivine reinforced sample as 118.6HB and in T6 heat treated sample the maximum mean hardness was measured from again 10 wt.% sample as 160 HB.

Three-point bend tests of metal matrix composites were also done for as cast and T6 heat treated samples. The maximum flexure strength was obtained from 5 wt. % olivine reinforced samples for both as-cast (434.8 MPa) and T6 heat treated samples (636 MPa). An average 45% improvement was seen in flexure strength after T6 heat treatment.

In optical microscope examination of metal matrix composite materials, relatively homogeneous distribution of reinforcement particles were obtained with some agglomerations.

SEM imaging showed that dendritic structure formed in as-cast samples were eliminated with T6 heat treatment and more homogeneous and relatively globular grained microstructure was obtained. In addition, It was seen that there is a good wettability of olivine particles by aluminum matrix. Precipitates were observed in T6 heat treated samples smaller than 1 micron. However, their chemical composition could not be detected. Thus, It can be concluded that TEM analysis is necessary to identify them.

Melt infiltration of sintered preforms were completed successfully without almost no matrix-preform interface delamination.

The maximum mean hardness value was obtained from melt infiltrated alumina samples that were sintered at 1400 °C as 393HB. For melt infiltrated olivine samples, the maximum mean hardness value was obtained from 80/20 olivine that were sintered at 1300 °C as 337HB.

In the three-point bend tests of melt infiltrated alumina samples, the maximum flexure strength value was obtained as 385 MPa for preform that were sintered at 1400 °C. In olivine samples, the maximum flexure strength was obtained from 80/20 preforms that

were sintered at 1250 °C as 487 MPa. The maximum flexure strength was found as 426 MPa for 90/10 preforms that were sintered at 1300 °C.

Finally, this study has showed that, functionally graded aluminum matrix composite materials can be produced by melt stirring and melt infiltration by squeeze casting. By adjusting particle size distribution of particles that are used in preform production and by changing sintering temperature, graded structures can be produced.

Olivine as a ceramic material can be used in ballistic applications since this study showed that it has similar or sometimes better mechanical properties compared to alumina ceramics when processed at the same way with lower cost of raw material

.

REFERENCES

[1] Yumak, N., Pekbey Y., Aslantaş K., 2014. Investigation of deformation characteristics of composite materials used in armor design, Electronic Journal of Machine Technologies, 10, 1-21.

[2] Bhatnagar, A., 2016. Lightweight ballistic composites- Military and law enforcement applications, Woodhead Publishing Series in Composite Science and Engineering, second edition.

[3] Durmaz, T., 2017. Development of high strength aluminum matrix composite backing plates for ballistic armor, MSc. Thesis, METU.

[4] Opportunities in protection materials science and technology for future army applications, 2011. Retrieved from http://nap.edu/13157, ISBN 978-0-309-38500-8, DOI 10.17226/13157

[5] Dhanashekar, M., Kumar, V.S., 2014. Squeeze casting of aluminum metal matrix composites – an overview, Procedia Engineering, 97, 412-420.

[6] Kieback, B., Neubrand, A., Riedel, H., 2003. Processing techniques for functionally graded materials, Materials Science and Engineering, A362, 81-105.

[7] Ebhota, S., Karun, A.S., Inambao, F.,L., 2016. Principles and baseline knowledge of functionally graded aluminum matrix materials (FGAMMs): fabrication techniques and applications, International Journal of Engineering Research in Africa ISSN: 1663-4144, 26, 47-67.

[8] Mahamood, R.M., Akinlabi, E.T., 2012. Functionally graded material: an overview. Proceedings of World Congress on Engineering, Vol III, London, UK.

[9] Birman, V., 2014. Functionally graded materials and structures, Encyclopedia of Thermal Stresses, 1858-1865.

[10] Mattern, A., Huchler, B., Staudenecker, D., Oberacker, R., Nagel, A., Hoffmann, M.J., 2004. Preparation of interpenetrating ceramic-metal composites, Journal of the European Ceramic Society, 24, 3399-3408.

[11] Ghomashchi, M.R., Vikhrov, A., 2000. Squeeze casting: an overview, Journal of Materials Processing Technology, 101, 1-9.

[12] Tekinbüğrü, C.M., 2013. Kompozit zırh malzemeleri, Sakarya Üniversitesi, Lecture Notes.

[13] Radhakrishna, B.V., Somaraju, K., Metal matrix composites as potential armour materials, Defense Metallurgical Research Laboratory, Hyderabad.

[14] Rajesh, N., Kumar, R., Tharmaraj, R., Velu, P., 2016. Production of aluminum metal matrix composites by liquid processing methods, AIP Conference Proceedings, 1728, 020558.

[15] Mahadevan, R., Gopal, R., 2008. Selectively reinforced squeeze cast pistons, 68th WFC –World Foundry Congress, 379-384.

[16] Mortensen, A., Michaud, V.J., Flemings M.C., 1993. Pressure-infiltration processing of reinforced aluminum, Journal of Materials, 36-43.

[17] Ballistic Standards, retrieved from https://www.bodyarmornews.com/ on 20.08.2019.

[18] Lausund, K.B., 2014. Adhesion between ceramic and composite materials for use in lightweight ballistic armour, MSc. Thesis, Oslo University.

[19] Naik, N.K., Doshi, A.V., 2008. Ballistic impact behaviour of thick composites: Parametric studies, Composite Structures, 82, 447-464.

[20] Sobczak, J.J., Drenchev, L., 2013. Metallic functionally graded materials: a specific class of advanced composites, Journal of Materials Science and Technology, 29 (4), 297-316.

[21] El-Wazery, M.S., El Desouky, A.R., 2015. A review on functionally graded ceramic-metal materials, Mater. Environ. Sci. 6 (5), 1396-1376.

[22] Udupa, G., Rao, S.S., Gangadharan, K.V., 2014. Functionally graded composite materials: An overview, Procedia Materials Science, 5, 1291-1299.

[23] Yılmaz, H.,S., 2004. Characterization of silicon carbide particulate reinforced squeeze cast aluminum 7075 matrix composite, MSc. Thesis, METU.

[24] Keleş, Ö., 2008. Production and characterization of alumina fiber reinforced squeeze cast aluminum alloy matrix composites, MSc. Thesis, METU.

[25] Furlani, E., Aneggi, E., Maschio S., 2014. Sintering behaviour of waste olivine/alumina blends, Materials, 7, 4773-4788.

[26] Küçükoğlu, Ö., Yücel O., 2016. Production of olivine based refractories from domestic sources, IMMC, 220-222.

[27] Furlani, E., Aneggi, E., Maschio S. Tonello, G., 2013. Possible use of waste olivine powders from a foundry process into the ceramic industry: sintering behaviour of olivine, kaolin and their blends.

[28] Rahaman, M.N., 2003. Ceramic processing and sintering, CRC Press, 2nd Edition, ISBN 9780824709884.

[29] Principle of optical emission spectrometry, retrieved from https://shimadzu.com/an/elemental/oes/oes.html on 4.9.2019

[30] Yungwith, C.J., O'Conor, J., Zakraysek, A., Deshpande, V.S., Wadley, H.G., 2011. Explorations of hybrid sandwich panel concepts for projectile impacts mitigation, Journal of American Ceramic Society, 94, 62-75.

[31] Wadley, H.N.G., O'Masta M.R., Dharmasena, K.P., Compton, B.G., Gamble, E.A., Zok, F.W., 2013, Effect of core topology on projectile penetration in hybrid aluminum/alumina sandwich structures, International Journal of Impact Engineering, 62, 99-133.

[32] Wadley, H.N.G., O'Masta M.R., Deshpande, V.S., 2016. Mechanism of projectile penetration in dyneema encapsulated aluminum structures, International journal of Impact Engineering, 74, 16-35.

[33] ASM International, 2001. Heat Treating Handbook vol.4. https://doi.org/10.1016/S0026-0576(03)90166-8.

[34] ASTM E-10-01 (Standard Test Method for Brinell Hardness of Metallic Materials)

[35] Medvedovski, E., 2006. Lightweight ceramic composite armour system, Advances in Applied Ceramics, 105, 241-245.

[36] Fahrenholtz, W.G., 2004. Ceramic engineering 111 sintering, University of Missouri-Rolla, Lecture notes.

[37] Arslan, G., Kalemtaş, A., Tunçer, N., Yeşilay, S., 2009. Effect of post infiltration heat treatments on the microstructure and properties of B_4C-Al composites, Anadolu University Journal of Science and Technology, 10, 267-276.

[38] Senthilvelan, T., Gopalakannan, S., Vishnuvarthan, S., Keerthivaran, K., 2013. Fabrication and characterization of SiC, Al2O3 and B4C reinforced Al-Zn-Mg-Cu (AA 7075) metal matrix composites: a study, Advanced Materials Research, ISSN: 1662-8985, vols: 622-623, 1295-1299.

[39] Yılmaz, S., Kalkanlı, A., 2008. Synthesis and characterization of aluminum alloy 7075 reinforced with silicon carbide particulates, Materials and Design, 29, 775-780.

[40] Balcı, E., Sarıkan, B., Übeyli, M., Camuşcu, N., Yıldırım, R. O., 2013. On the ballistic performance of the AA7075 based functionally graded material with boron carbide reinforcement, Kovove Mater., 51, 257-262.

[41] Durmaz, T., Kalkanlı, A., Kalemtaş, A., Arslan, G., 2017. Melt infiltration casting of alumina, silicon carbide and boron carbide reinforced aluminum matrix composites, Journal of Materials Science and Engineering, 6:357, doi: 10.4172/2169-0022.1000357.

[42] Demir, T., Übeyli, M., Yıldırım, R.O., 2009. Investigation on the ballistic impact behavior of various alloys against 7.62 mm armor piercing projectile, Materials and Design, 29, 2009-2016.

APPENDICES

A. SEM Examination

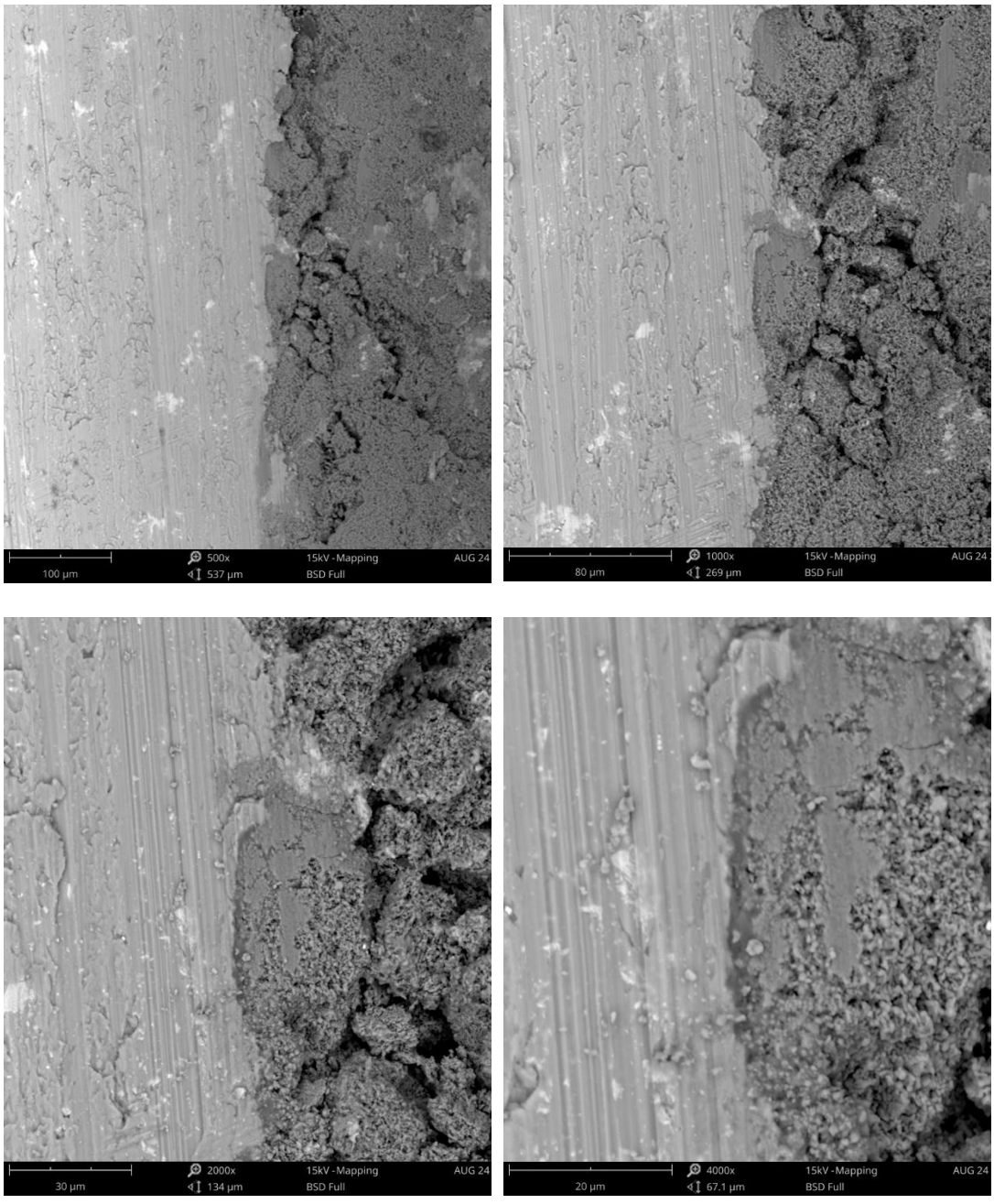

Figure A. 1. SEM images of interface of melt infiltrated alumina preform sintered at 1300 °C (500, 1000, 2000 and 4000X magnifications)

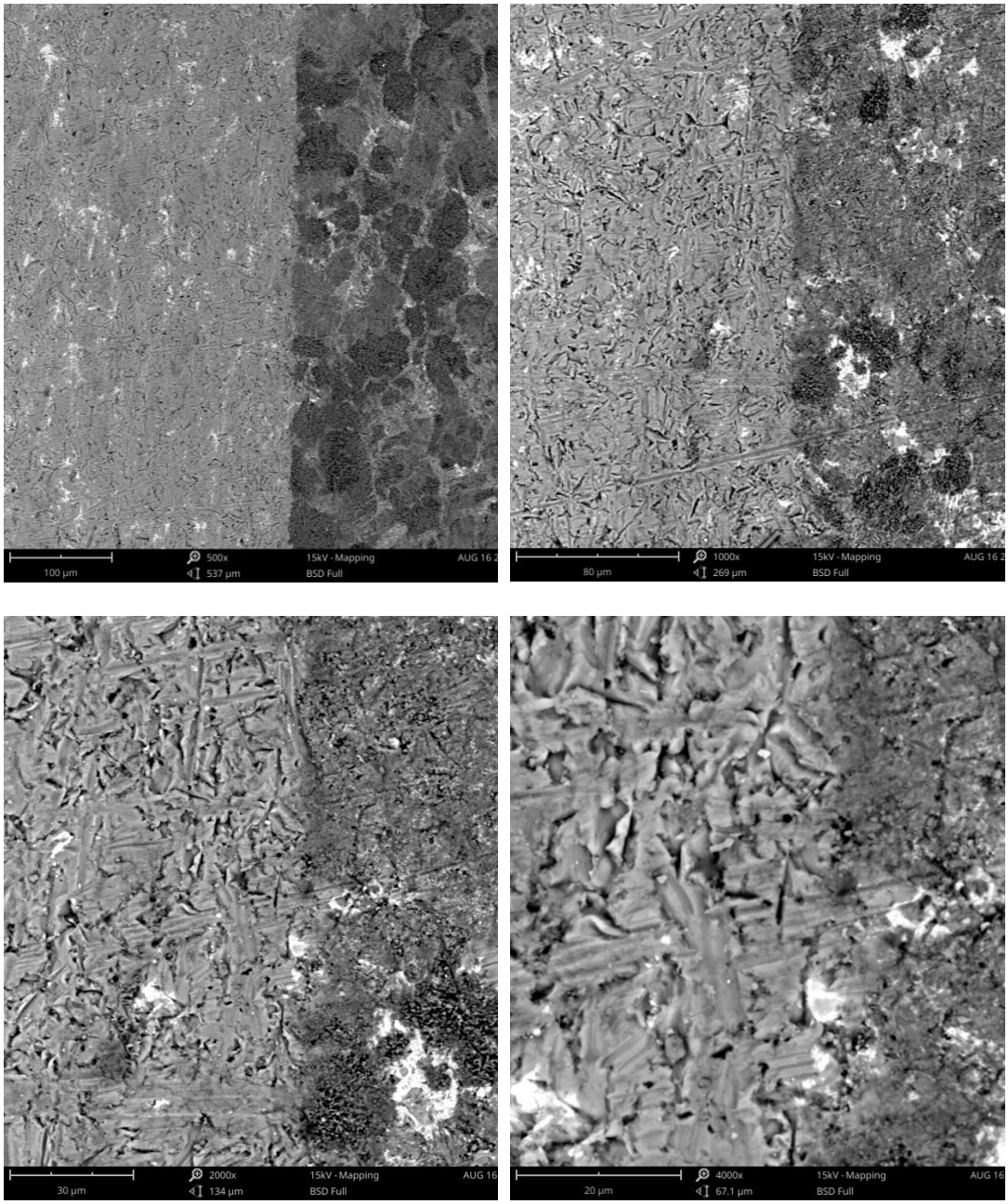

Figure A. 2. SEM images of interface of melt infiltrated alumina preform sintered at 1350 °C (500, 1000, 2000 and 4000X magnifications)

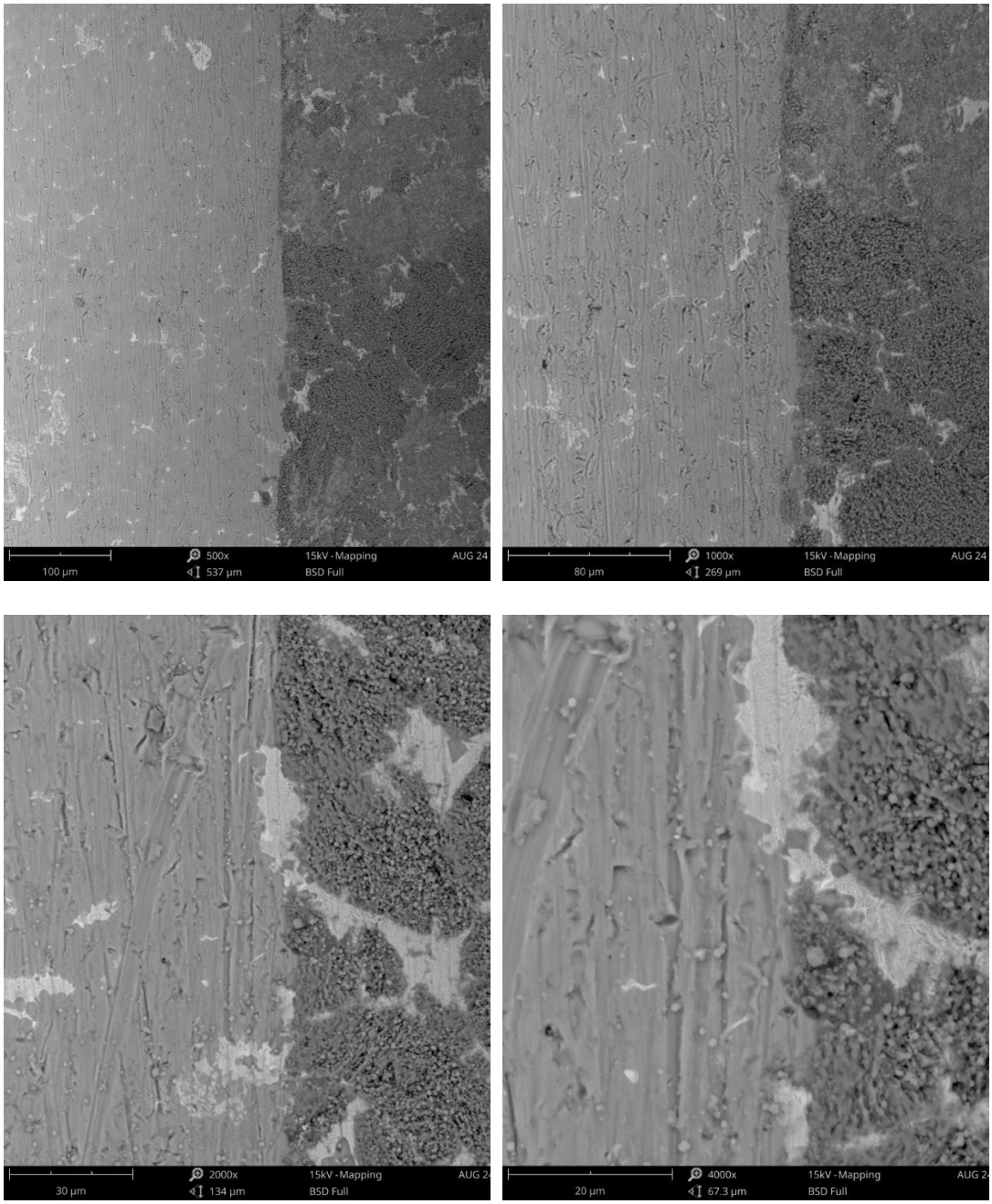

Figure A. 3. SEM images of interface of melt infiltrated alumina preform sintered at 1400 °C (500, 1000, 2000 and 4000X magnifications)

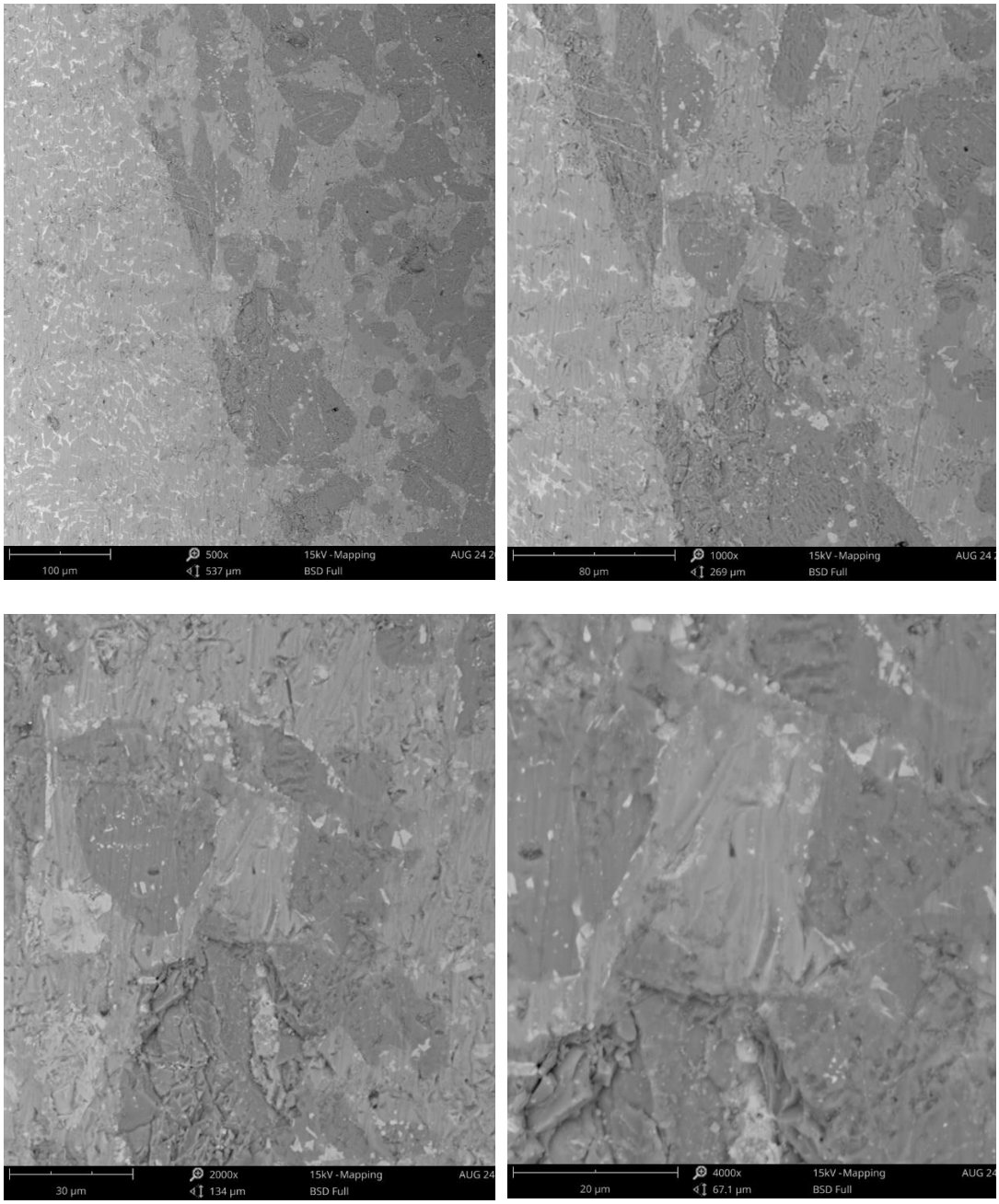

Figure A. 4. SEM images of interface of melt infiltrated 90/10 olivine preform sintered at 1300 °C (500, 1000, 2000 and 4000X magnifications)

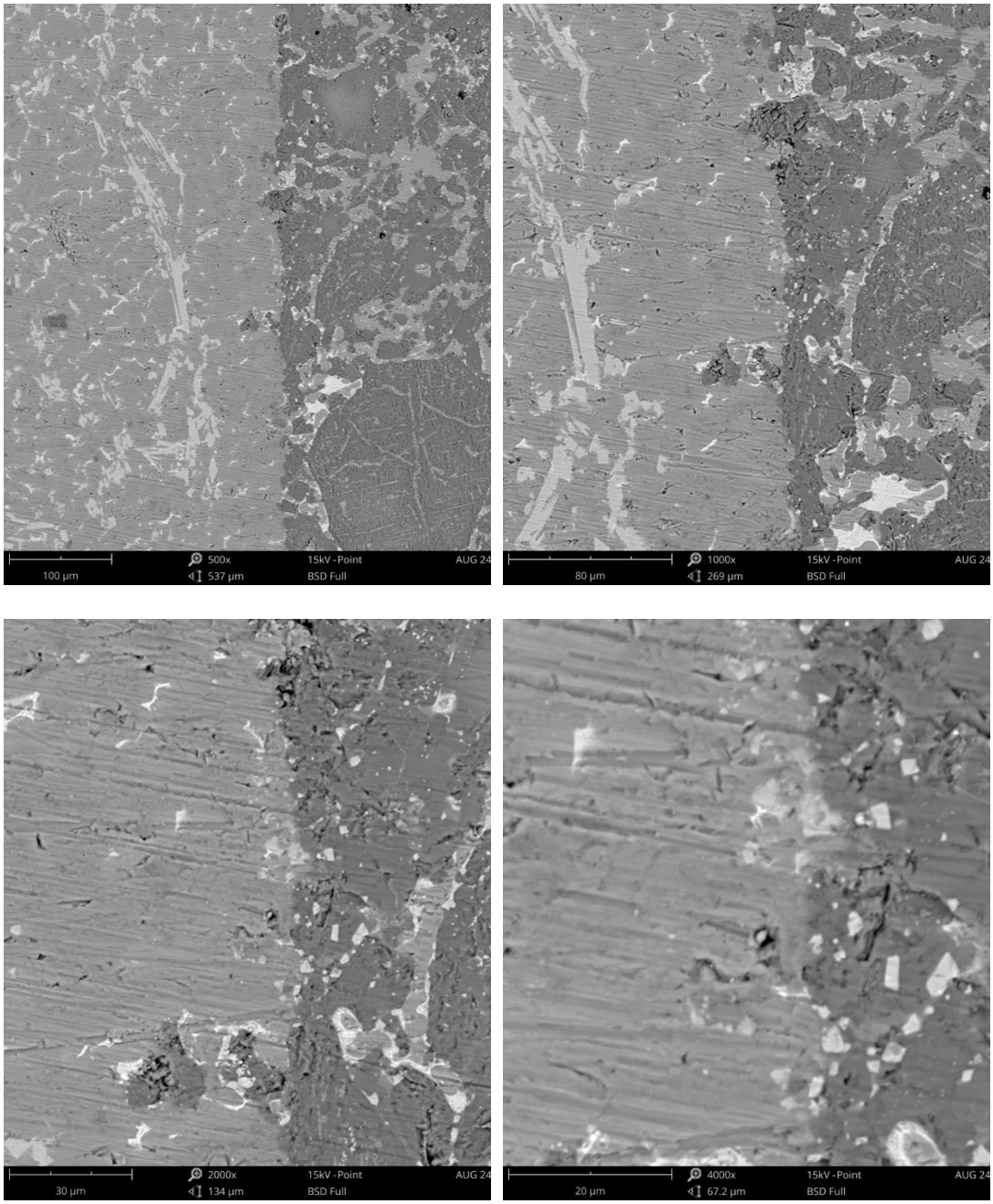

Figure A. 5. SEM images of interface of melt infiltrated 80/20 olivine preform sintered at 1300 °C (500, 1000, 2000 and 4000X magnifications)

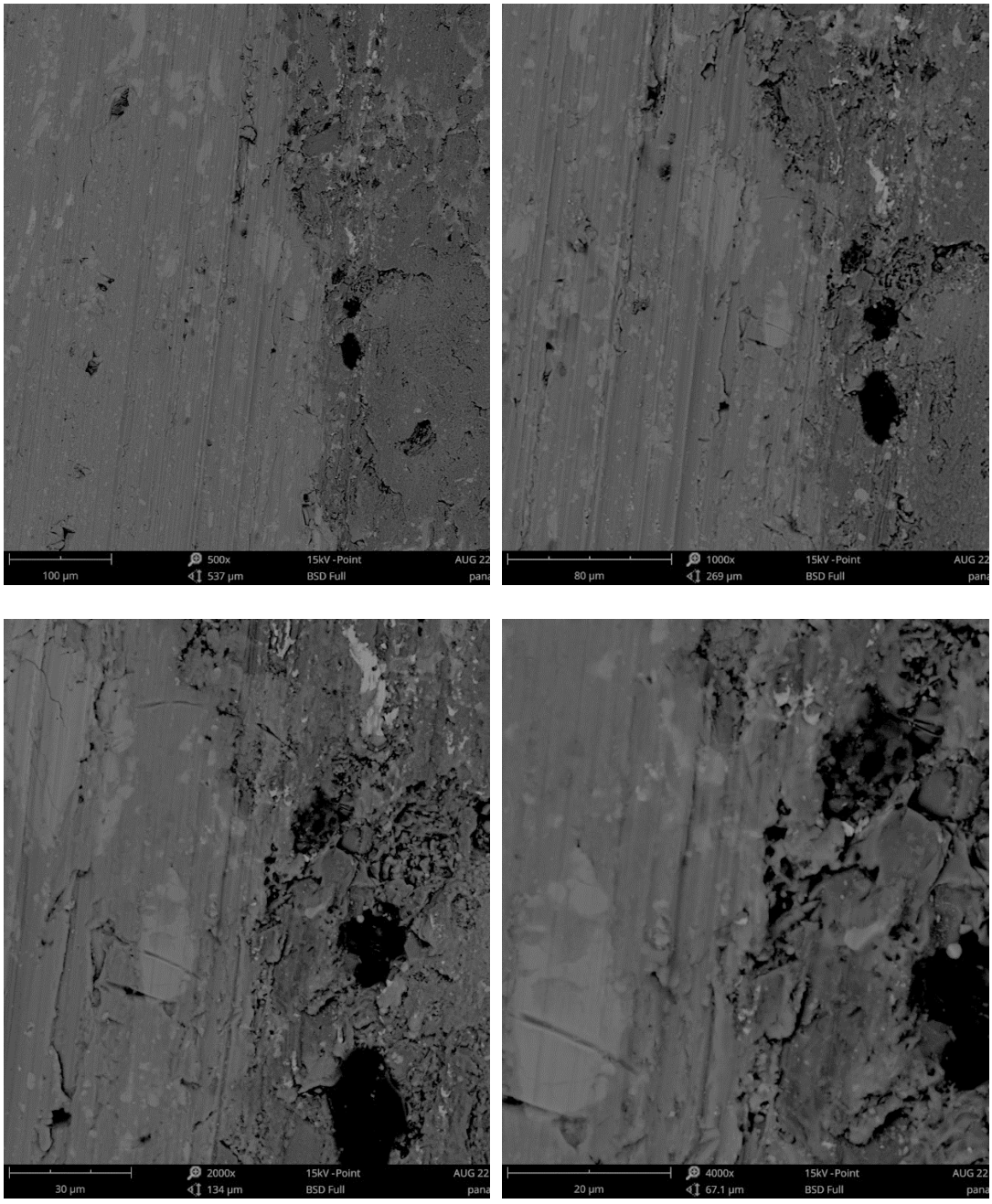

Figure A. 6. SEM images of interface of melt infiltrated 70/30 olivine preform sintered at 1300 °C (500, 1000, 2000 and 4000X magnifications)

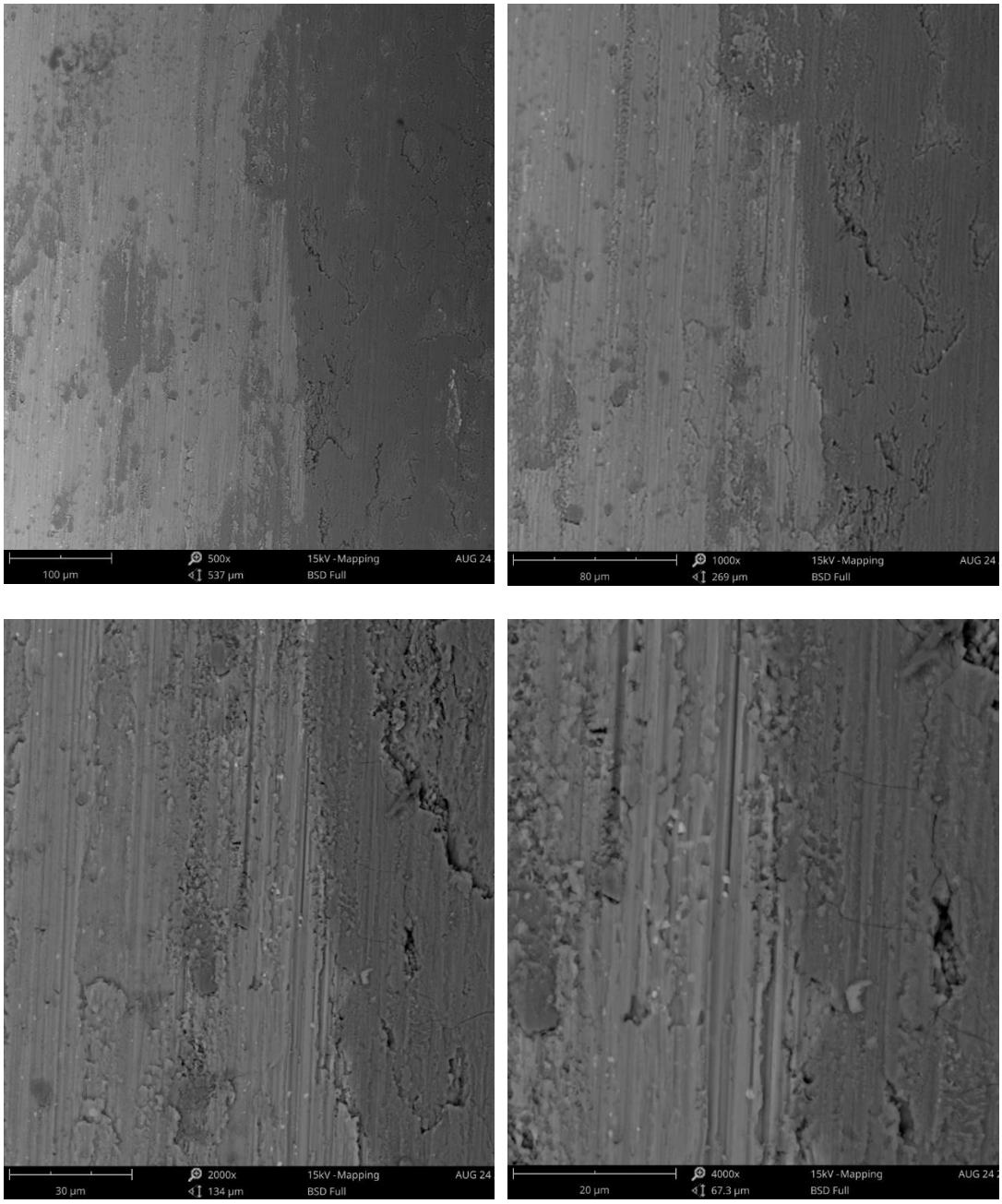

Figure A. 7. SEM images of interface of melt infiltrated 60/40 olivine preform sintered at 1300 °C (500, 1000, 2000 and 4000X magnifications)

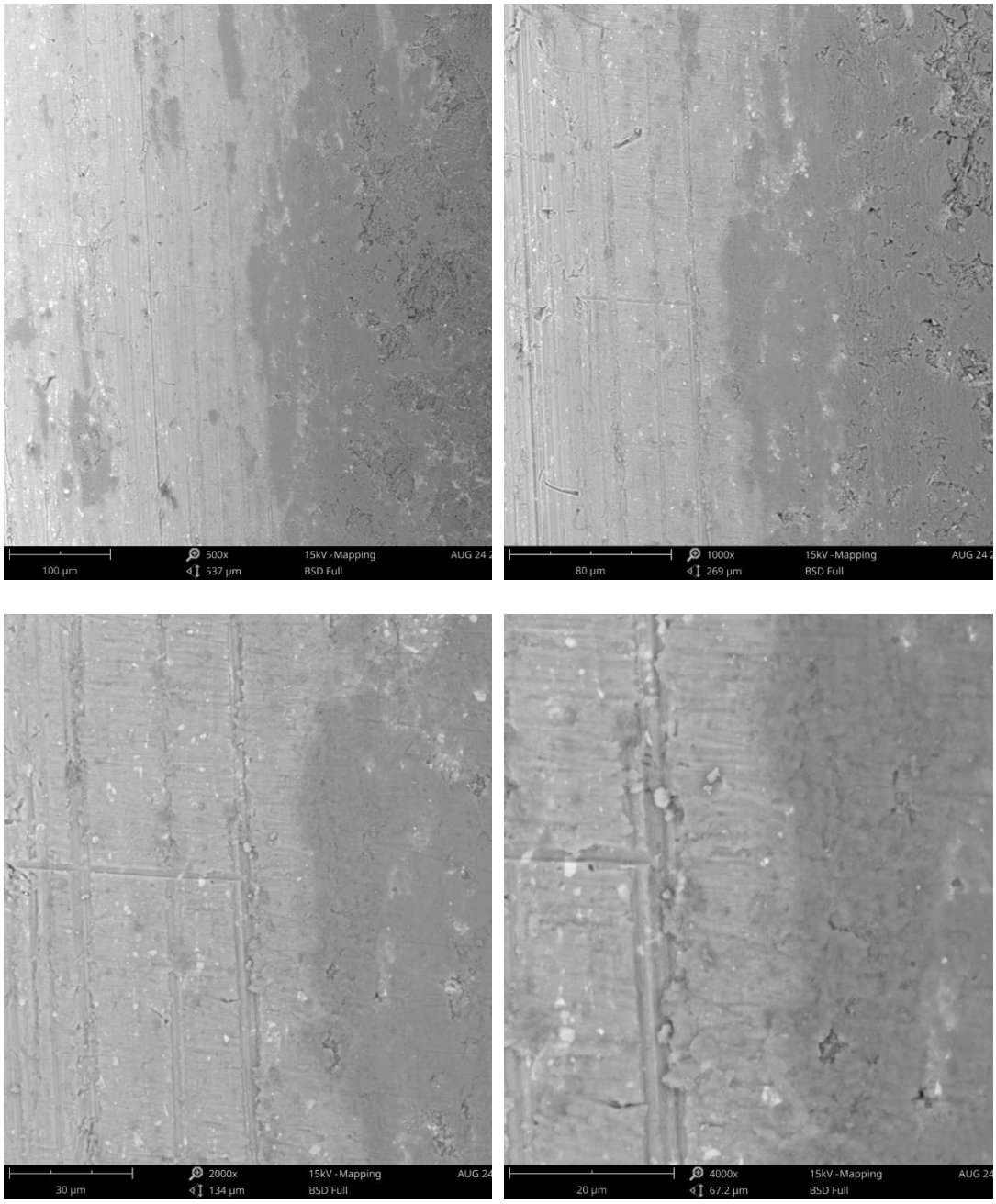

Figure A. 8. SEM images of interface of melt infiltrated 50/50 olivine preform sintered at 1300 °C (500, 1000, 2000 and 4000X magnifications)

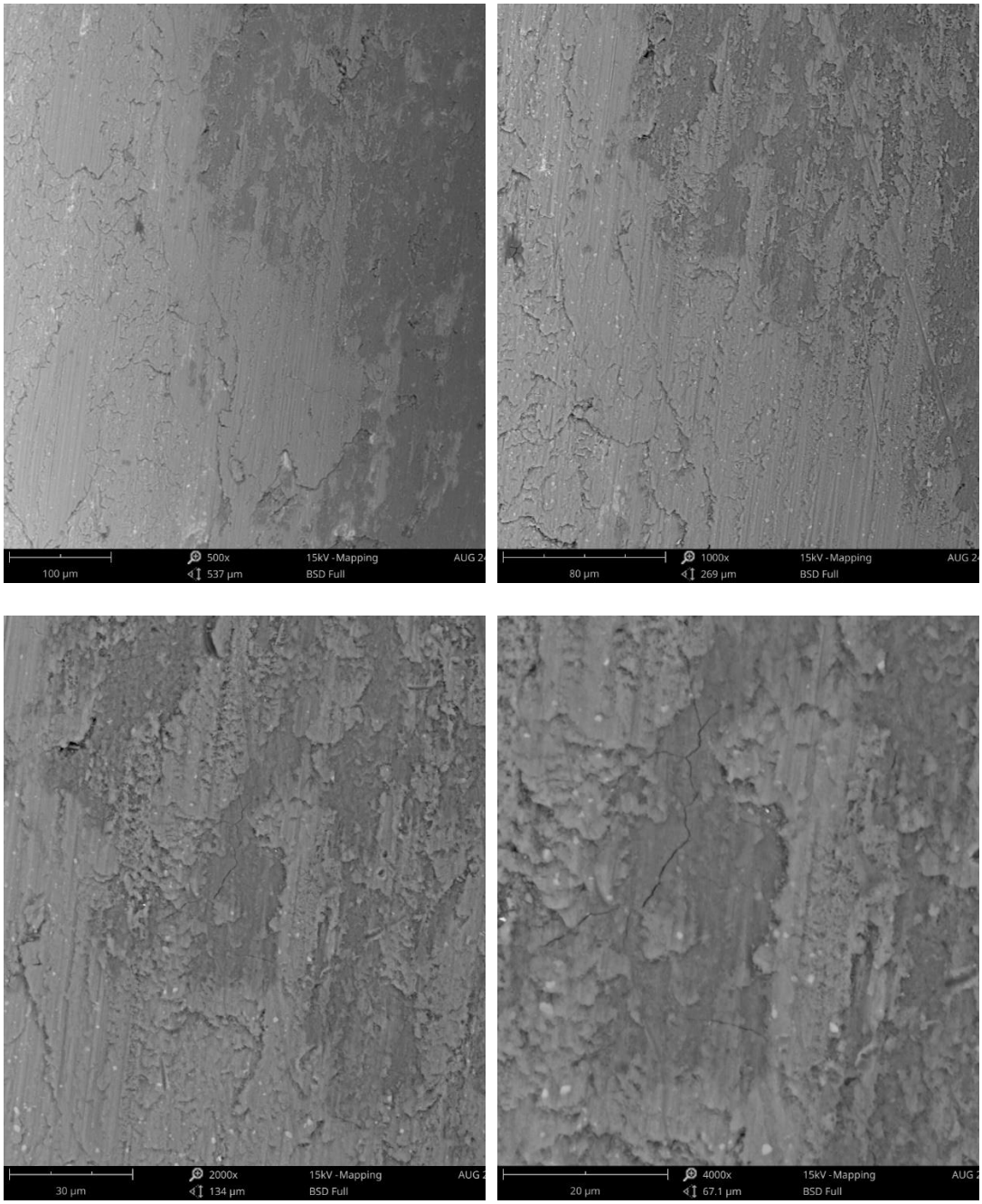

Figure A. 9. SEM images of interface of melt infiltrated 80/20 olivine preform sintered at 1250 °C (500, 1000, 2000 and 4000X magnifications)

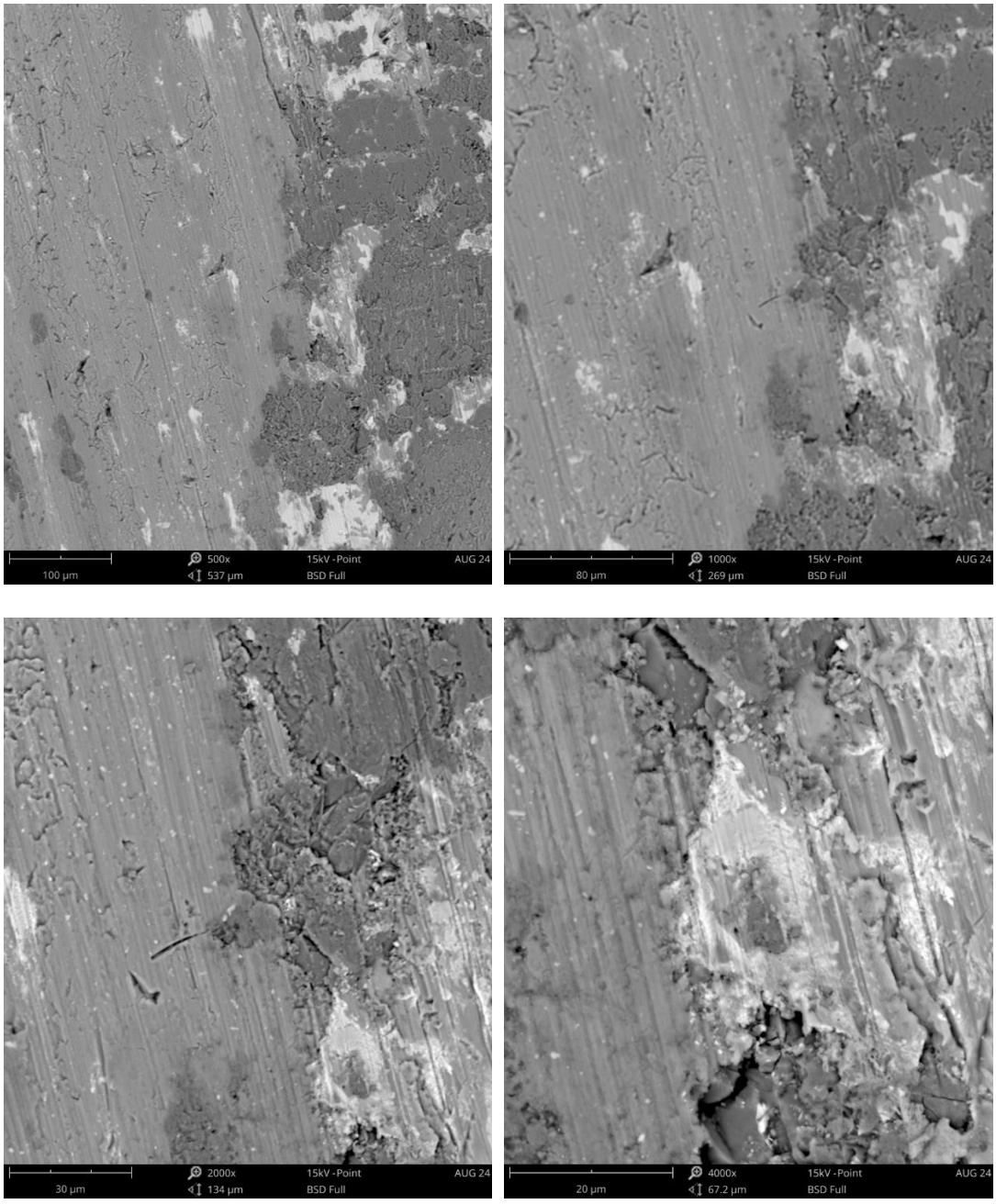

Figure A. 10. SEM images of interface of melt infiltrated 80/20 olivine preform sintered at 1350 °C (500, 1000, 2000 and 4000X magnifications

B. Image Analysis

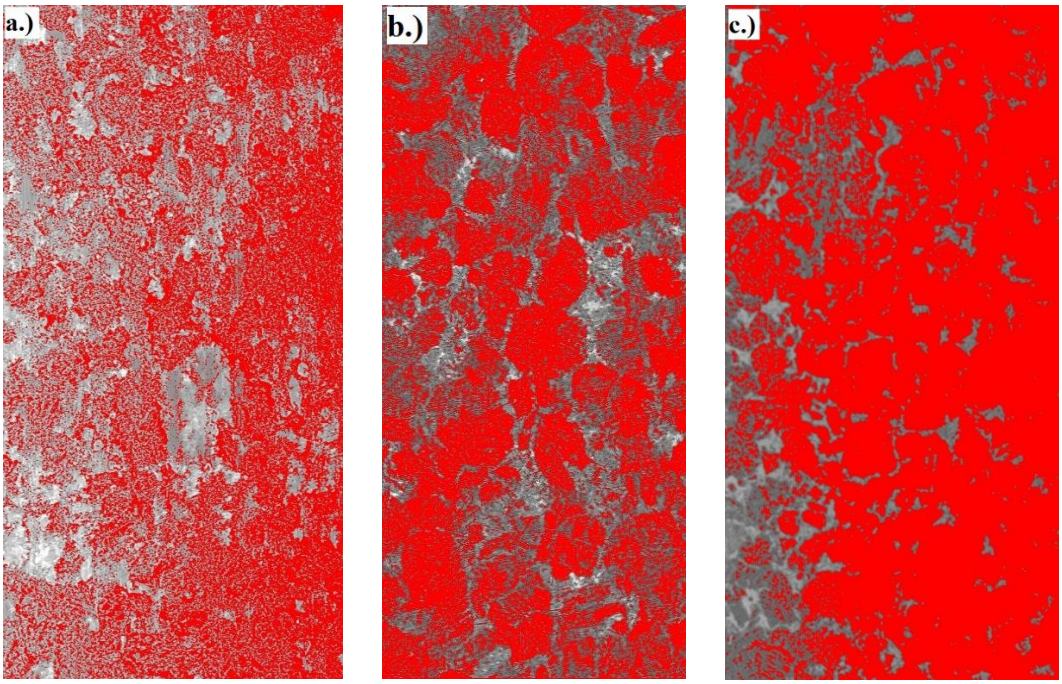

Figure B. 1. Image analysis of infiltrated alumina preforms sintered at a.)1300 °C, b.) 1350 °C and c.) 1400 °C

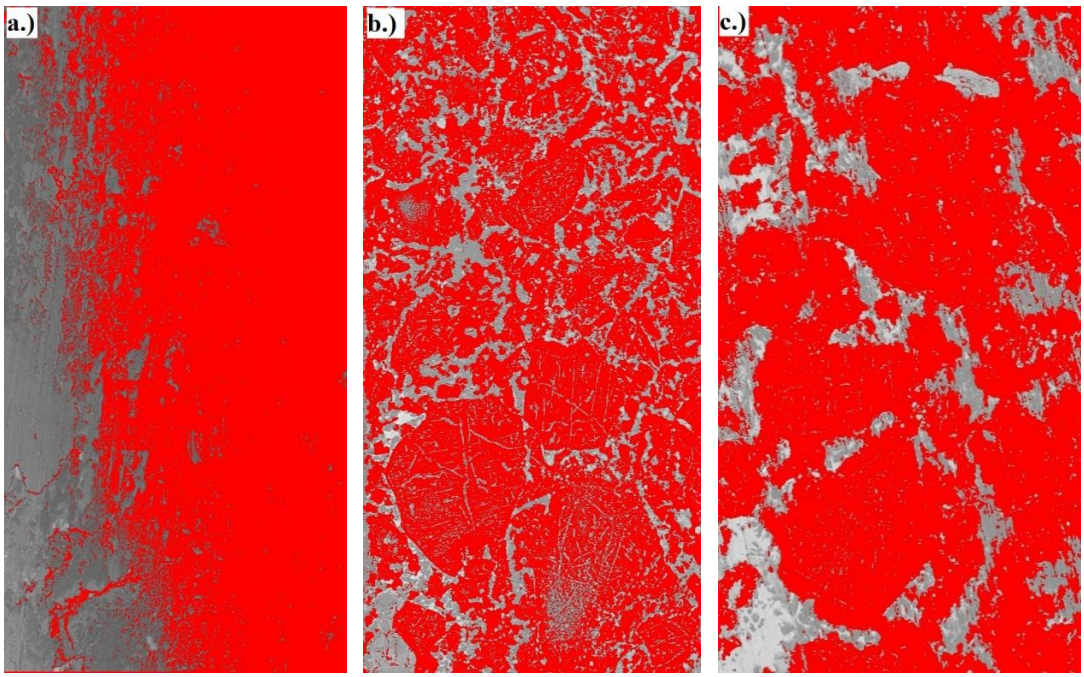

Figure B. 2. Image analysis of infiltrated olivine preforms sintered at a.)1250 °C, b.) 1300 °C and c.) 1350 °C

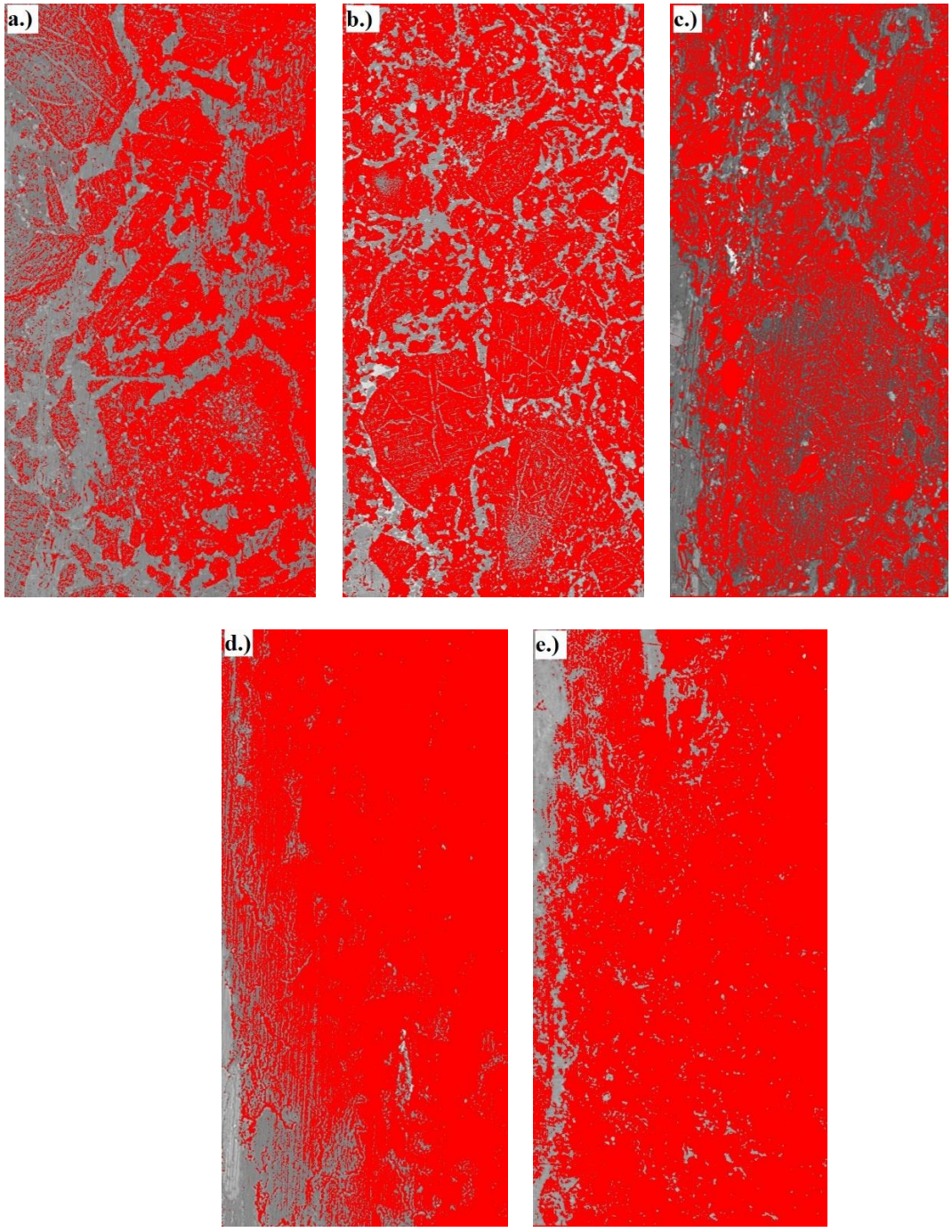

Figure B. 3. Image analysis of infiltrated olivine preforms of different coarse/fine fractions sintered at 1300 °C a.)90/10 , b.) 80/20, c.) 70/30, d.)60/40 amd e.)50/50